Synthesis of carboxymethyl cellulose (CMC)-based bionanogels for dual stimuli-responsive drug release and cancer therapy

Yifen Wen

A Thesis
In
The Department
of
Chemistry and Biochemistry

Presented in Partial Fulfillment of the Requirements
for the Degree of Master of Science (Chemistry) at
Concordia University
Montreal, Quebec, Canada

March 2015

CONCORDIA UNIVERSITY

School of Graduate Studies

This is to certify that the thesis prepared

By: Yifen Wen

Entitled: Synthesis of carboxymethyl cellulose (CMC)-based bionanogels for dual stimuli-responsive drug release and cancer therapy

and submitted in partial fulfillment of the requirements for the degree of

Master of Sciences (Chemistry)

complies with the regulations of the University and meets the accepted standards with respect to originality and quality.

Signed by the final Examining Committee:

_____ Chair

_____Dr. Pat Forgione_____ Examiner

_____Dr. Xavier Ottenwaelder_____Examiner

_____Dr. Jung Kwon (John) Oh _____Supervisor

Approved by _____

Chair of Department or Graduate Program Director

_____ 2015_____

Dean of Faculty

Abstract

Synthesis of carboxymethyl cellulose (CMC)-based bionanogels for dual stimuli-responsive drug release and cancer therapy

Yifen Wen

Polysaccharides possess great potential as building blocks in the development of drug delivery vehicles. This can be attributed to their outstanding virtues, such as biocompatibility, biodegradability, and possession of a plenty of functional groups. Their chemical flexibility allows for the modification of polysaccharides, leading to diverse functionalities that are valuable in biomedical applications. A promising functionality is stimuli-responsiveness that results in a change of physical or chemical properties of polysaccharide-based nanocarriers in response to an environmental change, such as pH, temperature, and light. Herein, recent strategies to develop polysaccharide-based nanomaterials for biomedical application are mapped out. Furthermore, using carboxymethyl cellulose (CMC) as a promising pH-sensitive polysaccharide, two types of stimuli-responsive polysaccharide-based nanomaterials were developed and evaluated as potential tumor targeting drug delivery nanocarriers.

The first system involves dual pH/reduction responsive polysaccharide-based bionanogels (ssBNGs) prepared by aqueous crosslinking polymerization. CMC is grafted with pendant oligo(ethylene oxide) containing methacrylate (OEOMA), and crosslinked with a disulfide-labeled dimethacrylate, yielding disulfide crosslinked ssBNGs with a diameter ≈ 24 nm measured by dynamic light scattering. ssBNGs exhibit dual pH/reduction-responsive drug release, attributed to less interactions between the encapsulated drug molecules and CMC at acidic pH and the reductive cleavage of disulfide crosslinkers. The possibility of conjugating a targeting ligand to ssBNGs is confirmed with a model water-soluble UV-active dye.

The second system includes dual pH/temperature responsive bionanogels (DuR-BNGs). Thermoresponsive polymers undergo volume change above their lower critical solution temperature (LCST) due to a hydrophilic/hydrophobic transition. DuR-BNGs were prepared by grafting thermoresponsive monomers: di(ethylene oxide) methyl ether methacrylate (MEO_2MA) and OEOMA from CMC in the presence of crosslinker via aqueous crosslinking polymerization.

The self-association of grafted P(MEO_2MA-co-OEOMA) above their LCST resulted in a micelle-like structure of DuR-BNGs as well as narrow size distribution. DuR-BNGs exhibit pH-responsive drug release due to the pH-dependent interaction of CMC with drug molecules. The temperature-responsive drug release was driven by the shrinkage of DuR-BNGs networks upon high temperature treatment, thereby expelling encapsulated cargoes causing rapid drug release. The non-specific protein absorption of DuR-BNGs is evaluated with bovine serum albumin (BSA) as a model.

The potential application of two types of dual stimuli-responsive bionanogels (BNGs) in drug delivery is demonstrated with cell viability by MTT assay and cellular uptake using confocal laser scanning microscopy and flow cytometry.

Acknowledgements

I would like to express my deepest gratitude to my supervisor, Dr. Jung Kwon (John) Oh, for his guidance and encouragement throughout my master's program. His enthusiasm and dedication in polymers encouraged me to devote myself to research. His kindness, patience and continuous support helped me go through the hardest time while I was injured. He always believed in my abilities as a scientist and helped me to make good choices. Under his supervision, I was able to build my own knowledge of polymers, develop an ability to solve problems, and improve my writing skills. Without his help, this dissertation would not have been written.

I would also like to thank my committee members Dr. Xavier Ottenwaelder and Dr. Pat Forgione for taking the time to attend my committee meetings and giving me insightful guidance and recommendations. Their questions helped me expand my understanding of my research.

I am most grateful for having the opportunity to work with the wonderful people in our group. I would like to thank Nicky, Soyoung, Nare, Puzhen, Samuel, Alexander, Behnoush, Tongbing, Kaiwan, Arunbabu, Depannita, and other group members for the great times we shared. I want to thank Dr. Nicky Chan for his great help in the beginning of my master's program and sharing his knowledge. Thanks to Soyoung and Puzhen for their great friendship and support. There were so many times I felt I was too frustrated to continue my experiment, they listened to me and cheered my up.

I wish to thank my best friend Poon. Whenever I fell depressed, Poon is the one I can talk to and rely on. Thanks to my parents for their belief in my abilities and constant moral and financial support. They have not experienced what I was facing, but their understanding and encouragement is the best gift for me. Without them, this degree would have never been possible. Words cannot express the gratitude and love I have for all of them.

Table of Contents

List of Figures ix
List of Abbreviations xii
Chapter 1 Introduction 1
1.1 Overview of research and goals 1
1.2 General concepts of polymer-based drug delivery and research goals 1
1.3 Polysaccharide-based drug carriers 2
1.3.1 Polysaccharide 2
1.3.2 Polysaccharide-based bionanogels (BNGs) 4
1.3.3 Strategies of BNGs preparation 4
1.4 Stimuli-responsive polymeric nanomaterials 5
1.4.1 Reduction-responsive degradation 6
1.4.2 Temperature-responsive volume change 7
1.4.3 pH-responsiveness 8
1.5 Scope of the thesis 9
Chapter 2 10
Review of recent strategies of developing polysaccharide-based nanocarriers for biomedical application 10
2.1 Introduction 11
2.2 Polysaccharide-based self-assembled aggregates 13
2.2.1 Amphiphilic polysaccharides modified with small hydrophobic molecules 13
2.2.2 Amphiphilic polysaccharides conjugated with polymers 14
2.3 Polysaccharide-based crosslinked microgels/nanogels 18
2.3.1. Chemical crosslinking by condensation 18
2.3.2. *In situ* disulfide-crosslinking method 19
2.3.3. Aqueous free radical crosslinking polymerization (FRCP) 21
2.3.4. Physical crosslinking method 24
2.4. Polysaccharide-based hydrogels 25
2.4.1. Physical crosslinking method 25
2.4.2. Chemical crosslinking method 27
2.5. Polysaccharide-based fibrous materials 29
2.6. Summary and Outlook 29
Chapter 3 Development of pH/reduction-responsive CMC-based bionanogels 31
3.1 Introduction 32

3.2 Experimental 34
3.2.1 Instrumentation and analysis 34
3.2.2 FT-IR measurements 35
3.2.3 Dynamic light scattering (DLS) measurements 35
3.2.4 Transmission electron microscopy (TEM) 36
3.2.5 Materials 36
3.2.6 Synthesis of ssBNGs crosslinked with disulfides 37
3.2.7 Loading of DOX 37
3.2.8 Dual-responsive release of DOX using UV/Vis spectroscopy 37
3.2.9 Cell culture 38
3.2.10 Confocal laser scanning microscopy (CLSM) 38
3.2.11 Cell viability using MTT assay 38
3.2.12 Conjugation of ssBNGs with APTS 38
3.3 Results and Discussion 39
3.3.1 Preparation of ssBNGs based on crosslinked POEOMA-g-CMC 39
3.3.2 Loading of anticancer drugs 42
3.3.3 Dual responsive release of encapsulated anticancer drugs 43
3.3.4 Intracellular release as anticancer drug delivery nanocarriers 45
3.3.5 Bioconjugation for active targeting 47
3.4 Conclusion 49
Chapter 4 50
Development of pH/temperature-responsive CMC-based bionanogels 50
4.1 Introduction 52
4.2 Experimental 54
4.2.1 Materials 54
4.2.2 Aqueous polymerization to synthesize CMC-g-P(MEO_2MA-co-OEOMA) 55
4.2.3 Synthesis of DuR-BNGs by temperature-driven self-association assisted method 55
4.2.4 Instrumentation and analysis 55
4.2.5 Size and morphology analysis 56
4.2.6 Determination of LCST using DLS 56
4.2.7 Colloidal stability 56
4.2.8 Non-specific BSA absorption of DuR-BNGs 56
4.2.9 DOX Loading 57
4.2.10 Dual stimuli-responsive release of DOX using UV/Vis spectroscopy 57
4.2.11 Cell culture 58

4.2.12 Cell viability using MTT assay 58
4.2.13 Confocal laser scanning microscopy (CLSM) 58
4.2.14 Flow cytometry 59
4.3 Results and Discussion 59
4.3.1 Synthesis of DuR-BNGs 59
4.3.2 Prolonged colloidal stability and non-specific protein absorption 61
4.3.3 Encapsulation of DOX 63
4.3.4 Dual stimuli-responsive release of encapsulated DOX 63
4.3.5 Intracellular trafficking and antitumor activity of DOX-loaded DuR-BNGs 65
4.4 Conclusion 68
Chapter 5 Conclusion and Future Work 69
References 71
Appendix A 84
Appendix B 91
List of publications 96

List of Figures

Figure 1.1. Illustration of EPR effect that allows nanocarriers to be accumulated in tumor tissues compared to normal tissues.[1] 2

Figure 1.2. Typical chemical structures of polysaccharides. Abbreviation of polysaccharides: HA: hyaluronic acid, ALG: alginate, CeL: cellulose, CS: chitosan, PuL: pullulan, DeX: dextran. 3

Figure 1.3. Typical example of stimuli-responsive drug delivery strategies.[35] 6

Figure 1.4. Reductive degradation of disulfide-containing bionanogels in response to cellular GSH..... 7

Figure 1.5. Schematic drawing showing the phase transition associated with LCST. 8

Figure 2.1. Chemical structures of typical polysaccharides and polysaccharide-based biomaterials, typically self-assembled micelles, crosslinked microgels/nanogels, three-dimensional hydrogels, and fibrous meshes, for various biomedical applications such as drug delivery, cell-encapsulation, tissue engineering, and regenerative medicine. Abbreviation of polysaccharides) DeX: dextran, PuL: pullulan, CeL: cellulose, CS: chitosan, ALG: alginate, HA: hyaluronic acid, HPCeL: hydroxypropyl cellulose, ECeL: ethyl cellulose, CMC: carboxymethyl cellulose, CT: chitin, and ChS: chondroitin sulfate. 12

Figure 2.2. Synthesis, self-assembly, and pH-responsive release of amphiphilic PuL conjugated with urocanic acid and cholesterol succinate via a carbodiimide coupling reaction. Reproduced with permission.[76] Copyright 2014, Royal Society of Chemistry. 14

Figure 2.3. Synthesis of amphiphilic brush-like ECeL grafted with thermoresponsive (co)polymers. Reproduced with permission.[45] Copyright 2012, Elsevier. 16

Figure 2.4. Synthesis of a thermoresponsive HA-polymer conjugate of HA-g-P(DEGMA-co-OEOMA) via thiol-ene Michael addition reaction and their self-assembly driven by change in temperature. Reproduced with permission.[23] Copyright 2012, Royal Society of Chemistry. 17

Figure 2.5. Synthesis, self-assembly at temperature above LCST, and oxidation of thiolated HPCeL to form disulfide-crosslinked nanogels. Adapted with permission.[118] Copyright 2011, Royal Society of Chemistry. 21

Figure 2.6. Schematic representation of dual enzymatic and light-degradable nanogels crosslinked with photo-labile linkage of DeX-g-PAAm. Reproduced with permission.[122] 22

Figure 2.7. Synthesis and dual reduction and acidic pH-responsive Dox release of nanogels crosslinked with disulfide linkages of POEOMA-grafted CMC.[33] Copyright 2014, Royal Society of Chemistry..... 24

Figure 2.8. Synthesis (A) and sol-gel transition (B) of HA-dopamine and SH-terminated Pluronic F127. Reproduced with permission.[153] Copyright 2010, Royal Society of Chemistry. 27

Figure 2.9. Synthetic scheme for Michael addition reaction of SH-modified HA with hyperbranched thermoresponsive copolymers labeled with acrylate groups to yield thiol-ene crosslinked hydrogels in aqueous solution. Reproduced with permission.[159] 28

Scheme 3.1. Synthesis by aqueous FRCP, bioconjugation, and dual stimuli-response of biopolymer-based ssBNGs crosslinked with disulfide linkages of POEOMA-g-CMC. 34

Figure 3.1. DLS diagram (a) and TEM image (b) of dialyzed ssBNGs. 40

Figure 3.2. FT-IR spectrum of ssBNGs, compared with that of POEOMA-g-CMC. 42

Figure 3.3. Release of DOX from DOX-loaded ssBNGs in aqueous buffer solutions at different pH of 3, 5.5, and 7 (a), and digital photos of outer water (upper) and the corresponding dialysis tubing (lower) before (b) and after release of DOX at pH = 3 (c), 5.5 (d), and 7 (e). 44

Figure 3.4. Release of DOX from DOX-loaded ssBNGs in aqueous buffer solutions at pH = 7 with and without 5 mM GSH. 45

Figure 3.5. CLSM images of HeLa cells incubated with empty ssBNGs for 8 hrs (a), DOX-loaded ssBNGs for 2 (b) and 8 hrs (c), as well as free DOX for 2 (d) and 8 hrs (e). Scale bar = 20 μm. 46

Figure 3.6. Viability of HeLa cells incubated with empty and DOX-loaded ssBNGs for 48 hrs determined by MTT assay. Data are presented as the average ± standard deviation (n = 12) 47

Figure 3.7. UV/Vis spectra and digital photos (insect) of aqueous solution of APTS-conjugated ssBNGs and free APTS at pH = 7. 48

Figure 4.1. LCST of CMC-g-P((MEO$_2$MA-co-OEOMA) as a function of the amount of hydrophobic MEO$_2$MA units. 60

Figure 4.2. DLS diagram and TEM image (inset) of DuR-BNGs measured at 25 ºC. 61

Figure 4.3. Evolution of diameter of DuR-BNGs in buffer solutions at pH = 5.5 and 7.0. 62

Figure 4.5. Release of DOX from DOX-loaded DuR-BNGs in aqueous buffer solution (pH = 7) at different temperatures of 25, 37, 40, and 43 ºC (a) and at pH = 5.5 and 7 (37 ºC) (b). 65

Figure 4.6. Flow cytometric histograms (a) and CLSM images of HeLa cells incubated with DuR-BNGs only (A), DOX-loaded DuR-BNGs (B), and free DOX (C) for 5 hrs (b). Scale bar = 10 μm. 66

Figure 4.7. Viability of HeLa cells incubated with different amounts of DuR-BNGs only (a), DOX-loaded DuR-BNGs and free DOX for 48 hrs (b) determined by MTT assay 67

Figure A.1. DLS diagrams with various concentrations of OEOMA in water from 0 to 10 mg/mL concentrations for aqueous FRP of OEOMA initiated with VA-44 = 0.2 wt% of OEOMA at 40 °C. 87

Figure A.2. FT-IR spectra of POEOMA-g-CMC, CMC and POEOMA homopolymer. 88

Figure A.3. UV absorbance at λ = 497 nm of free DOX in outer water during extensive dialysis. 89

Figure A.4. Comparison of UV/Vis spectra of DOX-loaded ssBNGs (0.2 mg/mL) with free DOX (7.7 μg/mL) in water. 89

Figure A.5. UV/Vis spectra of free APTS in aqueous solutions at various pH ranging from 2 to 10. 90

Figure A.6. UV/Vis spectra (a) absorbance (b) vs different concentrations of APTS in water (pH = 6.5) to determine the extinction coefficient (ε = 21,700 M^{-1} cm^{-1}). 90

Figure B.1. ^{1}H-NMR spectrum of CMC-g-P1 to determine monomer conversion. 92

Figure B.2. FT-IR spectrum of CMC-g-P6 (CMC-g-P(MEO_2MA-co-OEOMA)).....93

Figure B.3. Temperature dependence of normalized light scattering intensity by DLS for aqueous solutions of LCST vs amount of MEO_2MA units (mol%) in grafted P(MEO_2MA-co-OEOMA) at 4.3 mg/mL. 93

Figure B.4. Temperature dependence of normalized light scattering intensity by DLS for aqueous solutions of DuR-BNGs at 4.6 mg/mL. 94

Figure B.5. Calibration curve to determine the concentration of BAS in PBS at pH = 7.4. 94

Figure B.6. Release of DOX from DOX-loaded DuR-BNGs in aqueous buffer solution (pH = 7.0) at various temperatures of 25, 37, 40, and 43 ºC. Apparent diffusion constant (D_{app}) is determined from the slopes obtained by fitting the data to a linear regression. 95

Figure B.7. Release of DOX from DOX-loaded DuR-BNGs in NaCl aqueous solution (pH = 7.0, 37 ºC) at different ionic strengths of 154 and 308 mM. 95

List of Abbreviations

4-NC	4-nitrophenyl chloroformate
AAm	Acrylamide
ALG	Alginate
APTS	8-aminopyrene-1,3,6-trisulfonic acid trisodium salt
ATRP	Atom transfer radical polymerization
BNGs	Bionanogels
BSA	Bovine serum albumin
CD	Cyclodextrin
CeL	Cellulose
ChS	Chondroitin sulfate
CLSM	Confocal laser scanning microscopy
CMC	Carboxymethyl cellulose
CRP	Controlled radical polymerization
CS	Chitosan
CT	Chitin
DCC	*N,N′*-dicyclohexylcarbodiimide
DeX	Dextran
DLS	Dynamic light scattering
DMAP	4-(dimethylamino)pyridine
DOX	Doxorubicin
DTT	D,L-dithiothreitol
ECeL	Ethyl cellulose
EPR	Enhanced permeability and retention
FRCP	Free radical crosslinking polymerization
FRP	Free radical polymerization
GPC	Gel permeation chromatography
GSH	Glutathione
HA	Hyaluronic acid
HIV	Human immunodeficiency virus
HPCeL	Hydroxypropyl cellulose
ICG	Indocyanine green
IV	Intravenous
KHP	Potassium hydrogen phthalate
LA	Lipoic acid
LCST	Lower critical solution temperature
MBA	*N,N'*-methylene bisacrylamide
MEO_2MA	Di(ethylene oxide) methyl ether methacrylate
M_n	Number-average molecular weight
MTT	3-(4,5-dimethylthiazol-2-yl)-2,5-diphenyltetrazolium bromide
M_w	Weight-average molecular weight
MWCO	Molecular weight cut-off

NIR	Near infrared
NMR	Nuclear magnetic resonance
OEODMA	Oligo(ethylene oxide) methyl ether dimethacrylate
OEOMA	Oligo(ethylene oxide) monomethyl ether methacrylate
PAA	Poly(acrylic acid)
PAAPBA	Poly(acrylamidophenylboronic acid)
PCL	Polycaprolactone
PDDS	Polymer-based drug delivery systems
PDMAEMA	Poly(*N, N*-dimethylaminoethyl methacrylate)
PEG	Poly(ethylene glycol)
PGA	Polyglycolide
PLA	Polylactide
PLL	Poly(L-lysine)
PNIPAM	Poly(*N*-isopropylacrylamide)
PtBMA	Poly(*t*-butyl methacrylate)
PuL	Pullulan
RAFT	Reversible addition fragmentation chain transfer
RES	Reticulo-endothelial system
ROP	Ring opening polymerization
ssDMA	Dithiopropionyl poly(ethylene glycol) dimethacrylate
TEM	Transmission electron microscopy
TPP	Pentasodium triphosphate
UV/Vis	Ultraviolet/Visible
W/O	Water-in-oil

Chapter 1
Introduction

1.1 Overview of research and goals

My Master's research is aimed at exploring dual stimuli-responsive polysaccharide-based crosslinked nanogels (bionanogels) for enhanced/controlled release of anticancer drugs. A facile aqueous crosslinking polymerization method has been employed to synthesize two types of monodispersed bionanogels with diameter < 20 nm: redox/pH-responsive and pH/temperature-responsive bionanogels. In response to dual stimuli, they exhibit rapid release of encapsulated anti-cancer drugs in cellular environment (*in vitro*). Furthermore, these smart bionanogels were evaluated as effective tumor-targeting intracellular delivery nanocarriers for cellular uptake and cell viability in HeLa cancer cell lines.

1.2 General concepts of polymer-based drug delivery and research goals

In cancer treatment, chemotherapy generally uses small anti-cancer therapeutic drugs, such as doxorubicin, paclitaxel, cytarabine and so on.[1] They are usually administered through intravenous (IV) injection. However, these small drug molecules are presented by two main challenges: low bioavailability and non-specific targeting.[2, 3] During blood circulation, small drugs are rapidly eliminated from the body through kidney filtration (called renal clearance), significantly reducing drug efficiency. Moreover, they quickly diffuse into normal tissues through undesired extravasation.[4, 5] This non-specific targeting causes cytotoxicity to normal cells, leading to dose-related side effects.[6] To circumvent these challenges facing small drugs, polymer-based drug delivery systems have been proposed. Typical example includes self-assembled micellar aggregates, fibers, and crosslinked nanogels.[7, 8] Drug molecules are encapsulated in these nanomaterials through physical interactions or covalent attachments. The encapsulation can improve the solubility of hydrophobic drugs and protect drug molecules from deactivation.[3] More importantly, tumor tissues present irregularly-aligned vasculatures as a consequence of rapid growth in the process of cancer angiogenesis. [1, 5] The fenestration of endothelial cells in tumor vasculatures ranges at 300 - 4700 nm, promoting extravasation of

nanocarriers designed with their size of 50 - 150 nm to tumor tissues (enhanced permeability). Due to the lack of effective lymphatic drainages, the nanocarriers extravasated from blood circulation retain inside tumor tissues (retention).[5, 6, 9] This phenomenon is called Enhanced Permeability and Retention (EPR) effect, also referred as passive targeting (Figure 1.1), which is the main mechanism of nanocarriers for specific targeting to tumor tissues not to normal tissues.

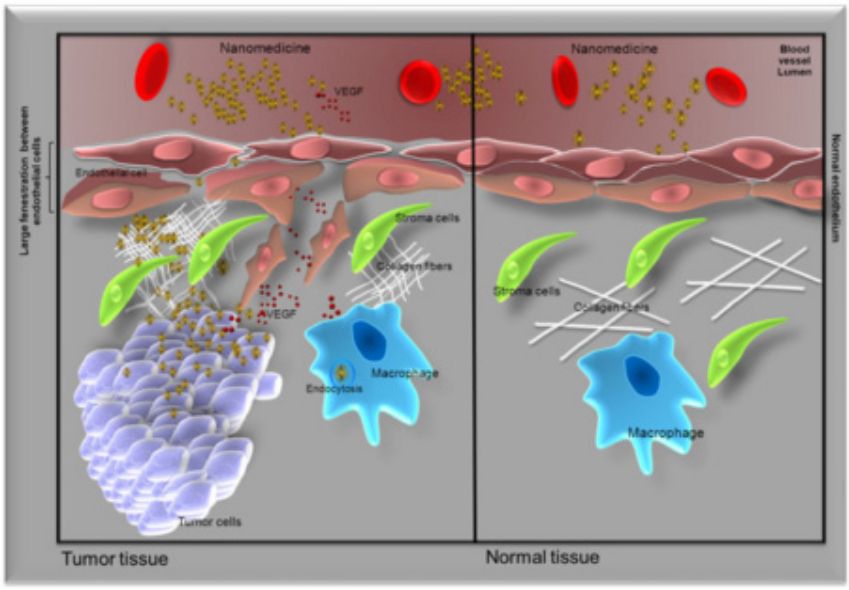

Figure 1.1. Illustration of EPR effect that allows nanocarriers to be accumulated in tumor tissues compared to normal tissues.[1]

1.3 Polysaccharide-based drug carriers

1.3.1 Polysaccharide

Among diverse polymeric materials that are feasible for the construction of drug delivery nanocarriers, polysaccharides display unique advantages. Firstly, polysaccharides are naturally-occurring biopolymers composed of one or more types of monosaccharides as repeating units connecting with glycosidic linkages.[10] Typical examples include hyaluronic acid, alginate, cellulose, chitosan, pullulan, and dextran (Figure 1.2). They are hydrophilic, intrinsically biocompatible, and widely exist in nature such as plants, animals, and bacteria.[11] Moreover, most of polysaccharides can be degraded by enzymatic reactions.[12] The resulting degraded species are small to be removed from the body. Secondly, polysaccharides possess a variety of

reactive functional groups such as COOH, NH_2, and OH groups. These groups can be used for the modification of polysaccharides toward effective biomaterials, particularly biocompatible nanocarriers.[13-15] For example, cellulose can be easily modified into its derivatives such as hydroxypropyl cellulose and carboxymethyl cellulose (CMC) with new functionalities.[16] Furthermore, the presence of functional groups can promote their bioconjugation with specific cell-targeting ligands for active targeting as well as facile conjugation with reactive synthetic polymers for new physical or chemical properties (e.g. hydrophobicity, surface charge, and stimuli-responsive property).[17-19] Thirdly, polysaccharides provide various physical properties such as molecular structure, hydrophobic/hydrophilic balance, and charge for various delivery applications. For example, β-cyclodextrin with seven glucopyranose rings can accommodate a wide variety of hydrophobic molecules through guest-host interactions to form inclusion complex.[20] Chitosan, a natural cationic polysaccharide, can bind to anionic phosphates in nucleic acids through ionic interactions to be useful as gene delivery nanocarriers.[21] These unique properties promote the use of polysaccharides as effective building blocks in the development of versatile bionanomaterials such as nanogels,[22, 23] self-assembled micelles,[24, 25] and hydrogels for biomedical applications.[26]

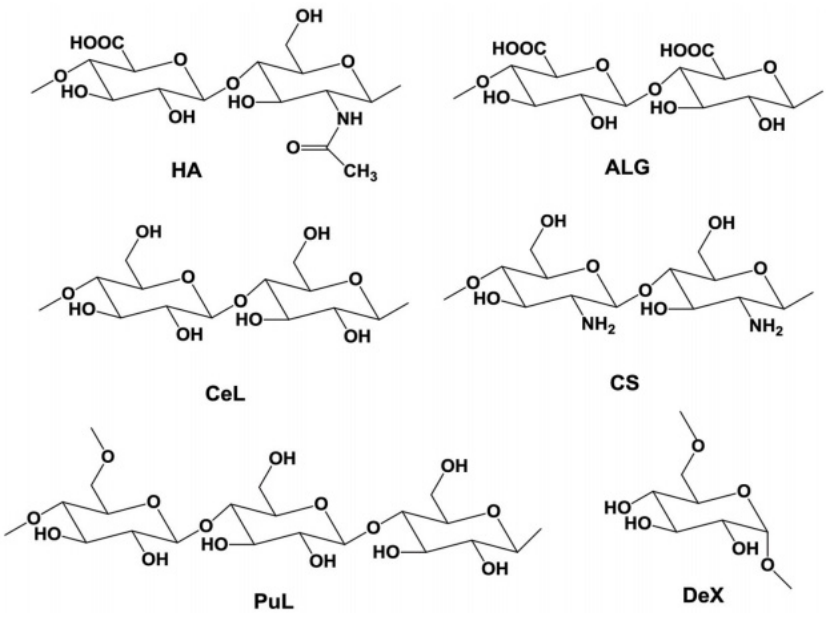

Figure 1.2. Typical chemical structures of polysaccharides. Hyaluronic acid (HA), Alginate (ALG), Cellulose (CeL), Chitosan (CS), Pullulan (PuL), Dextran (DeX).

1.3.2 Polysaccharide-based bionanogels (BNGs)

BNGs are defined as three-dimensionally crosslinked biopolymer-based networks that are confined into nanometer-sizes. They display great properties as drug delivery vehicles. Due to their hydrophilic polymer networks, BNGs possess high water content and good biocompatibility.[27] Because of being crosslinked, BNGs retain excellent colloidal stability upon dilution in blood after IV injection. Furthermore, their particle sizes can be adjusted from 10 to 100 nm by the selection of synthetic strategies. Benefiting from their small particle sizes, bionanogels have large surface area and plenty of functional groups for surface modification.[10, 11]

In fact, the small particle size of BNGs plays a key role in efficient drug delivery. After bionanogels are injected into the body, BNGs should avoid multiple clearance mechanisms before reaching target sites.[28] Most of the clearance mechanisms are size-related. Renal clearance and urinary excretion rapidly eliminates nanoparticles with diameter <5 nm and MW <45 KDa.[29] Reticulo-endothelial system (RES) located in liver, spleen and lung enables recognizing and clearing nanoparticles that are larger than 200 nm.[8] Therefore, in order to minimize renal clearance as well as RES elimination, nanocarriers with the particle size ranging from 50 to150 nm would be an optimum size for drug delivery application.[5]

1.3.3 Strategies of BNGs preparation

The reported synthetic strategies can be classified into two methods: physical or chemical crosslinking. Physical crosslinking is mainly achieved via non-covalent interactions.[30] For example, chitosan−pentasodium triphosphate (TPP) nanogels were formed based on electrostatic interaction between positively charged amino groups of chitosan (in acidic pH) and phosphate anions of TPP.[31] One limitation of physical crosslinking method involves the instability of nanogel networks due to weak interactions between polymeric chains. The formed BNGs are sensitive to environmental changes and can easily be destabilized. In contrast, chemical crosslinking involves the formation of covalent linkages of polymeric chains. A typical example to introduce covalent linkage is the use of external crosslinkers. For example, *N,N'*-methylene bisacrylamide (MBA) was used to prepare dextran-based crosslinked nanogels.[32] Another facile

way to introduce chemical linkages is through the modification of polymers with reactive groups such as carboxylic acid, amine, vinyl and thiol groups.[7]

For the synthesis of well-defined BNGs, a water-in-oil (W/O) heterogeneous system is a typical technique. It consists of small water droplets stabilized by an oil-soluble surfactant dispersed in organic phase.[27] Polymerization and crosslinking occur simultaneously in the system, yielding BNGs with narrow size distribution. In order to maintain colloidal stability, a large amount of surfactants has to be used and then removed from BNGs.

Compared to W/O heterogeneous systems, aqueous polymerization is a more convenient method that can be conducted under a mild condition with no use of surfactants. Because polymerization occurs in homogeneous medium, inter-particles crosslinking could lead to the occurrence of undesired aggregation.[33] In order to achieve uniform size distribution, several synthetic strategies have been proposed; the detailes will be discussed in Chapter 2.

1.4 Stimuli-responsive polymeric nanomaterials

Polymeric nanomaterials have been designed to release drugs through physical or chemical changes in response to stimuli (Figure 1.3).[34] These stimuli-responsive materials are also referred as “smart” materials. Internal stimuli are based on specific micro-environmental difference within tissues and cells, including redox potential, pH, temperature, and ionic strength. In contrast, external stimuli include heat, light, magnetic field, and ultrasound.[35] Once “smart” materials are subjected to the presence of stimuli, they undergo chemical degradation or physical change of volume. As a consequence, encapsulated drugs can be rapidly released from nanomaterials. Among numerous stimuli, pH, redox potential, and temperature have intrigued considerable attention because these micro-environmental differences exist between normal and pathological cells.[36] The constant gradient provides an effective driving force to trigger responsive drug release of nanomaterials.

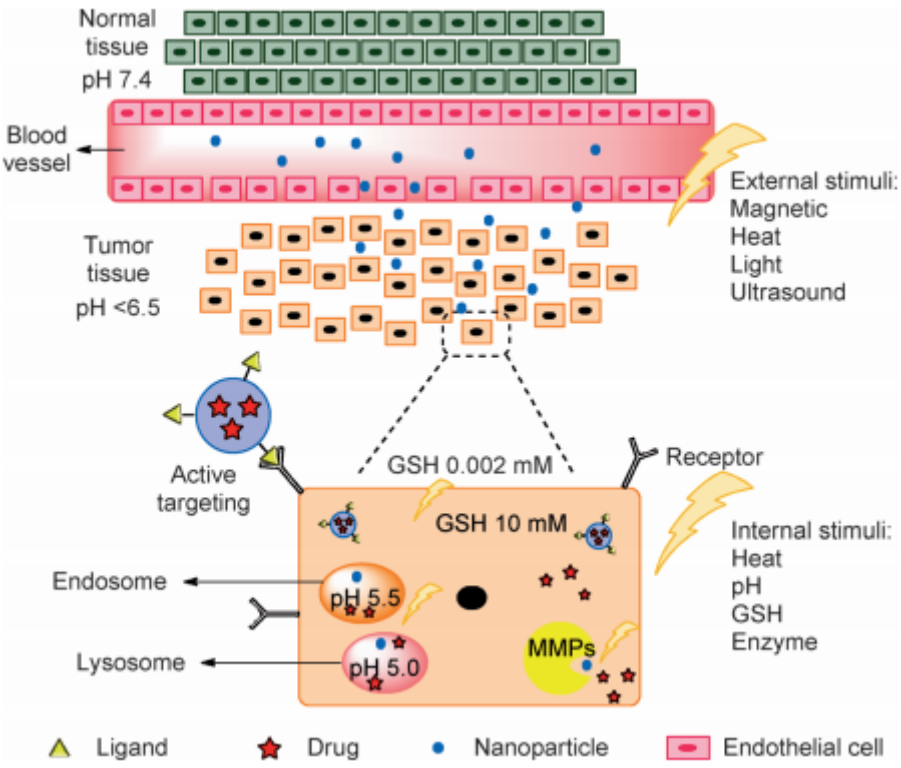

Figure 1.3. Typical example of stimuli-responsive drug delivery strategies.[35]

1.4.1 Reduction-responsive degradation

Reduction-responsive polymeric materials are promising biomaterials for controlled release. They are designed with reductively-cleavable linkages that can be broken in response to reduction reaction, resulting in the degradation of polymeric materials, thereby triggering rapid drug release. One of the typical redox-labile linkages is the disulfide bond (SS). It can be cleaved in the presence of glutathione (GSH), a cellular reducing agent, to the corresponding thiols.[37] In extracellular environment, GSH exists at < 2 μM, while it presents at ≈ 10 mM in intracellular environment. Compared to normal cells, GSH are found at elevated concentration in tumor tissues due to up-regulation metabolism of glutathione disulfide reductase.[35] Such significant difference of redox potential between intra- and extracellular compartments in tumor tissues enables the rapid cleavage of disulfide linkages, thus leading to enhanced/controlled drug release (Figure 1.4). Typical methods to introduce disulfide linkages into biomaterials include 1) copolymerization of a disulfide-labeled crosslinker[33] and 2) thiol-disulfide exchange reaction to create intra- or inter-chain disulfide crosslinks.[38]

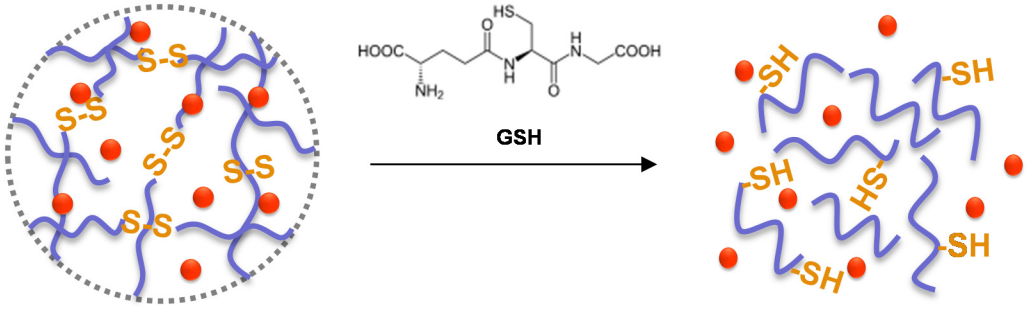

Figure 1.4. Reductive degradation of disulfide-containing bionanogels in response to cellular GSH.

1.4.2 Temperature-responsive volume change

Temperature gradient can be found between diseased and normal tissues.[39] Moreover, high temperature treatment (between 40 - 44 ºC), referred as hyperthermia, is commonly employed in cancer therapy to kill cancer cells while limit the effect to normal cells.[40] In response to a temperature change, thermoresponsive polymers undergo phase transition, causing volume change of nanocarriers, thereby triggering rapid drug release.[26] The thermoresponsive behavior can be characterized with lower critical solution temperature (LCST), which is the critical point where polymers undergo hydrophilic/hydrophobic transition (Figure 1.5). Below the LCST, polymers are hydrophilic and dissolved in water. Above LCST, polymers become hydrophobic due to the loss of H-bonding between polymers and water molecules.[41] Thus, polymers collapse to form aggregates in water. LCST is also referred as a cloud point, which describes macroscopic thermal behavior of polymers.[42] The cloud point can be usually determined as an onset point of light scattering (LS) intensity of polymers in aqueous solutions. At above LCST, LS intensity increases, which is attributed to the occurrence of large aggregates.

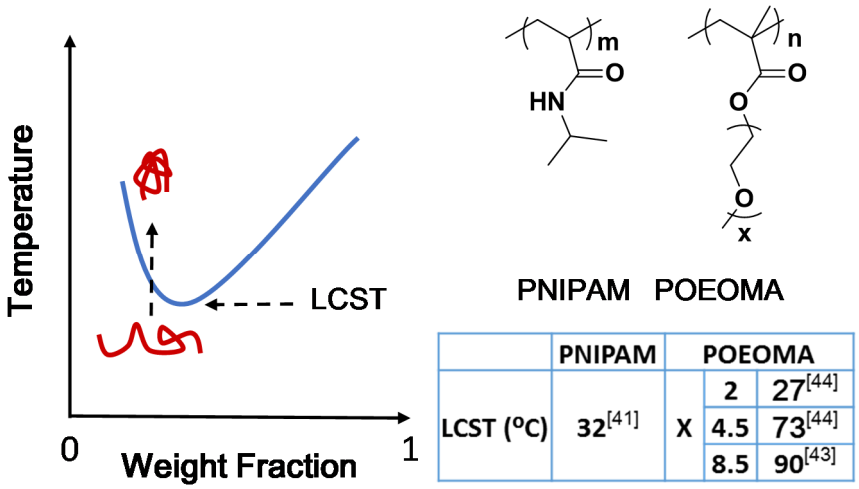

	PNIPAM	POEOMA		
LCST (°C)	32[41]	X	2	27[44]
			4.5	73[44]
			8.5	90[43]

Figure 1.5. Schematic drawing showing the phase transition associated with LCST.

A typical thermoresponsive polymer is poly(*N*-isopropylacrylamide) (PNIPAM), whose LCST is 32 ºC close to body temperature. The LCST of PNIPAM can be adjusted by copolymerization of NIPAM with hydrophilic or hydrophobic monomers.[43] However, the cytotoxicity of NIPAM monomer presenting in PNIPAM could lead to potential biocompatibility issues, which limits its biomedical applications. Alternatively, PEO containing methacrylates such as poly(oligo(ethylene glycol) monomethyl ether methacrylate) (POEOMA) are analogs of PEO, which has good biocompatibility and capability of preventing non-specific protein absorption.[44] The LCST of POEOMA ranges from 20 to 80 °C, depending on the length of pendent ethylene oxide (EO) repeating units. Their LCST can be tuned by varying the component fraction of different OEOMA monomers (Figure 1.5).[45, 46]

1.4.3 pH-responsiveness

The physiological pH of body fluid is kept at 7.4. While cancer cells and inflammatory tissues are presented in a slightly acidic environment (pH ≈ 6.5) due to enhanced metabolic rates. Acidic pH is also found in cell organelles such as endosomes (pH ≈ 5.5) and lysosomes (pH ≈ 5.0).[35] Such pH gradient can be used to trigger rapid drug release.

Three approaches allow for introducing pH-sensitivity into nanocarriers. Approach I is to incorporate acid-labile linkages such as acetal, orthoester, imine, or hydrazone linkages, into nanogels.[34] In acidic pH, these acid-labile linkages are cleaved causing nanogel degradation.

Approach II is to introduce pH-dependent functional groups such as carboxylic acid or amine groups into nanogels.[47, 48] In response to pH change, nanogels undergo volume change, which can promote the diffusion of encapsulated cargoes.[49] Approach III involves the change in interactions between pH-sensitive nanogels and cargoes containing pH-sensitive groups, which also promote the enhanced drug release.[50]

1.5 Scope of the thesis

The purpose of this thesis is to provide a detailed study of preparing different dual stimuli-responsive CMC-based BNGs as effective delivery nanocarriers for tumor-targeting enhanced drug release. A literature review focusing on recent strategies of synthesizing polysaccharide-based nanomaterials is presented in Chapter 2.

In Chapter 3, a dual pH/reduction-responsive bionanogel (ssBNG) containing pH-sensitive carboxymethyl cellulose (CMC) and disulfide linkages is reported. The proposed ssBNGs were synthesized by facile aqueous free radical polymerization in the presence of a disulfide-containing dimethacrylate as a crosslinker. The enhanced drug release was examined upon acidic pH and reducing agent (a cellular trigger, glutathione). In response to acidic pH, the electrostatic interaction between CMC and encapsulated cargoes are decreased. Under the treatment of GSH, the cleavage of disulfide crosslinkers causes the degradation of polymer networks. The two mechanisms lead to enhanced drug release. Furthermore, the potential application of ssBNGs as drug delivery vehicles was evaluated through *in vitro* studies.

In Chapter 4, another dual pH/temperature-responsive bionanogel (DuR-BNG) is presented. Temperature-responsive POEOMA were grafted from CMC in the presence of a permanent OEO-containing dimethacrylate crosslinker via aqueous polymerization. Micelle-like DuR-BNGs were synthesized through self-association assisted process. The resulting DuR-BNGs were evaluated for their prospective drug delivery applications. A significant enhanced drug release was achieved at temperatures above the LCST and in acidic pH. Furthermore, the DuR-BNGs had excellent colloidal stability and negligible non-specific interaction with proteins.

Finally, conclusion and future directions to develop effective polysaccharide-based nanomaterials are presented in Chapter 5.

Chapter 2

Review of recent strategies of developing polysaccharide-based nanocarriers for biomedical application

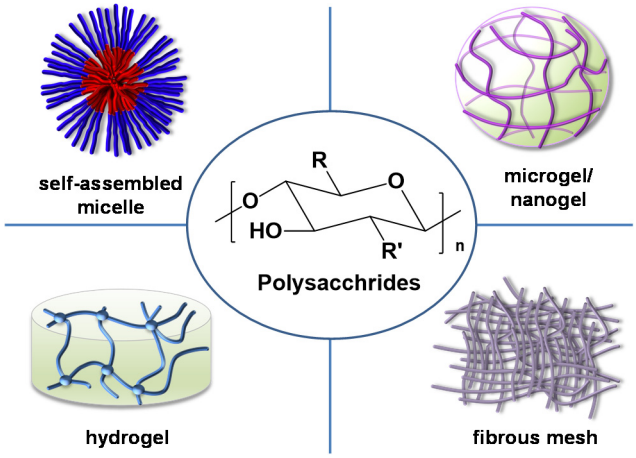

Polysaccharides are abundant in nature, renewable, nontoxic, and intrinsically biodegradable. They possess a high level of functional groups including hydroxyl, amino, and carboxylic acid groups. These functional groups can be utilized in further modification of the polysaccharides with small molecules, polymers, and crosslinkers; the modified polysaccharides have been used as effective building blocks in fabricating novel biomaterials for various biomedical applications as drug delivery carriers, cell-encapsulating biomaterials, and tissue engineering scaffolds. This review describes recent strategies to modify polysaccharides for the development of polysaccharide-based biomaterials; typically self-assembled micelles, crosslinked microgels/nanogels, three-dimensional hydrogels, and fibrous meshes. In addition, the outlook is briefly discussed on the important aspects for the current and future development of polysaccharide-based biomaterials, particularly tumor-targeting intracellular drug delivery nanocarriers.

This chapter contains information that was published in *Macromolecular Rapid Communications*, **2014**, *35*, 1819-1832 and part of the chapter is reproduced from the article with the permission from the publisher.

2.1 Introduction

Polysaccharides are naturally-occurring polymers or biopolymers. Typical examples of the polysaccharides include dextran (DeX), pullulan (PuL), cellulose (CeL), chitosan (CS), hyaluronic acid (HA), alginate (ALG), and many others (Figure 2.1a).[51-56] HA, as a main component of extracellular matrix, consists of *N*-acetyl-D-glucosamine and D-glucuronic acid. ALG composes of β-D-mannuronic acid and α-L-guluronic acid residues. CeL, as a main component of plant cells, has been considered as the most abundant polysaccharide in nature. It consists of homopolymeric β(1→4) linked of D-glucose. With a similar structure, CS is composing of β(1→4) linked 2-amino-deoxy-D-glucan, resulting from the deacetylation of *N*-acetyl-D-glucosamine of chitin (CT). It is almost the only cationic polysaccharide. PuL is a product of starch, formed of α(1→6) linked maltotriosyl units. DeX composes of α(1→6) glycosidic linkages between D-glucopyranose residues.[57]

Polysaccharides are abundant in nature, renewable, nontoxic, intrinsically biodegradable, and relatively cheap. Furthermore, they possess a high content of functional groups including hydroxyl, amino (i.e. CS), and carboxylic acid groups (i.e. HA and ALG). These functional groups can be utilized for further modification of the polysaccharides. These features have attracted significant efforts to develop polysaccharide-based biomaterials for various biomedical applications as drug delivery carriers, cell-encapsulating biomaterials, tissue engineering scaffolds, and regenerative medicine.[27, 58-60] However, polysaccharides also have several drawbacks; they have broad molecular weight distribution and suffer from batch to batch variability. In addition, most polysaccharides including typically CeL, ALG, and CS have limited solubility in common organic solvents.[61]

Toward those promising applications, various strategies utilizing well-defined organic synthesis and polymerization methods have been extensively explored; thus, the modified polysaccharides were used as effective building blocks to fabricate self-assembled micelles, crosslinked microgels/nanogels, three-dimensional hydrogels, and fibrous meshes. As examples, polysaccharides have been modified with small hydrophobic molecules or conjugated with hydrophobic polymers to render them to be amphiphilic for novel core/shell-type micellar aggregates. For the various forms of crosslinked materials (i.e. microgels, nanogels, and

hydrogels), polysaccharides have been crosslinked through chemical reactions or physical associations.

In this review, we summarize the recent development of polysaccharide-based biomaterials with a focus on novel approaches for the modification of polysaccharides to synthesize self-assembled micelles, crosslinked microgels, nanogels, hydrogels, and fibrous materials for bio-related applications. This review focuses on the polysaccharides in linear structures shown in Figure 2.1. Cyclodextrin (CD)-based supramolecular assemblies and hydrogels with the focus on recent advances are summarized in a recent review[62] and other reports.[63] In addition, polysaccharide-based hybrid materials containing inorganic metal nanoparticles[64-66] and carbon dots[67] are not covered in this review.

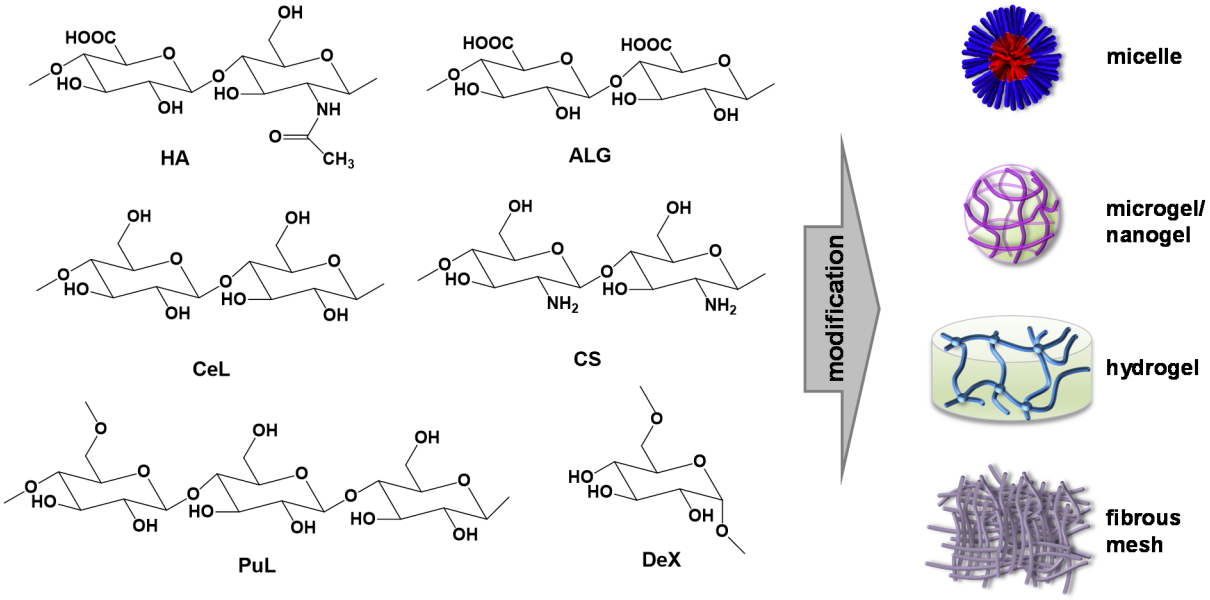

Figure 2.1. Chemical structures of typical polysaccharides and polysaccharide-based biomaterials, typically self-assembled micelles, crosslinked microgels/nanogels, three-dimensional hydrogels, and fibrous meshes, for various biomedical applications such as drug delivery, cell-encapsulation, tissue engineering, and regenerative medicine. Abbreviation of polysaccharides) DeX: dextran, PuL: pullulan, CeL: cellulose, CS: chitosan, ALG: alginate, HA: hyaluronic acid, HPCeL: hydroxypropyl cellulose, ECeL: ethyl cellulose, CMC: carboxymethyl cellulose, CT: chitin, and ChS: chondroitin sulfate.

2.2 Polysaccharide-based self-assembled aggregates

For the preparation of self-assembled micellar aggregates, the modification of polysaccharides (hydrophilic or water-soluble) with hydrophobic species is required, yielding amphiphilic polysaccharides. The hydrophobic species for the modification are small molecules, oligomers, or high molecular weight polymers which bear reactive functional groups. The resulting amphiphilic polysaccharides self-assemble to form micellar aggregates in aqueous solutions, consisting of hydrophobic cores surrounded with polysaccharide coronas. A variety of novel strategies have been explored to synthesize amphiphilic polysaccharide-based micellar aggregates.

2.2.1 Amphiphilic polysaccharides modified with small hydrophobic molecules

Various small hydrophobic molecules have been conjugated to polysaccharides to yield amphiphilic polysaccharides. An example includes the conjugation of HA with hydrophobic aminoethyl 5β-cholanomide having a terminal amino group, derived from 5β-cholanic acid, through a carbodiimide coupling reaction. The resulting amphiphilic HA self-assembled to form micellar aggregates surrounded with HA coronas with a diameter = 350 - 400 nm as potential drug delivery nanocarriers.[68] Other examples include the synthesis of HA conjugated with cholesteryl group,[69] DeX conjugated with terpene (an extract from resin produced by conifer trees),[70] DeX tethered with doxorubicin (Dox; a clinically-used anticancer drug),[71] and several others.[72, 73] The Dox-conjugated DeX as a biopolymer-based prodrug exhibits improved tumor penetration. These examples of amphiphilic polysaccharides involve the covalent conjugation of polysaccharides with hydrophobic molecules through strong covalent linkages.

In contrast, an introduction of stimuli-responsive cleavable linkages into the design of amphiphilic polysaccharides allow for the synthesis of amphiphilic nanocarriers that can be degraded in response to external triggers (degradable amphiphilic polysaccharides). Such stimuli-responsive cleavage of the labile linkages facilitates the controlled/enhanced release of encapsulated drugs. Examples include an acid-labile cholesteryl-modified PuL[74] and a reduction-responsive Dox-conjugated DeX.[75] Recently, amphiphilic PuL was synthesized by conjugation of pH-sensitive urocanic acid and hydrophobic cholesterol succinate to PuL (Figure 2.2). It self-assembled to form micellar aggregates with a diameter = 150 - 300 nm. Due to the

presence of pendant urocanic acids, the amphiphilic PuL micelles exhibited pH-responsiveness with swelling/deswelling transition at around pH 6.5. Such pH-responsiveness enabled to enhance intracellular release of encapsulated anticancer drugs, evidenced by cell viability, confocal laser scanning microscopy, and flow cytometry.[76]

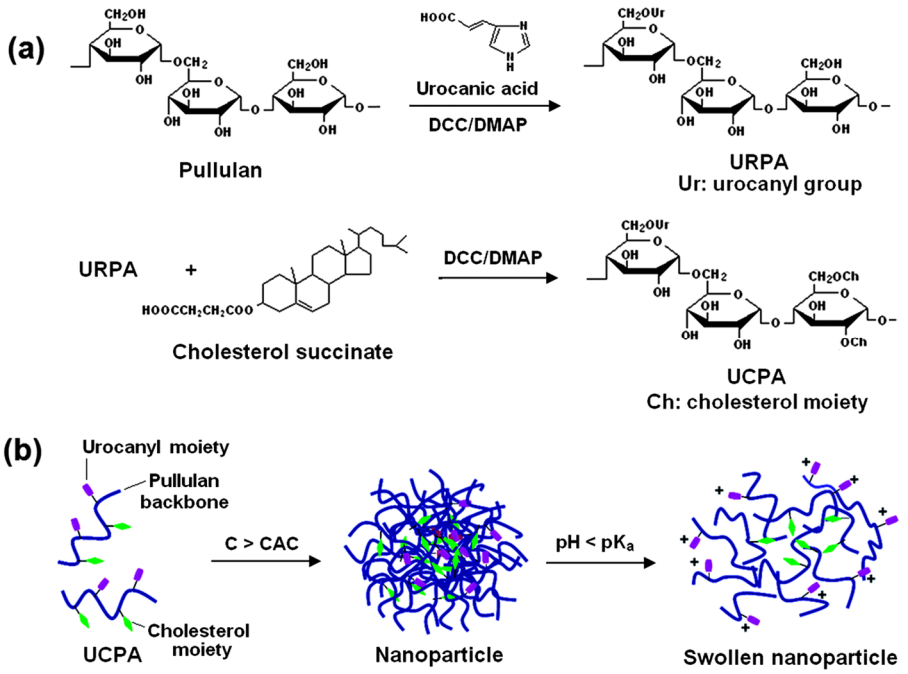

Figure 2.2. Synthesis, self-assembly, and pH-responsive release of amphiphilic PuL conjugated with urocanic acid and cholesterol succinate via a carbodiimide coupling reaction. Reproduced with permission.[76] Copyright 2014, Royal Society of Chemistry.

2.2.2 Amphiphilic polysaccharides conjugated with polymers

Numerous approaches have been explored to synthesize polymer-conjugated polysaccharides. One approach is the synthesis of diblock polysaccharides (i.e. polysaccharide-b-polymer) where one end of polysaccharides is directly attached to one end of synthetic polymers. This approach requires the modification of polysaccharides to have terminal reactive groups. For example, glycosaminoglycan was oxidized to have terminal aldehyde groups, which were involved in oxime click reaction to form glycosaminoglycan-b-poly(ethylene glycol) (PEG) block copolymers. These anionic copolymers enabled to form micelloplexes through ionic interactions with cationic poly(L-lysine) (PLL), a model protein; the resulting micelloplexes can be useful as

delivery vehicles for positively charged proteins.[77] However, most approaches involve the synthesis of polymer-grafted polysaccharides though "grafting from" and "grafting to" methods.

The "grafting from" method employs novel polymerization methods such as ring opening polymerization (ROP),[78, 79] controlled radical polymerization (CRP),[80] or oxidative polymerization.[81] Well-defined synthetic polymers with narrow molecular weight distribution ($M_w/M_n < 1.4$) can be grown from polysaccharide chains, yielding polymer-grafted polysaccharides (polymer-g-polysaccharides). ROP is utilized to synthesize biodegradable aliphatic polyesters such as polylactide (PLA), polycaprolactone (PCL), polyglycolide (PGA), and their copolymers grafted from polysaccharides. Pendant hydroxyl (OH) groups in polysaccharides are generally used as initiating species for the ROP of the cyclic monomers. Typical examples include CeL-g-PCL,[82] DeX-g-PCL,[83] CeL-g-(PCL-b-PLA),[84] HPCeL-g-PCL.[85] CRP is utilized to synthesize poly(meth)acrylates grafted from polysaccharides. Typical CRP methods that have been explored include atom transfer radical polymerization (ATRP)[86, 87] and reversible addition fragmentation chain transfer (RAFT)[88, 89] polymerization. The pendant OH groups in polysaccharides are modified to convert the corresponding initiating moieties such as bromines for ATRP and dithiocarbonyl groups for RAFT polymerization. The detailed synthesis of various polysaccharide-g-polymethacrylates using CRP methods is described in the previous review.[90]

The "grafting to" method utilizes well-known organic reactions such as click-type or condensation reactions of polysaccharides with pre-synthesized polymers. The click-type reactions are highly selective and orthogonal, thus resulting in quantitative conversion under mild conditions.[91-93] A typical click-type reaction is 1,3-cycloaddition of alkynes and azides in the presence of Cu(I) complexes.[94, 95] This reaction has been utilized after the modification of polysaccharides with pendant alkyne or azido groups. The modified polysaccharides then react with polymers in the presence of Cu(I) complexes, yielding brush-like, amphiphilic polysaccharides. Most reports describe the modification of polysaccharides including CD,[96] oligosaccharide,[97] ECeL,[45] and CS[98] with azido groups. The resulting azido-containing polysaccharides reacted with alkynyl-labeled PEG, PLA, PCL homopolymers, and their copolymers. As a typical example, Figure 2.3 illustrates an approach to synthesize amphiphilic ECeL grafted with thermoresponsive polymethacrylates. ECeL was first modified with 2-bromoisobutyryl bromide to form 2-bromoisobutyryl ECeL (ECeL-Br) *via* a simple

esterification, followed by its reaction with sodium azide (NaN_3), yielding ECeL-N_3. Meanwhile, well-defined alkynyl-poly(*N,N*-dimethylaminoethyl methacrylate) (alkynyl-PDMAEMA) and alkynyl-poly(di(ethylene oxide) monomethyl ether methacrylate (DEGMA or MEO_2MA) -co-oligo(ethylene oxide) monomethyl ether methacrylate (alkenyl-P(MEO_2MA-co-OEOMA)) were synthesized by ATRP in the presence of an alkenyl-labeled bromine ATRP initiator. These thermo-responsive (co)polymers were grafted to ECeL-N_3 via the click reaction. The resultant ECeL-grafted copolymers were double-hydrophilic, thermoresponsive; thus, they self-assembled at temperatures above LCST to form aqueous aggregates.

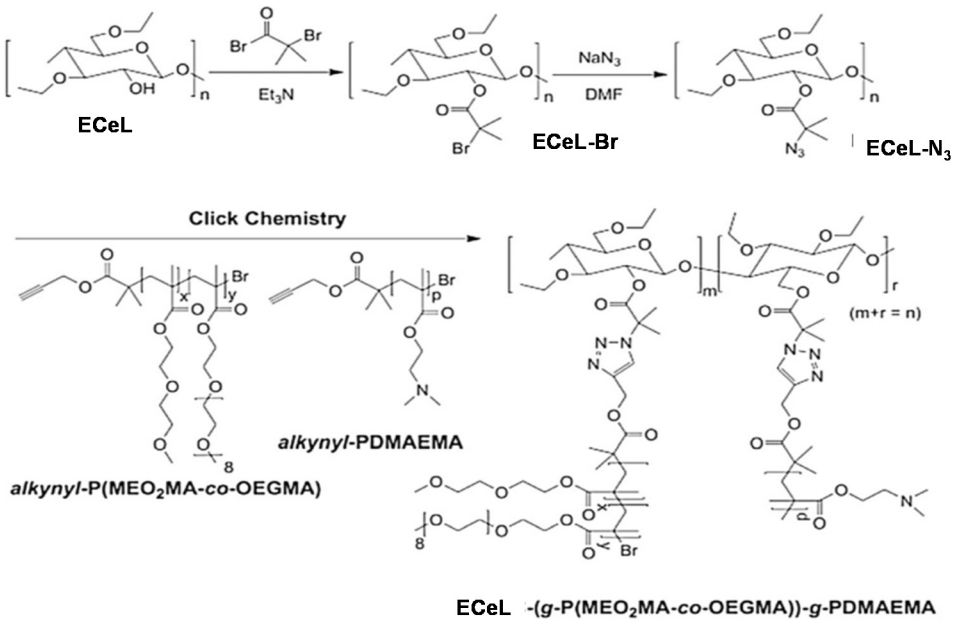

Figure 2.3. Synthesis of amphiphilic brush-like ECeL grafted with thermoresponsive (co)polymers. Reproduced with permission.[45] Copyright 2012, Elsevier.

Another click-type reaction is Michael addition reaction. Thiol-ene Michael addition[99-102] has been explored to synthesize a thermoresponsive HA-polymer conjugate, thus HA-g-P(DEGMA-co-OEOMA) (Figure 2.4).[23] A pendant maleimide-labeled HA was synthesized by reaction of HA with aminoethylmaleimide. A thiol (HS)-terminated P(DEGMA-co-OEOMA) was separately synthesized by RAFT polymerization, followed by aminolysis of terminal RAFT agent in the presence of a primary base. Two polymers reacted via a base-catalyzed Michael addition reaction. The resulting HA-g-P(DEGMA-co-OEOMA) exhibited tunable thermoresponsive properties with varying amounts of thermoresponsive P(DEGMA-co-

OEOMA) block. Furthermore, they self-assembled to form aggregates as a consequence of the hydrophobic transition of P(DEGMA-co-OEOMA) block at above LCST.

Facile coupling reactions have also been reported to synthesize amphiphilic polysaccharides. Typical examples include HA-g-PLGA in the presence of dicyclohexyl carbodiimide,[103] CD grafted with PEO-b-PCL in the presence of *N,N*-carbonyl diimidazole (CDI),[104] β-CD grafted with PCL-b-PEO-b-PCL triblock copolymer,[105] and HA grafted with a thermoresponsive polymer.[106] Recently, PCL was grafted to HA through a carbodiimide coupling reaction to form PCL-HA, which self-assembled to form anionic micelles in physiological conditions. The anionic HA coronas were ionically interacted with cationic CS to form CS/PCL-HA polyelectrolyte complex aggregates for oral delivery.[107]

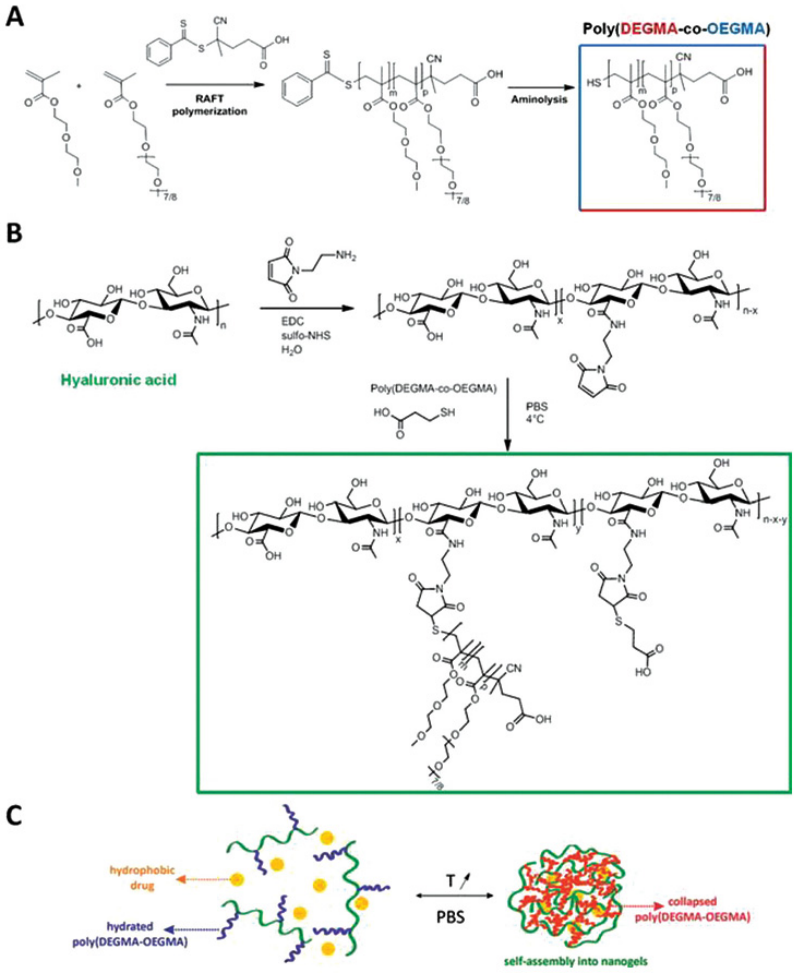

Figure 2.4. Synthesis of a thermoresponsive HA-polymer conjugate of HA-g-P(DEGMA-co-OEOMA) via thiol-ene Michael addition reaction and their self-assembly driven by change in temperature. Reproduced with permission.[23] Copyright 2012, Royal Society of Chemistry.

2.3 Polysaccharide-based crosslinked microgels/nanogels

For targeted drug delivery applications *in vivo*, a challenge of physically aggregated micelles is to retain their colloidal stability upon dilution. After *in vivo* injection, drug loaded micelles are significantly diluted by several orders of magnitude in the blood. As a consequence, the micelles are subjected to local environment far below the critical micellar concentration. The dilution could result in dissociation of micelles, leading to the premature of encapsulated cargoes. Several strategies have been explored, including the design of block copolymers with lower critical micellar concentration[108] and brush-like graft copolymers.[109] A promising strategy is to introduce effective crosslinking chemistry into the synthesis of crosslinked nanogels/microgels based on polysaccharides. The microgels are a class of three-dimensionally crosslinked hydrogels confined in micrometer-sized particles; when the microgels are nanometer-sized, they are known to be nanogels.[57]

2.3.1. Chemical crosslinking by condensation

This method centers on the synthesis of reactive polysaccharides grafted (or conjugated) with small molecules or polymeric chains bearing reactive functional groups. These reactive groups are then involved in the crosslinking reactions to form polysaccharide-based microgels/nanogels in aqueous solutions. HPCeL was modified with poly(acrylic acid) (PAA) by multiple steps; 1) ROP of CL, 2) esterification of the resulting PCL-grafted HPCeL to the corresponding bromide, and 3) chain extension with poly(*t*-butyl methacrylate) (PtBMA) by ATRP, yielding HPCeL grafted with PCL-b-PtBMA block copolymer. The following hydrolytic cleavage of *t*-butoxy groups to the COOH groups yielded reactive HPCeL grafted with PCL-b-PAA block copolymers. The pendent COOH groups reacted with amino groups of external crosslinkers, allowing for the synthesis of nanogels crosslinked with amide linkages in water.[110] PuL was also modified with vitamin B6 (pyridoxal) by an alkyne-azido click-type reaction to yield pyridoxal phosphate-bearing PuL having aldehydes. The reactive PuL was crosslinked with a protein (lysozyme) containing several amino groups through a Schiff-base reaction with reactive aldehydes in aqueous solution.[111] However, these nanogels could have broad size distribution due to the occurrence of crosslinking in aqueous solution (not in compartmentalized locations). For the preparation of well-defined nanogels with narrow size distribution, the control of concentrations

could be important to minimize of undesired inter-chain crosslinking reactions, which leads to the occurrence of large aggregation.

A promising approach to narrow size distribution utilizes self-assembly driven by either amphiphilicity or temperature-change, followed by chemical crosslinking reactions. For the approach, polysaccharides are first modified to be amphiphilic or thermoresponsive; the resulting amphiphilic polysaccharides bearing reactive functional groups self-assemble in aqueous solution to form reactive micellar aggregates. For example, PuL was conjugated with hydrophobic cholesterols and reactive groups. The resulting reactive amphiphilic PuL self-assembled to form nano-assemblies with a diameter = 18 nm in aqueous solution. The reactive acrylate groups were then involved in interparticle crosslinking with a thiol-terminated 4-arm star PEG crosslinker through thiol-ene Michael addition reaction, yielding raspberry-like nanogels with diameter ranging from 40 to 120 nm by varying the initial ratio of $[SH]_0/[acrylate]_0$ groups. The resulting nanogels exhibit the prolonged release profile of encapsulated proteins.[112] HA was also modified with pendant hydrophobic pyrene moieties and reactive hydrazine (-C(O)-NH-NH_2) groups. The reactive HA self-assembled to form aqueous micellar aggregates, and further stabilized by chemical crosslinking (through the formation of hydrazones) of HA chains to form HA-based nanogels.[113]

2.3.2. *In situ* disulfide-crosslinking method

Covalent crosslinking strategy provides enhanced colloidal stability against dilution. However, the use of permanent crosslinkers hampers enhanced/controlled release of encapsulated drugs. An introduction of stimuli-responsive degradation strategy of dynamic covalent bonds (cleavable linkages) in response to external stimuli enables the enhanced drug release.[114-116] In contrast to the addition of external crosslinkers bearing cleavable linkages, *in situ* disulfide-crosslinking method is more promising in that the method results in the formation of reduction-responsive disulfide dynamic covalent bonds as crosslinks through two ways: disulfide-thiol exchange reaction and oxidation. The resulting disulfide-crosslinked nanogels exhibit enhanced colloidal stability as well as promoted drug release in response to reduction reactions.

For the disulfide-thiol exchange reaction, polysaccharides were modified with pendant disulfide linkages. For example, lipoic acid (LA) was conjugated to starch[24] and DeX[117] to

form LA-starch and LA-DeX, which self-assembled to form micellar aggregates. The partial cleavage of disulfides in response to a catalytic amount of D,L-dithiothreitol (DTT), a reducing agent, resulted in the formation of disulfide-crosslinked nanogels. These nanogels having enhanced colloidal stability as well as reduction-responsive promoted drug release have a potential for tumor-targeted chemotherapy.

For oxidation of pendant thiol groups of copolymers, different strategies have been explored to introduce pendant thiol groups into polysaccharides. A RAFT polymerization and following aminolysis has been examined. The RAFT polymerization allowed for the chain extension of PuL[19] and DeX[38] with PNIPAM, yielding PNIPAM-grafted polysaccharides. The following aminolysis of terminal RAFT agents in the presence of a primary amine resulted in the synthesis of pendant HS-terminated PNIPAM-grafted polysaccharides. At a temperature above the LCST, they self-assembled upon temperature change to form pendant thiol-functionalized micelles, and further to temperature responsive disulfide-crosslinked nanogels upon oxidation. A facile coupling reaction was also examined for the reaction of cysteamine with HPCeL activated with 4-nitrophenyl chloroformate (4-NC) (Figure 2.5). The resulting thiolated HPCeL (HPCeL-SH) was collapsed to form nanospheres upon the LCST transition. The pendant SH groups in the nanostructures were then oxidized by DMSO, yielding disulfide-crosslinked nanogels with diameter = 72 - 88 nm.[118] These disulfide-crosslinked nanogels exhibited reduction-responsive degradation in the presence of excess reducing agents.

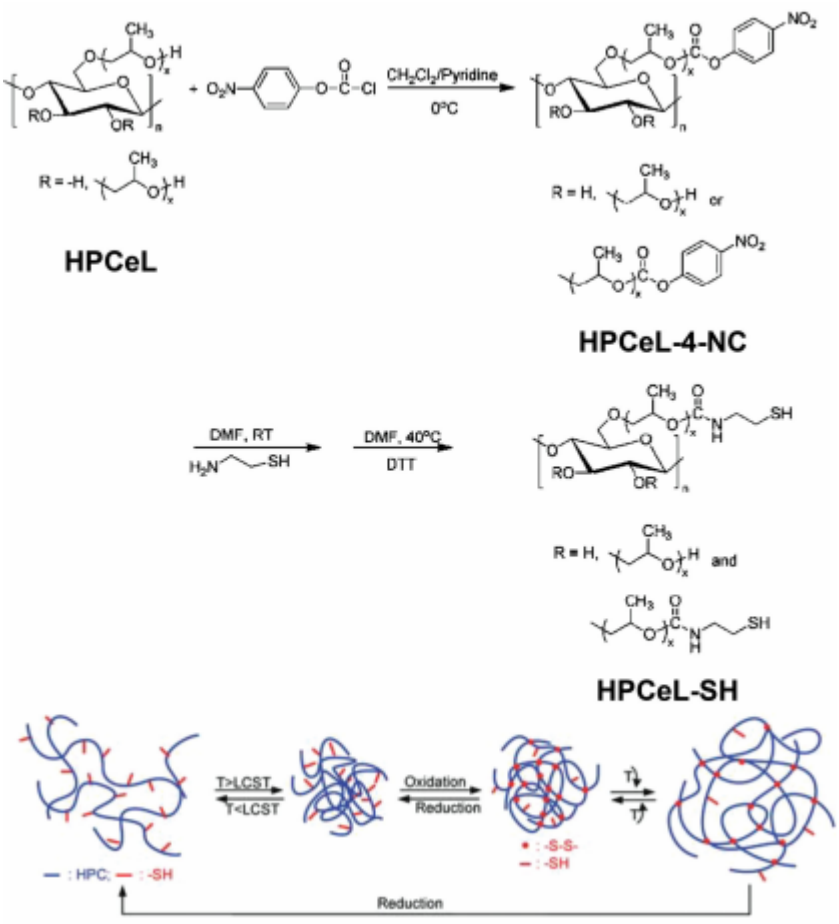

Figure 2.5. Synthesis, self-assembly at temperature above LCST, and oxidation of thiolated HPCeL to form disulfide-crosslinked nanogels. Adapted with permission.[118] Copyright 2011, Royal Society of Chemistry.

2.3.3. Aqueous free radical crosslinking polymerization (FRCP)

Aqueous FRCP has been explored to synthesize polysaccharide-based nanogels crosslinked with vinyl polymers (including polymethacrylates). An approach includes the functionalization of polysaccharides with methacrylate moieties. The resulting methacrylated polysaccharides are used as multifunctional crosslinkers for FRCP.[119] Oil-in-water inverse miniemulsion polymerization has been widely explored to synthesize crosslinked nanogels with narrow size distribution due to the occurrence of polymerization in compartmented locations (i.e. inverse miniemulsion).[120] Recently, this approach has been advanced to synthesize enzymatically degradable nanogels by inverse miniemulsion polymerization of acrylamide (AAm) with a

methacrylated-modified DeX crosslinker.[121] Furthermore, the interesting technique has been explored for the synthesis of dual enzymatic and light-degradable nanogels (Figure 2.6).[122]

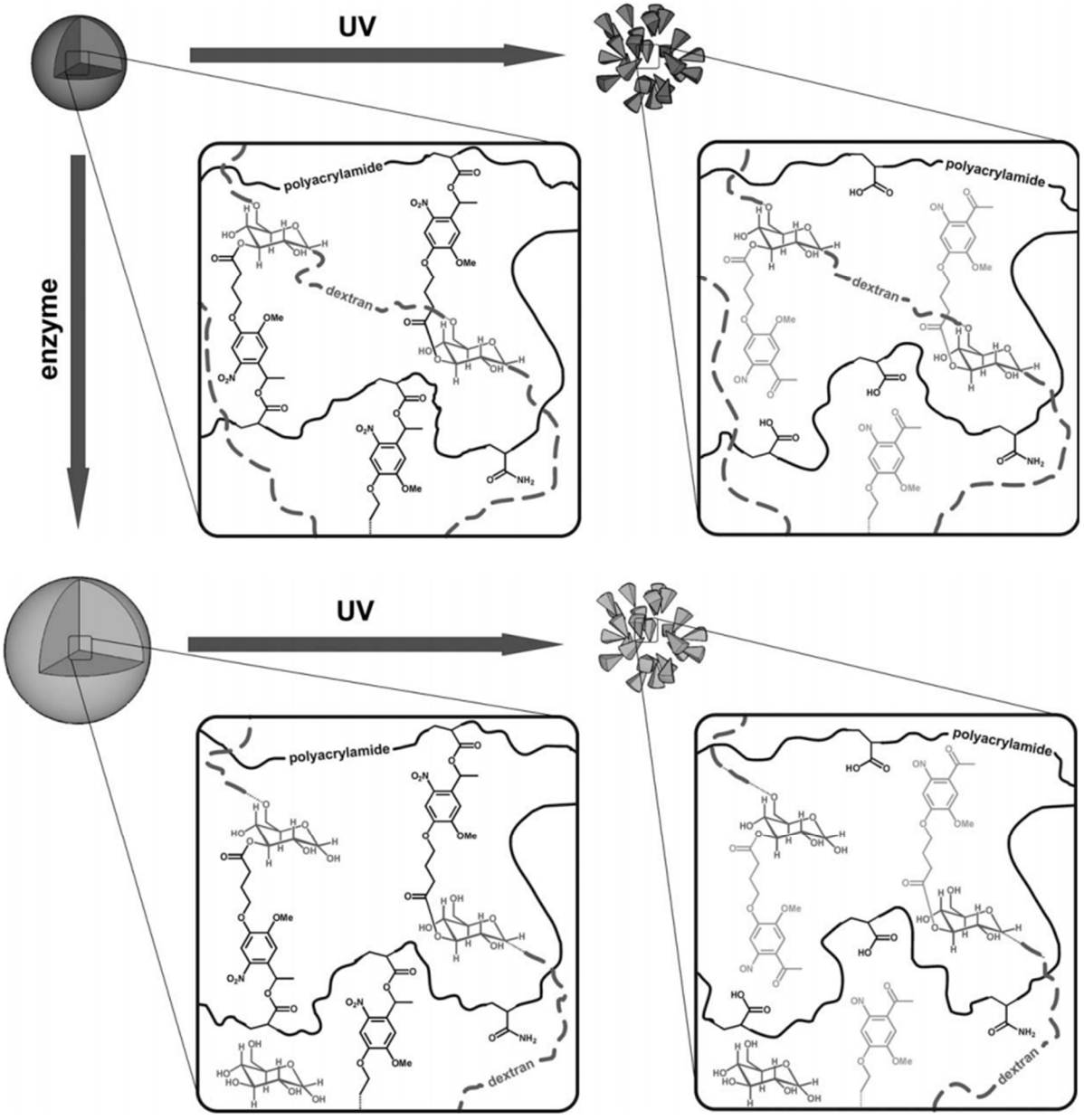

Figure 2.6. Schematic representation of dual enzymatic and light-degradable nanogels crosslinked with photo-labile linkage of DeX-g-PAAm. Reproduced with permission.[122]

Another approach utilizes aqueous FRCP of vinyl monomers in the presence of polysaccharides, resulting in the formation of vinyl polymer-grafted polysaccharides. By varying the vinyl monomers, the properties of the grafted polysaccharide can be tuned. Typical examples

of grafted vinyl polymers include PAA for pH response[123] as well as PNIPAM and PAAm for temperature response.[124, 125] In the presence of difunctional crosslinkers, this approach allows for the synthesis of crosslinked nanogels such as PNIPAM-grafted CS nanogels.[126-128] Oridon known to be an anticancer agent against liver cancers was loaded into pH-responsive nanogels decorated with galactose ligands. These nanogels show the potential for hepatoma-targeted delivery.[126] Recently, glucose-responsive nanogels based on poly(acrylamidophenylboronic acid) (PAAPBA) were synthesized by a self-assembly assisted strategy. This method utilizes thermoresponsive properties of PAAPBA; during polymerization at temperatures above LCST, PAAPBA-grafted DeX in the presence of difunctional crosslinker self-assembled to form well-defined nanogels. Since boronic acid moieties incorporated in the nanogels recognize glucose, the nanogels can be useful as potential glucose sensor.[32] More recently, new dual stimuli reduction and acidic pH-responsive nanogels were developed by a facile aqueous FRCP of OEOMA in the presence of CMC and a disulfide-labeled dimethacrylate crosslinker (ssDMA). As show in Figure 2.7, the nanogels are crosslinked with reductive-responsive disulfide linkages of POEOMA-grafted CMC, exhibiting enhanced release of encapsulated anticancer drugs to dual responses: reductive cleavage of disulfide crosslinkers and acidic pH responsive of COOH groups in CMC. The intracellular release of anticancer drugs after internalization into HeLa cancer cells, combined with the ability to facile bioconjugation suggest as a promising intracellular nanocarrier platform exhibiting multi-controlled drug release.[33]

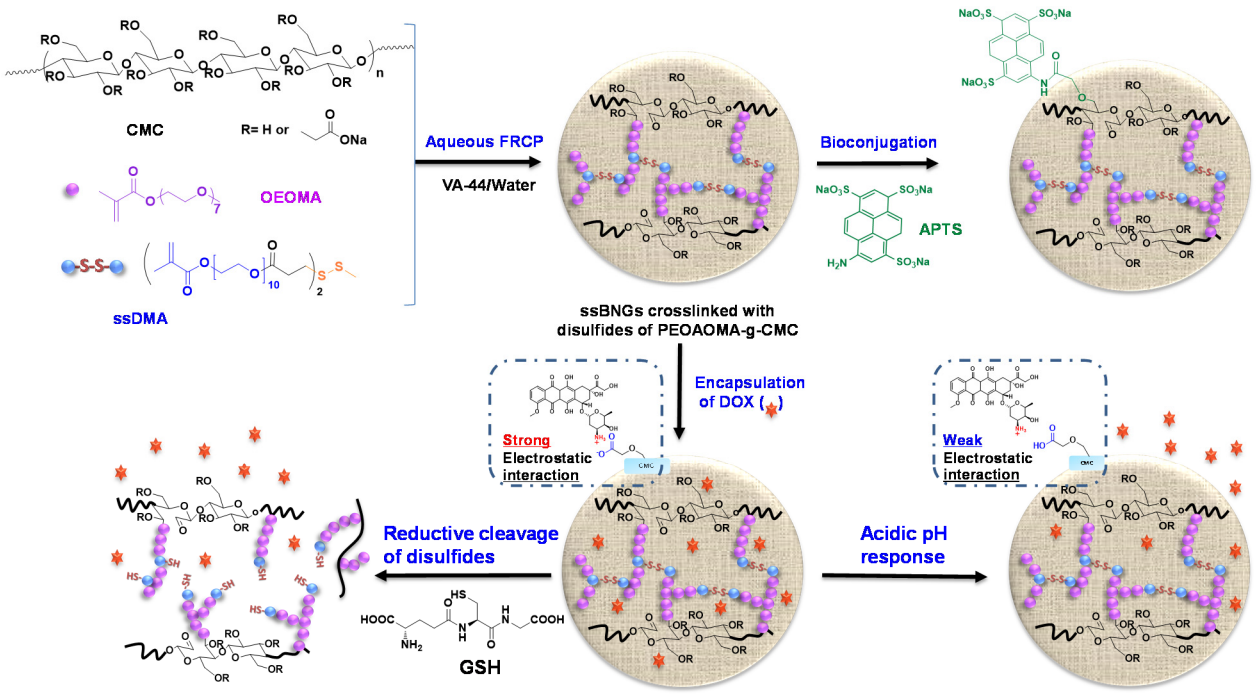

Figure 2.7. Synthesis and dual reduction and acidic pH-responsive Dox release of nanogels crosslinked with disulfide linkages of POEOMA-grafted CMC.[33] Copyright 2014, Royal Society of Chemistry.

2.3.4. Physical crosslinking method

In contrast to chemical crosslinking that allows for the formation of covalently-crosslinked nanogels, physical crosslinking yields supramolecular nanogels by utilizing non-covalent interactions between polysaccharides and external crosslinkers. Of these interactions including stereocomplexation of PLA-based DeX[129] and host-guest molecular recognition of DeX,[130, 131] the ionic interaction has been widely explored to synthesize polysaccharide-based nanogels. Without further modification, CS possessing pendant amino groups interacted with anionic crosslinkers such as tripolyphosphate (TPP)/ALG (containing pendant COOH groups) for ionic gelation. The resulting CS/TPP/ALG nanogels were evaluated for insulin release[132] or cell response;[133] however, they had relatively large diameters (d > 250 nm) due to the formation of more expanded structures. Such a large size could have a short blood circulation due to uptake by RES. A smaller sized CS-based nanogels were synthesized by ionic complexation of CS with PEO-b-poly(sodium 2-(acrylamindo)-2-methylpropanesulfonate), followed by an addition of genipin. Genipin is an irridoid glucoside extracted from Gardenia, and reacts with primary amine

groups. The resulting nanogels had a diameter ≈ 50 nm in the swollen state by dynamic light scattering (DLS) and ≈ 20 nm in dry state by transmission electron microscopy (TEM).[134]

In addition, further modification of polysaccharides is required for ionic gelation. DeX was modified with PEG and cystamine to yield PEO-DeX-ss-NH_2. The protonated amino groups interacted with negatively-charged indocyanine green (ICG), a tricarbocyamine dye, to form ICG/DeX nanogels. Since ICG is a FDA-approved near infrared (NIR) fluorescent dye to be used in clinics, the resulting nanogels are useful for NIR imaging and photothermal therapy.[135] In another report, wood CeL was modified with carboxymethyl groups, yielding negatively charged CMC. Wood CeL was also quarternized with ammonium salts, yielding positively charged CeL (QCeL). Mixing of the CeL-based polysaccharides in aqueous solutions resulted in the formation of ionically crosslinked CeL-based nanogels for protein delivery. Their sizes could be modulated by adjusting either CMC and QCeL in the feed, ranging from 150 to 800 nm in diameter.[136]

2.4. Polysaccharide-based hydrogels

2.4.1. Physical crosslinking method

Similar to crosslinked nanogels, several approaches to synthesize physically crosslinked supramolecular hydrogels have been explored. Typical approaches include ionic interactions, host-guest inclusion complexation, and thermoresponsive sol-gel transition.

Ionic interaction includes the interaction of ionic polysaccharides with a broad selection of ionic crosslinkers.[137] Examples include ALG bearing COOH groups with Ca^{2+} and Fe^{3+} ionic species[138-141] and HA bearing COOH groups with gelatin,[142] yielding hydrogels. In contrast to homogenous hydrogels, a dual-structure hydrogel was also reported. The amino groups of CS were modified, and the formed amphiphilic CS self-assembled to form CS-based nanostructures dispersed in aqueous ALG solution. By adding Ca^{2+} crosslinkers through ionic interactions, the resulting mixtures turned to hydrogels composed of CS-based nanostructures embedded in ALG-hydrogels. The dual-structure gels enabled to encapsulate hydrophobic drug in self-assembled nanostructured cores. Additionally, the hydrogels exhibit self-healing property in the presence of

glycerol.[143] Other examples include HA with cationic PLL[144] and CS with anionic azopolymers,[145] yielding multilayer films.

Host-guest inclusion complexation utilizes CD with a hydrophobic cavity, which is capable of inclusion with guest molecules, typically PEG derivatives. Examples include pyrene-terminated PEG star polymers,[146] cholesterol-derived linear PEG,[147] PEG-PPG-PEG triblock copolymer,[148] and PEG-grafted disulfide-containing poly(amino amine).[149] These CD/polymer inclusion complexes could be useful as injectable smart biomaterials for controlled-drug delivery applications.

Temperature-induced sol-gel transition involves the design of thermoresponsive polymers that undergo a volume change due to hydrophobic/hydrophilic transition in respond to temperature change. This property enables sol-gel transition of the polymers at higher concentrations, resulting in the formation of *in situ* formed hydrogels. This approach involves the modification of polysaccharides with thermoresponsive polymers. For example, CS was modified with PEG-based block copolymers of polyalanine, yielding CS-g-(PA-b-PEG),[150] and poly(L-alanine-co-L-phenyl alanine), yielding CS-g-(PAF-b-PEG).[151] HA was also grafted with PNIPAM by RAFT polymerization, yielding HA-g-PNIPAM.[152] Recently, HA was conjugated with dopamine (Figure 2.8); the resulting HA-dopamine reacted with HS-terminated Pluronic F127 block copolymer to prepare lightly crosslinked HA/Pluronic gel structure based on a click-type catechol-thiol addition. The resulting hydrogels exhibit thermoresponsive sol-gel transition at temperature above 37 ºC.[153]

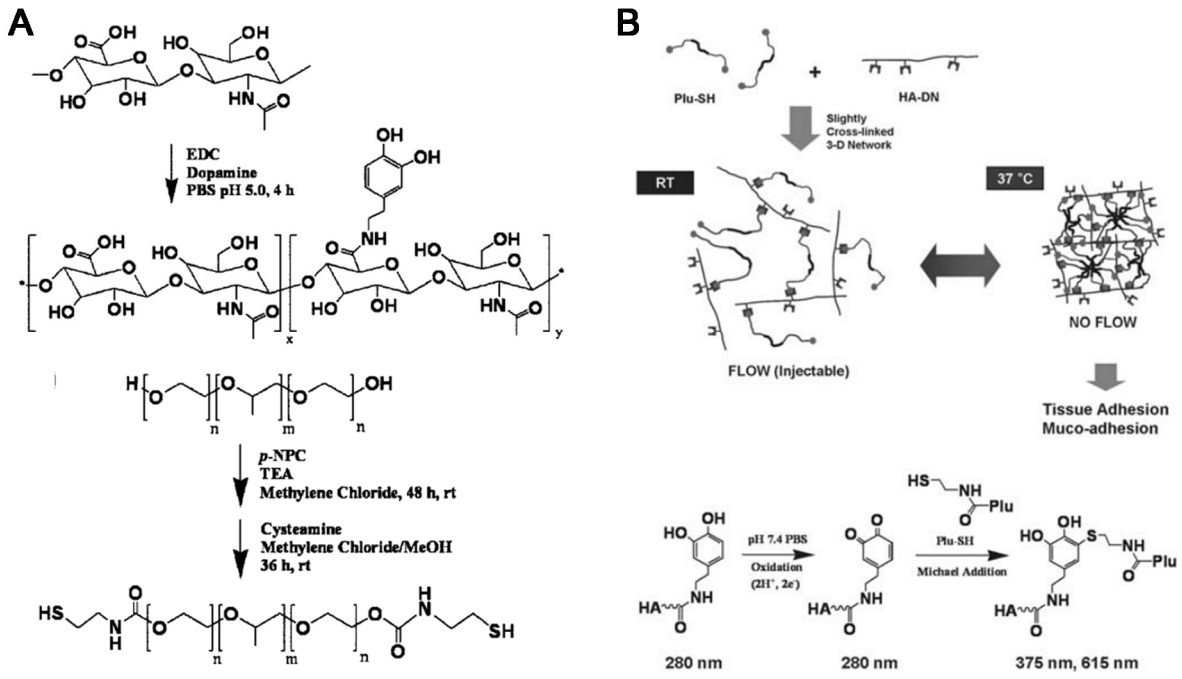

Figure 2.8. Synthesis (A) and sol-gel transition (B) of HA-dopamine and SH-terminated Pluronic F127. Reproduced with permission.[153] Copyright 2010, Royal Society of Chemistry.

2.4.2. Chemical crosslinking method

Compared to physical crosslinking exhibiting poor ability to tune mechanical properties, chemical crosslinking possesses several advantages, including facile control of moduli, swelling ratio, and porosity of hydrogels by varying crosslinkers and crosslinking densities.

FRCP has been explored as a robust method to fabricate polysaccharide-based hydrogels. Similar to the preparation of microgels/nanogels of polysaccharides, this approach involves the modification of polysaccharides with vinyl or (meth)acrylate moieties to polymerizable polysaccharides. Typical examples include methacrylated ChS,[154] methacrylated HA,[155] and methacrylated CT,[156] as well as xanthan gum functionalized with maleic anhydride[157] and acetylated galactoglucomannan functionalized with alkenes.[158] Different from the microgels/nanogels, however, these polymerizable polysaccharides are polymerized in aqueous solutions, mostly photopolymerized upon UV irradiation, to form highly crosslinked hydrogels for tissue engineering.

Facile coupling reactions or condensation reactions have also been explored to fabricate polysaccharide-based hydrogels in mild conditions. For the click-type thiol-ene reaction, polysaccharides are modified with either SH or vinyl groups. As illustrated in Figure 2.9, HA was modified with cysteamine to form SH-modified HA. In addition, hyperbranched thermoresponsive copolymers labeled with acrylate groups were synthesized by ATRP of thermoresponsive OEOMA in the presence of a difunctional methacrylate (DMA). These copolymers reacted with SH-HA through Michael addition reaction, yielding thiol-ene crosslinked hydrogels in aqueous solutions.[159, 160] Other examples include thiol-ene crosslinking reactions of maleimide modified DeX with thiol-modified β-CD[20] and methacrylate-modified HA with DTT.[161] In addition to thiol-ene reaction, copper-free alkyne-azido reaction,[162] Schiff base reaction,[163-165] and Diels-Alder reaction[166] have been explored.

Oxidative crosslinking of dopamine-conjugated polysaccharides provides an alternative route to synthesis of crosslinked hydrogels. An example includes the preparation of calcium-free ALG hydrogels in the presence of $NaIO_4$, an oxidizing agent for catechol-conjugated ALG.[167] Another example is rutin-releasing CS-based hydrogels composed of rutin-conjugated CS-PEG-tyramine crosslinked by enzymatically-catalyzed oxidation of phenol groups.[168]

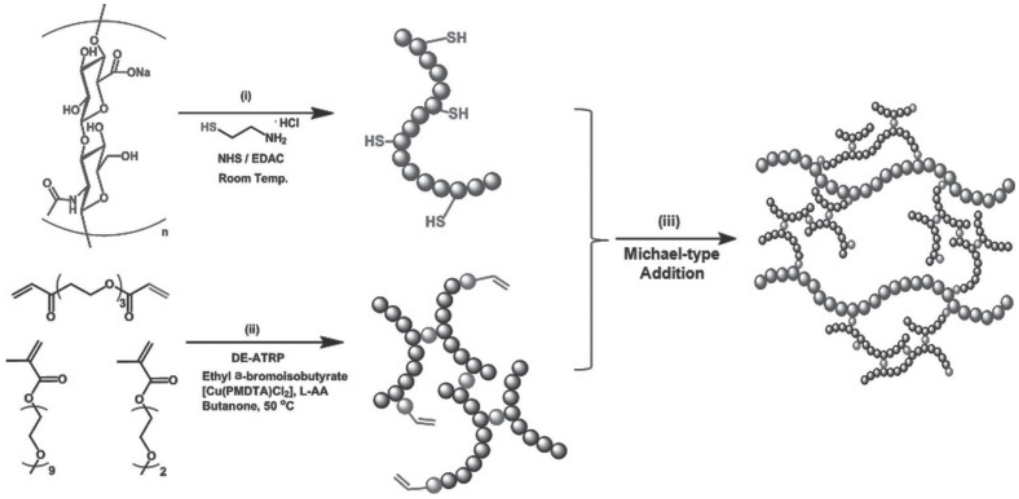

Figure 2.9. Synthetic scheme for Michael addition reaction of SH-modified HA with hyperbranched thermoresponsive copolymers labeled with acrylate groups to yield thiol-ene crosslinked hydrogels in aqueous solution. Reproduced with permission.[159]

2.5. Polysaccharide-based fibrous materials

Electrospinning is a powerful method to fabricate polymer substrates into fibrous materials with nanoscale diameters. These fibers possess high specific surface areas, controlled compositions, and high porosities; thus they have found their application in various biomedical fields.[169, 170] Due to the unique features, electrospun polysaccharide-based fibers enable the encapsulation of diverse therapeutic cargo; thus the resulting drug-loaded nanofibers have been considered as effective drug delivery carriers. Examples include cellulose acetate phthalate fibers for semen induced anti-HIV (human immunodeficiency virus) vaginal drug delivery[171] as well as a sodium ALG/PEG blend fibers containing ibuprofen for pulsatile drug release[172] and ammonium ALG fibers carrying antibiotics and enzymes.[173] Furthermore, the surfaces of electrospun polysaccharide nanofibers have been immobilized with proteins[174] or functionalized with lysostaphin[175] for wound healing applications. A challenge to electro-spinning of most polysaccharides is associated with their poor solubility in organic solvents. The use of room temperature ionic liquids offers a solution to overcome these difficulties.[176, 177]

2.6. Summary and Outlook

The recent advances in the development of polysaccharide-based biomaterials for bio-related applications are summarized. Polysaccharides possess a high content of hydroxyl, amino, and carboxylic acid groups. These functional groups have been used for modification of polysaccharides; the resulting modified polysaccharides are extensively explored as effective building blocks to fabricate self-assembled micelles, crosslinked microgels, nanogels, hydrogels, and fibrous materials. Self-assembled micelles were prepared by both “grafting to” and “grafting from” methods. To form well-defined micellar aggregates, the hydrophobic/hydrophilic balance of modified polysaccharides is a key criteria. It can be achieved by tuning the substitution degree of hydrophobic moieties. For grafting to method, click-type reactions such as 1,3-cycloadditon of alkynes and azides and thiol-ene addition have been utilized to modify polysaccharides with small hydrophobic molecules and polymers. For grafting from method, well-known polymer synthesis methods such as ROP and CRP have been utilized. Crosslinked nanomaterials (microgels, nanogels, and hydrogels) were fabricated by both chemical and physical crosslinking reactions. Chemical crosslinking methods include further click-type, facile coupling reactions,

and in situ disulfide crosslinking methods as well as FRCP, while physical crosslinking methods include ionic interactions, host-guest inclusion complexation, and thermoresponsive sol-gel transition.

Future development of polysaccharide-based biomaterials, particularly for tumor-targeting intracellular drug delivery, requires a high degree of control over properties. One property is the controlled/enhanced release of encapsulated therapeutics. Although polysaccharides are biodegraded by enzymatic reactions, the enzymatic degradation is intrinsically slow; such slow degradation causes slow release of encapsulated therapeutics from polysaccharide-based nanocarriers and scaffolds in cellular environments. A promising solution to circumvent the challenge is the multiple stimuli-responsive degradation platform. Multi-stimuli responses to each stimulus can independently and precisely regulate encapsulated drug release. Another property is the narrow size distribution. Although the inverse (mini)emulsion technique has been explored to synthesize polysaccharide-based nanogels with relatively narrow size distribution, harsh conditions are required for the complete removal of residual oil-soluble surfactants remaining in the products. Temperature-driven self-assembly/crosslinking is a promising method that should be further explored to nanogels with narrow size distribution. Combined with these properties, the applicability of these biomaterials in response to cellular components toward tumor-targeting delivery applications *in vivo* is an exploratory research area.

Chapter 3

Development of pH/reduction-responsive CMC-based bionanogels

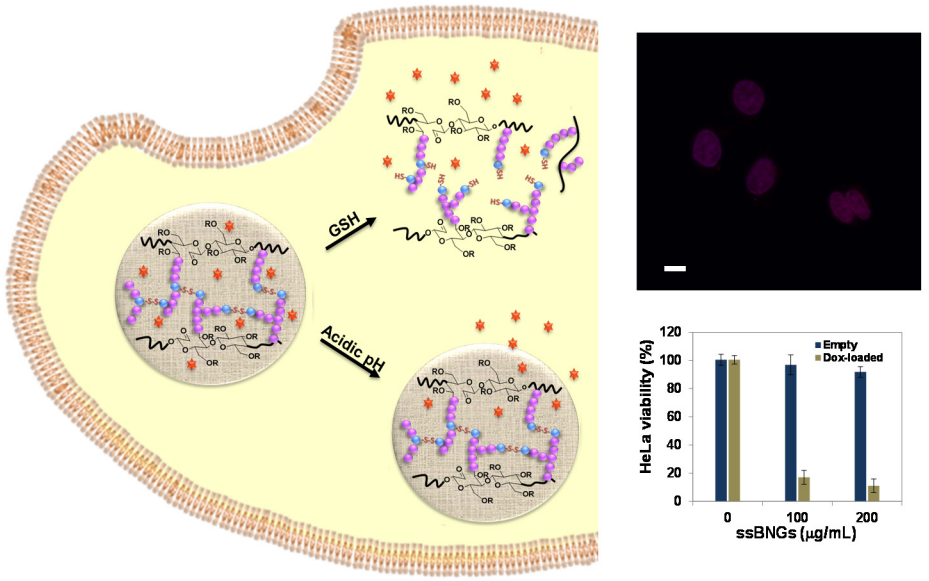

Biopolymer-based nanogels (bionanogels) are a promising platform as polymer-based drug delivery systems encapsulating hydrophilic anticancer therapeutics; however, enhanced/controlled drug release is highly desired. Herein, we report new dual stimuli-responsive bionanogels (ssBNGs) as potential intracellular delivery nanocarriers with multi-controlled and enhanced drug release. A facile aqueous crosslinking polymerization of oligo(ethylene oxide)-containing methacrylate (OEOMA) in the presence of carboxymethyl cellulose (CMC) and a disulfide-labeled dimethacrylate allows for the synthesis of ssBNGs crosslinked with disulfide linkages of POEOMA-grafted CMC. These ssBNGs exhibit dual response release of encapsulated anticancer drugs: reductive cleavage of disulfide crosslinks and acidic pH-response of carboxylic acid groups in CMC. Their applicability toward tumor-targeting drug delivery applications is demonstrated with confocal laser scanning microscopy for cellular uptake and cell viability, as well as a facile bioconjugation with a water-soluble UV-active dye as a model cell-targeting biomolecule.

This chapter contains information that was published in *RSC Advances*. **2014**, *4*, 229-237 and part of the chapter is reproduced from the article with permission from the publisher.

3.1 Introduction

Polymer-based drug delivery systems (PDDS) are a promising platform in biomedical applications such as tissue engineering, biomedical implants, bionanotechnology, and drug delivery. Drug molecules are either physically encapsulated inside particles or covalently attached to polymeric chains, thus enhancing therapeutic efficacy while reducing side effects common to small drugs.[178-182] Typical examples of PDDS include drug conjugates (prodrugs),[183-185] hydrophobic particulates,[186-188] vesicles,[189] nanocapsules,[190, 191] and self-assembled micellar aggregates.[192-194] Particularly, nanogels are crosslinked hydrogel particles that are confined to nanometer-sized dimensions, which are smaller than micron-sized hydrogel particles (i.e. microgels).[195-198] They have the unique properties of hydrogels including high water content, biocompatibility, adjustable chemical and mechanical properties. These nanogels also possess tunable size, a large surface area for multivalent bioconjugation, and an interior network for the incorporation of therapeutics.[199-203]

Biopolymer-based nanogels (bionanogels) have all the properties of synthetic counterparts (i.e. nanogels) as well as all benefits from biopolymers being intrinsically biodegradable, abundant in nature, renewable, nontoxic, and relatively cheap.[56, 204-206] They also possess a high content of functional groups including hydroxyl, amino, and carboxylic acid groups. These functional groups can be further utilized for bioconjugation with cell targeting agents. In addition to bionanogels, the development of biopolymer-based hydrogels,[207-209] capsules,[72, 210] nanofibrous membranes,[211] and polyplexes[212] have been explored for various biomedical applications. Despite these advances, the controlled/enhanced release from bionanogels remains challenging.

Enhanced and controlled release of encapsulated anticancer therapeutics in targeted cancer cells is a highly desired property in constructing effective PDDS, particularly nanogels/microgels.[213-215] A promising method is to incorporate stimuli-responsive properties into nanogels/microgels. In response to external stimuli, these stimuli-responsive materials either undergo volume changes[216, 217] or are degraded by cleavage of dynamic covalent bonds;[114, 116] such changes enable the enhanced release of encapsulated cargoes. Typical external triggers include temperature,[218, 219] pH,[220-222] light,[223, 224] and salts,[225] as well as enzymatic[226-228] and reductive reactions.[229-232] Of our interest, low pH-sensitive systems, while stable at

physiological pH, are destabilized in acidic conditions, facilitating the release of encapsulated drugs in a controlled manner. Tumor tissue as well as endosomes and lysosomes present slightly acidic pH (5.0 - 6.5). Reduction-responsive degradable systems typically employ disulfide-thiol chemistry where disulfides are cleaved to the corresponding thiols in response to reductive reactions.[233, 234] In biological systems, glutathione (GSH reduced form) exhibit the largely different redox potential between intracellular and extracellular compartments; furthermore, GSH exists at elevated concentration in cancer cells (> 10 mM).[235, 236] In the design and development of smart bionanogels, surprisingly, the stimuli-responsive drug release has not been extensively studied yet. Most stimuli-responsive bionanogels were formed through self-assembly of amphiphilic biopolymers modified with pendant dynamic linkages.[118, 237-239]

Several methods utilizing chemical crosslinking have been proposed to synthesize various bionanogels in aqueous solution. Typical methods include free radical polymerization (FRP) of methacrylate-modified polysaccharides[120, 240] and polycondensation/or polyaddition of polysaccharides bearing reactive functional groups.[24, 241-243] A promising method involves aqueous FRP of methacrylate monomers in the presence of polysaccharides that allows for the synthesis of polymethacrylate-grafted polysaccharides. This method is versatile in that the properties of polysaccharides can be tuned with varying polymethacrylates. Examples of grafted polymethacrylates include poly(acrylic acids) for pH response,[244] as well as poly(N-isopropyl acrylamide)[245] and poly(acrylamide)[125] for temperature response. However, only few reports describe the synthesis of microgels or nanogels utilizing the aqueous FRP in the presence of dimethacrylate crosslinkers.[126, 127]

This paper describes dual-stimuli reduction and low pH-responsive bionanogels crosslinked with disulfide linkages (ssBNGs) as intracellular delivery nanocarriers with enhanced release. Scheme 3.1 illustrates our approach. Aqueous FRP of oligo(ethylene oxide) (OEO)-containing methacrylate (OEOMA) in the presence of carboxymethyl cellulose (CMC) was examined to synthesize POEOMA-grafted CMC (POEOMA-g-CMC). Water-soluble POEOMA was targeted to be grafted from CMC as the scaffold materials. POEOMA is an analog of poly(ethylene oxide) (PEO); PEO is biocompatible material that has been FDA-approved for clinical use, has low toxicity, and prevents nonspecific protein adsorption.[246, 247] An introduction of a disulfide-labeled dimethacrylate (ssDMA) as a crosslinker into aqueous free radical crosslinking polymerization (FRCP) yielded ssBNGs based on disulfide-crosslinked POEOMA-g-CMC.

These ssBNGs exhibit dual-controlled release of encapsulated anticancer drugs: reductive cleavage of disulfide crosslinks and acidic pH-response of carboxylic acid (COOH) groups in CMC. Their applicability as intracellular anticancer drug delivery nanocarriers was evaluated using confocal laser scanning microscopy (CLSM) for cellular uptake and cell viability measurements. Furthermore, their facile bioconjugation with a water-soluble UV-active dye as a model cell-targeting biomolecule was demonstrated.

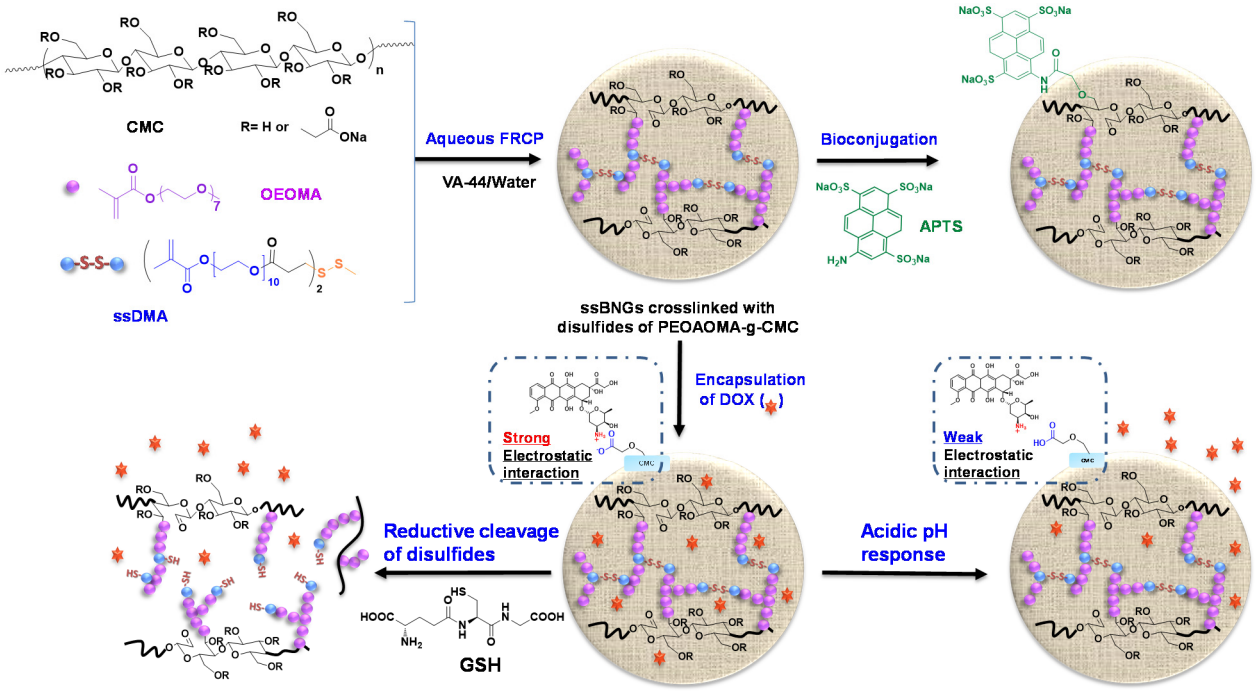

Scheme 3.1. Synthesis by aqueous FRCP, bioconjugation, and dual stimuli-response of biopolymer-based ssBNGs crosslinked with disulfide linkages of POEOMA-g-CMC.

3.2 Experimental

3.2.1 Instrumentation and analysis

^{1}H-NMR spectra were recorded using a 500 MHz Varian spectrometer. The D_2O singlet at 4.8 ppm and the $CDCl_3$ singlet at 7.26 ppm were selected as reference standards. Spectral features are tabulated in the following order: chemical shift (ppm); multiplicity (s, singlet; d, doublet; t, triplet; m, complex multiple); number of protons; position of protons. Conversion was determined by ^{1}H-NMR. Molecular weight and molecular weight distribution were determined by gel permeation chromatography (GPC). An Agilent GPC was equipped with a 1260 Infinity

Isocratic Pump and a refractive index (RI) detector. Two Agilent PLgel mixed-C and mixed-D columns were used with DMF containing 0.1 mol% LiBr at 50 °C at a flow rate of 1.0 mL/min. Linear poly(methyl methacrylate) (PMMA) standards from Fluka were used for calibration. Aliquots of polymer samples were dissolved in DMF/LiBr. The clear solutions were filtered using a 0.25 μm PTFE filter to remove any DMF-insoluble species. A drop of anisole was added as a flow rate marker. UV/Vis spectra were recorded on Agilent Cary 60 UV/Vis spectrometer equipped with an external probe.

3.2.2 FT-IR measurements

FT-IR spectra of all the samples were taken on a Nicolet 6700 FT-IR spectrometer using KBr pellets. All spectra were recorded with 32 scans in resolution of 4 cm^{-1} at room temperature in the range of 500 - 4000 cm^{-1}. Background noises were corrected with pure KBr. For data processing, the baselines of all spectra were corrected. To prepare specimens, as-synthesized aqueous polymer solutions (≈15 mL) were precipitated from acetone (300 mL) under stirring for 12 hrs. The resulting mixtures were centrifuged under the conditions of 6,000 rpm x 10 min x 4 °C. After vacuum filtration, the precipitated polymers were dried in a vacuum oven at 50 °C for 1 day. The dried polymer samples were then mixed with KBr powders to prepare pellets for FT-IR measurements.

3.2.3 Dynamic light scattering (DLS) measurements

The sizes in hydrodynamic diameters by volume of POEOMA-g CMC polymers and ssBNGs in aqueous solution were measured by dynamic light scattering (DLS) at a fixed scattering angle of 173° at 20 °C with a Malvern Instruments Nano S ZEN1600 equipped with a 633-nm He-Ne gas laser. The number average diameter (D_n) = $\frac{\sum \boldsymbol{d_i V_i}\%}{\sum \boldsymbol{V_i}\%}$, weight average diameter (D_w) = $\frac{\sum \boldsymbol{d_i^2 V_i}\%}{\sum \boldsymbol{d_i V_i}\%}$, and polydispersity = $\frac{\boldsymbol{D_w}}{\boldsymbol{D_n}}$, where d_i is a diameter of particle i and V_i% is a volume faction of particle i. Note that volume faction < 0.5% was not included in the calculation.

3.2.4 Transmission electron microscopy (TEM)

TEM images were taken using a Philips Tecnai 12 TEM, operated at 120 kV and equipped with a thermionic LaB6 filament. An AMT V601 DVC camera with point to point resolution of 0.34 nm and line resolution of 0.2 nm was used to capture images at 2048 by 2048 pixels. To prepare specimens, the nanogel dispersions were dropped onto copper TEM grids (400 mesh, carbon boated), blotted and then allowed to air dry at room temperature.

3.2.5 Materials

Carboxymethylcellulose sodium salts (CMC) with average MW ≈ 250 kg/mol and viscosity = 400 - 800 cP at 2 wt% in water, oligo(ethylene oxide) methacrylate (OEOMA-OH) with MW = 526 g/mol and #EO units ≈ 10, 3,3′-dithiopropionic acid (ssDCOOH, 99%), *N,N′*-dicyclohexyl carbodiimide (DCC), *N,N*-dimethylaminopyridine (DMAP), doxorubicin hydrochloride (DOX, -$NH_3^+Cl^-$ salt forms, > 98%), glutathione (GSH, reduced form), potassium phosphate monobasic (KHP), and KBr (FT-IR grade, ≥ 99%) from Aldrich Canada, 2,2'-azobis[2-(2-imidazolin-2-yl)propane]dihydrochloride (VA-44) from Wako Chemie, and 8-aminopyrene-1,3,6-trisulfonic acid trisodium salt (APTS, MW = 523.4 g/mol) from Biotium were purchased and used as received. Dialysis tubing with MWCO = 12,000 g/mol with a diameter = 25 mm was purchased from Spectrum Laboratories. Oligo(ethylene oxide) monomethyl ether methacrylate (OEOMA) with MW = 475 g/mol and #EO units ≈ 9 was purchased from Aldrich Canada and purified by passing through a column filled with basic alumina to remove inhibitors before used.

Dithiopropionyl poly(ethylene glycol) dimethacrylate (ssDMA) was synthesized as described in our previous report.[248] Briefly, ssDCOOH (4.6 g, 20 mmol) dissolved in THF (60 mL) reacted with OEOMA-OH (20 g, 38 mmol) in the presence of DCC (7.8 g, 38 mmol) and a catalytic amount of DMAP in dichloromethane (DCM, 120 mL). The product was purified by vacuum filtration and solvent evaporation. ^{1}H-NMR ($CDCl_3$, 7.26 ppm): 1.9 (s, 6H, -CH_3), 2.7 (t, 4H, -C(O)-$\underline{CH_2}$-CH_2-SS-), 2.9 (t, 4H, -C(O)-CH_2-$\underline{CH_2}$-SS-), 3.5-3.8 (m, EO protons), 4.0-4.3 (m, 8H, -C(O)O-CH_2- and –CH_2-O(O)C-), 5.6 (s, 2H, CH=), and 6.1 (s, 2H, CH=).

3.2.6 Synthesis of ssBNGs crosslinked with disulfides

OEOMA (50 mg, 0.11 mmol), CMC (50 mg), and an aqueous stock solution of ssDMA (0.5 mL, 2 mg/mL, 0.82 μmol) were dissolved in water (15 mL) in 25mL of Schlenk flask. The resulting clear mixture was purged with nitrogen for 30 min under magnetic stirring and then heated to 40 °C in a water bath for 10 min. A nitrogen-prepurged aqueous stock solution of VA-44 (0.3 mL, 10 mg/mL) was added using a syringe to initiate the polymerization. The polymerization stopped at 5 hrs by cooling down to room temperature. The resulting ssBNGs were purified by intensive dialysis for 24 hrs against water for DLS and conjugation experiments as well as against PBS for cell culture experiments.

3.2.7 Loading of DOX

DOX (2.3 mg, 5 wt% of ssBNGs solids) was dissolved in aqueous ssBNGs solution (5.9 mg/mL, 8 mL). The resulting mixture was stirred at room temperature for 24 hrs and dialyzed against water (1 L). Outer water was changed every 12 hrs to remove free DOX for 36 hrs, yielding aqueous DOX-loaded ssBNGs solution at 4.3 mg/mL. Their UV/Vis spectra were recorded and the loading level of DOX was calculated by the weight ratio of loaded DOX to dried polymers.

3.2.8 Dual-responsive release of DOX using UV/Vis spectroscopy

For acidic pH-responsive release, aliquots of aqueous DOX-loaded ssBNGs solution (2 mL) were placed in a dialysis tubing and immersed in aqueous KHP buffer solutions at different pH values (50 mL). The absorbance of DOX in outer water was recorded at an interval of 5 min using a UV/Vis spectrometer equipped with an external probe at λ_{ex} = 497 nm. For quantitative analysis, the solution in the tubing was combined with outer water and the UV/Vis spectrum of the resulting mixture was recorded. For reduction-responsive release of DOX, the similar procedure was applied except for the use of outer aqueous buffer solution with and without 5 mM GSH at pH = 7.

3.2.9 Cell culture

HeLa cancer cells were cultured in DMEM (Dulbecco's modified Eagle's medium) containing 10% FBS (fetal bovine serum) and 1% antibiotics (50 units/mL penicillin and 50 units/mL streptomycin) at 37 °C in a humidified atmosphere containing 5% CO_2.

3.2.10 Confocal laser scanning microscopy (CLSM)

Cells plated at 2×10^5 cells/well into a 6-well plate were incubated with DOX-loaded ssBNGs (200 μL for DOX = 21 μg) and free DOX (21 μg) as a control at 37 °C for 2 and 8 hrs. After culture medium was removed, cells were washed with PBS three times. After the removal of supernatants, the cells were fixed with cold methanol (-20 °C) for 20 min at 4 °C. The slides were rinsed with tris-buffered saline Tween-20 (TBST) three times. Cells were stained with 2-(4-amidinophenl)-6-indolecarbamidine (DAPI) for 5 min. The fluorescence images were obtained using a LSM 510 Meta/Axiovert 200 (Carl Zeiss, Jena, Germany).

3.2.11 Cell viability using MTT assay

Cells were plated at 5 x 10^5 cells/well into a 96-well plate and incubated for 24 hrs in DMEM (100 μL) containing 10% FBS for the following experiments. They were then incubated with various concentrations of empty and DOX-loaded ssBNGs for 48 hrs. Blank controls (cells only) were run simultaneously. Cell viability was measured using CellTiter 96 Non-Radioactive Cell Proliferation Assay kit (MTT, Promega) according to manufacturer's instruction. Briefly, 3-(4,5-dimethylthiazol-2-yl)-2,5-diphenyltetrazolium bromide (MTT) solutions (15 μL) was added into each well. After 4 hrs incubation, the medium containing unreacted MTT was carefully removed. DMSO (100 μL) was added into each well in order to dissolve the formed formazan blue crystals, and then the absorbance at λ = 570 nm was recorded using Powerwave HT Microplate Reader (Bio-Tek). Each concentration was 12-replicated. Cell viability was calculated as the percent ratio of absorbance of mixtures with nanogels to control (cells only).

3.2.12 Conjugation of ssBNGs with APTS

An aqueous APTS stock solution (0.83 mL, 5 mg/mL) was mixed with aqueous ssBNGs solution (1 mL, 6 mg/mL) in the presence of an aqueous stock solution of EDC (1.1 mL, 10

mg/mL) under stirring at room temperature for 1 day. The mixture was then dialyzed against water for 3 days to completely remove unreacted APTS dyes, yielding aqueous APTS-conjugated ssBNGs solution at 1.1 mg/mL.

3.3 Results and Discussion

3.3.1 Preparation of ssBNGs based on crosslinked POEOMA-g-CMC

Our approach to synthesize dual stimuli-responsive ssBNGs involves the aqueous free radical polymerization (FRP) of OEOMA in the presence of CMC and a disulfide-labeled dimethacrylate (ssDMA). The synthesis of ssDMA using a facile carbodiimide coupling reaction is reported.[248] A water-soluble VA-44 azo-type free-radical initiator was selected because of its short half-life at lower temperature ($\tau_{1/2}$ = 10 hrs at 44 °C). For FRP of OEOMA initiated with VA-44, conversion reached > 80% within 2 hrs at 40 °C (Table A.1). Due to the high molecular weight of CMC, the viscosity of its aqueous solution strongly relies on the concentration of CMC. It was found that 1 wt% aqueous CMC solution is suitable for FRP. For the concentration of OEOMA, a series of aqueous FRP of different amounts of OEOMA in the presence of 1 wt% CMC without ssDMA was carried out. The results show that the average diameter of the resulting particles based on POEOMA-grafted CMC increased with an increasing amount of OEOMA (Figure A.1 and Table A.2). Such increase is attributed to an increase in probability of intra- or inter-particle coupling reaction. At 3.3 mg/mL concentration, the resulting particles based on POEOMA-grafted CMC had an average diameter ≈ 14 nm with a monomodal distribution.

A 1.5 mol% of ssDMA was introduced into aqueous FRP of OEOMA in the presence of CMC = 1wt% and VA-44 = 2 wt% of OEOMA at 3.3 mg/mL. After 5 hrs, monomer conversion was determined by ^{1}H-NMR to be > 80%. The resulting ssBNGs were then purified by intensive dialysis to remove unreacted monomers. DLS results suggest the presence of two populations. The main population (> 90% volume) is smaller-sized aggregates with $D_n \approx 24$ nm, which is larger than that (≈ 14 nm) prepared in the absence of ssDMA. In addition, a smaller population (< 10% volume) is larger-sized aggregates with the diameter > 0.8 μm (Figure 3.1a). TEM images

indicate near-spherical shapes of ssBNGs with average diameter = 19.5 ± 4.1 nm, which is similar to that determined by DLS (Figure 3.1b).

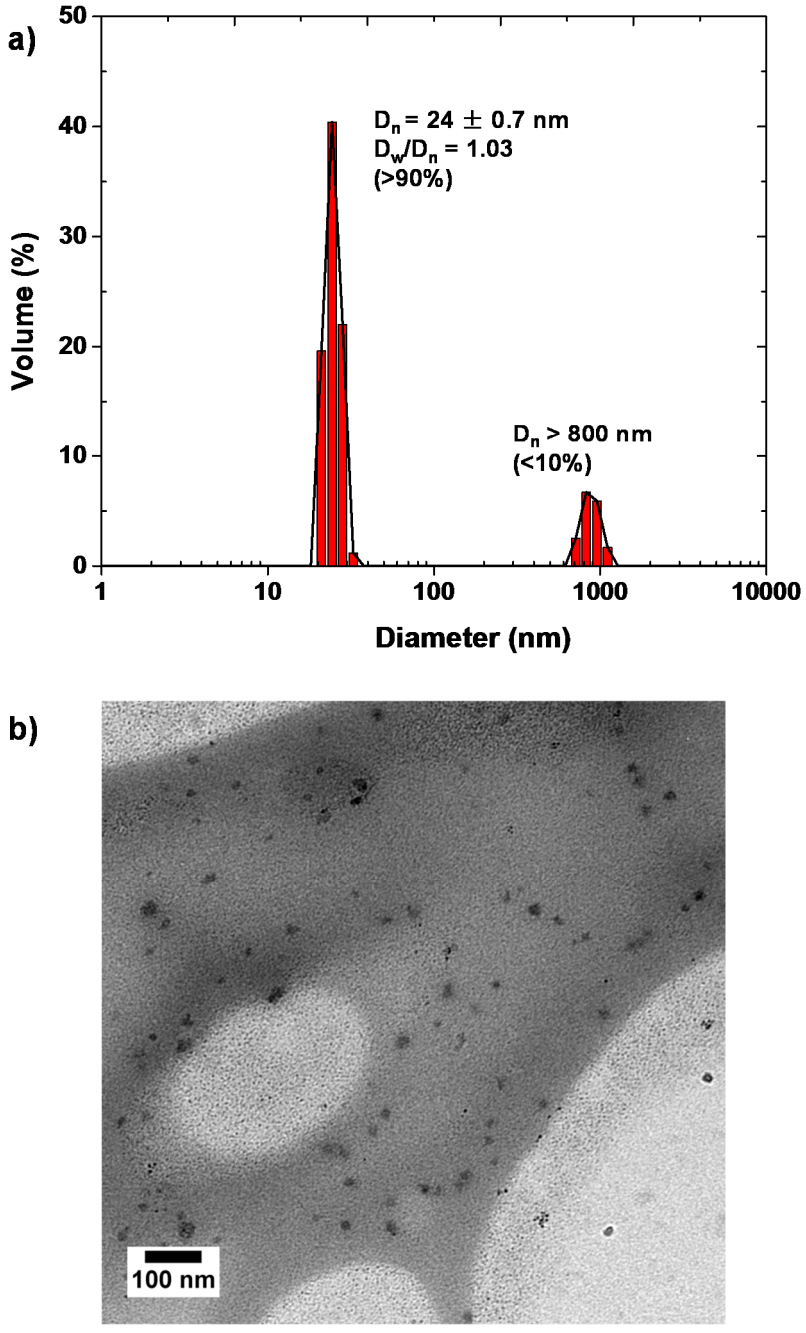

Figure 3.1. DLS diagram (a) and TEM image (b) of dialyzed ssBNGs.

Aqueous FRP process allows for the synthesis of polymethacrylates grafted from polysaccharide-based biopolymers.[249, 250] However, this process also forms undesired polymethacrylate homopolymers; such as polyacrylamide,[125] poly(methyl methacrylate),[251] and poly(3-dimethyl-(methacryloyloxyethyl) ammonium propane sulfonate).[252] They were removed by intensive extraction with appropriate solvents.

In our control experiment without ssDMA, the results from our solubility tests suggest that acetone and a mixture of ethanol and acetic acid could be good solvents to POEOMA homopolymers, but poor solvents to CMC (Table A.3). Accordingly, the POEOMA-g-CMC prepared without ssDMA (FRP-C1) was precipitated from acetone to remove undesired POEOMA homopolymers and unreacted OEOMA. As seen in Figure A.2, the FT-IR spectrum of the POEOMA-g-CMC exhibits two characteristic bands at 1605 cm^{-1} corresponding to carboxylate ($C(=O)O^-$) anion absorption of CMC and at 1730 cm^{-1} corresponding to ester C=O vibrational absorption of POEOMA, suggesting the formation of POEOMA-g-CMC. Similarly, ssBNGs prepared in the presence of ssDMA were precipitated from acetone. Note that the undesired products of POEOMA homopolymers crosslinked in the presence of ssDMA could be dissolved in acetone as microgel particles and thus they will be removed. As seen in Figure 3.2, the FR-IR spectrum of the precipitated ssBNGs exhibits the two typical vibrational absorptions at 1605 and 1730 cm^{-1}; this is similar to POEOMA-g-CMC prepared without ssDMA.

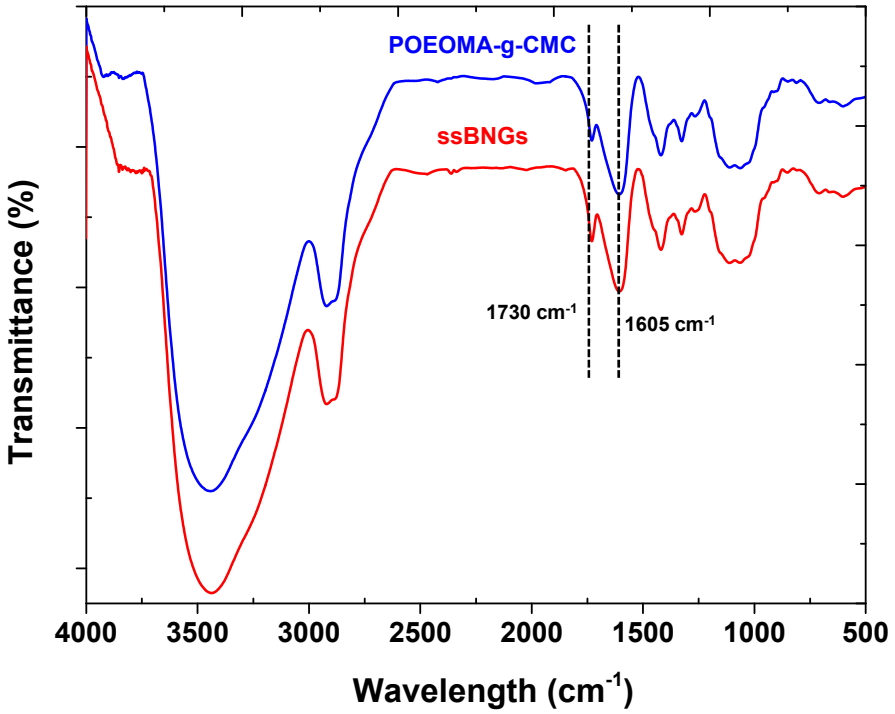

Figure 3.2. FT-IR spectrum of ssBNGs, compared with that of POEOMA-g-CMC.

3.3.2 Loading of anticancer drugs

To preliminarily evaluate ssBNGs as a platform with enhanced release for tumor-targeting drug delivery, doxorubicin (DOX), a DNA-interacting anticancer drug used in chemotherapy, was encapsulated in ssBNGs. An aqueous DOX stock solution was mixed with ssBNGs in water (pH = 6.5). Free (not encapsulated) DOX was removed by intensive dialysis for 36 hrs. The removal of free DOX was monitored by measuring the absorbance of DOX at 497 nm in outer water (Figure A.3). In this way, DOX-loaded ssBNGs in aqueous solution at 4.3 mg/mL was prepared. The loading level of DOX for DOX-loaded ssBNGs was determined using UV/Vis spectroscopy. UV/Vis spectrum of DOX-loaded ssBNGs is similar to that of free DOX, suggesting no signification change in the structure of DOX encapsulated in ssBNGs (Figure A.4). The Beer-Lambert equation with the absorbance and the extinction coefficient of 10,000 M^{-1} cm^{-1} at λ = 497 nm[253] was used to determine the loading level of DOX to be 3.4 ± 0.1% and its loading efficiency to be 68.6 ± 3.1% at the weight ratio of DOX/ssBNGs = 1/20.

3.3.3 Dual responsive release of encapsulated anticancer drugs

The release of DOX from DOX-loaded ssBNGs in response to both acidic pH and thiol reducing agents was investigated. To examine acidic pH-responsive release, aliquots of DOX-loaded ssBNGs in dialysis tubing were placed in aqueous KHP buffer solutions at different pH values of 3, 5.5, and 7. Figure 3.3 shows the significant dependence of DOX release upon acidic pH values. Figure 3.3b - e show the digital photos of outer water and the corresponding dialysis tubing before and after release. The release of DOX was enhanced in the order of pH 3 > pH 5.5 > pH 7. This enhancement is attributed to the extent of interactions between COOH groups of CMC in ssBNGs and amine (NH_2) groups of DOX. Because of pKa of DOX = 8.3, most amine groups of DOX exist as protonated forms (NH_3^+ forms) in the range of pH values examined here. However, COOH groups exist as their neutral forms (COOH forms) at below pKa = 4.8 or their deprotonated forms (COO^- forms) at above pKa. It is obvious that protonated NH_3^+ forms of DOX have weaker interactions with neutral COOH forms of CMC than deprotonated COO^- forms. As a consequence, the release of DOX was faster at pH = 3 than pH = 7.

Next, reductively responsive release of DOX was examined at pH = 7 in a way that aliquots of DOX-loaded ssBNGs in dialysis tubing was placed in aqueous buffer solution with and without (control) 5 mM GSH. As seen in Figure 3.4, the release of DOX was relatively faster in the presence of 5 mM GSH, compared to no GSH. Such slight enhancement is the result of GSH-induced degradation of ssBNGs by cleavage of disulfides. These results suggest that acidic pH-response is more significant than thiol-response in enhancing the release of DOX from ssBNGs crosslinked with disulfide linkages of POEOMA-g-CMC.

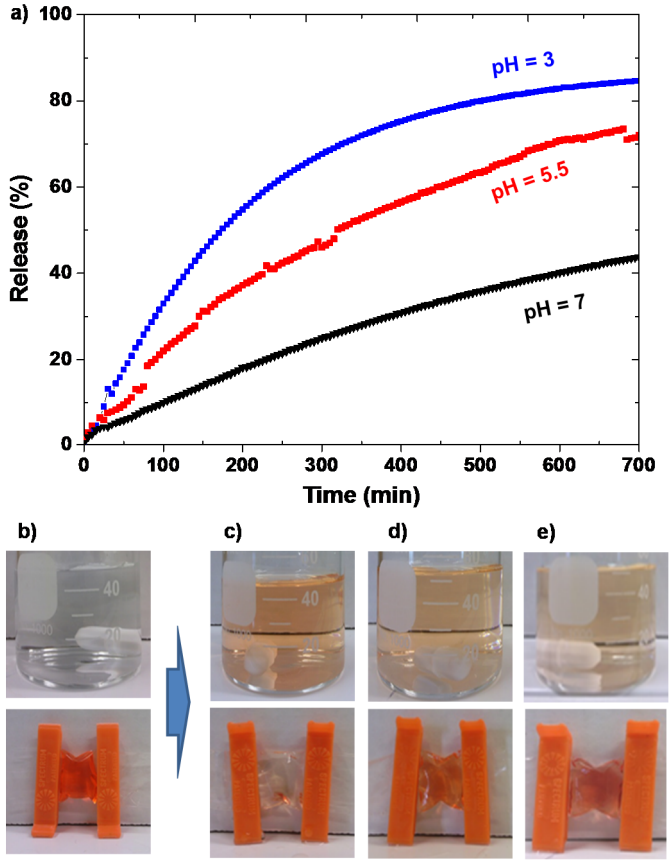

Figure 3.3. Release of DOX from DOX-loaded ssBNGs in aqueous buffer solutions at different pH of 3, 5.5, and 7 (a), and digital photos of outer water (upper) and the corresponding dialysis tubing (lower) before (b) and after release of DOX at pH = 3 (c), 5.5 (d), and 7 (e).

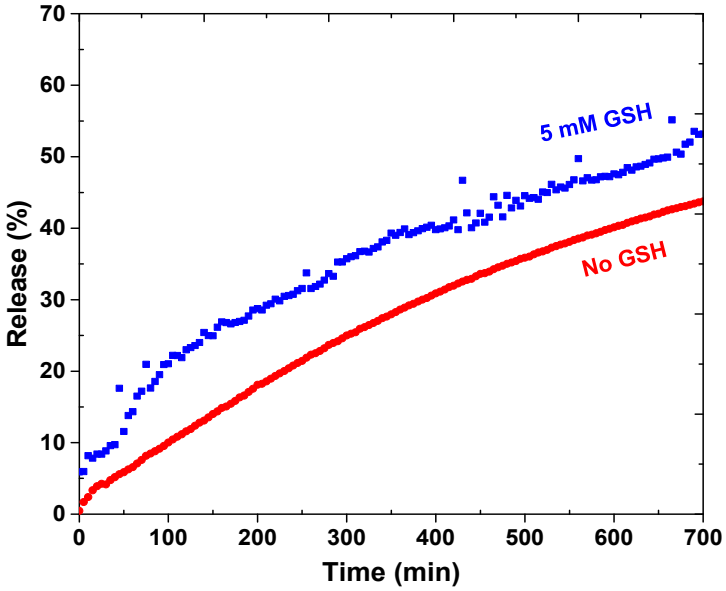

Figure 3.4. Release of DOX from DOX-loaded ssBNGs in aqueous buffer solutions at pH = 7 with and without 5 mM GSH.

3.3.4 Intracellular release as anticancer drug delivery nanocarriers

Intracellular trafficking of DOX from DOX-loaded ssBNGs after cellular uptake was examined using CLSM. Figure 3.5 shows CLSM images of HeLa cells incubated with and without DOX-loaded ssBNGs for 2 and 8 hrs. For comparison, HeLa cells were also incubated with free DOX. HeLa nuclei were stained with DAPI to provide enhanced contrast and clarity. Compared to free DOX as a control (Figure 3.5d and e), the images from DOX fluorescence suggest that DOX-loaded ssBNGs were internalized and DOX was released to reach cell nuclei within 2 hrs (Figure 3.5b). When the incubation time increased to 8 hrs, the DOX fluorescence became brighter, suggesting more DOX reached cell nuclei (Figure 3.5c).

A MTT colorimetric assay was used to evaluate cytotoxicity of HeLa cells in the presence of empty and DOX-loaded ssBNGs (Figure 3.6). The empty crosslinked ssBNGs exhibited > 90% HeLa cell viability at concentrations up to 200 μg/mL, suggesting non-toxicity of ssBNGs to cells. In the presence of DOX-loaded ssBNGs at 200 μg/mL (≈ 3.5 μg/mL DOX), however, the viability decreased to below 20%, suggesting inhibition of cell proliferation in the presence of DOX. The results from cell viability and CLSM measurements suggest that DOX release from

DOX-loaded ssBNGs, possibly triggered by intracellular GSH and acidic pH inside cancer cells, enhanced the inhibition of the cellular proliferation.

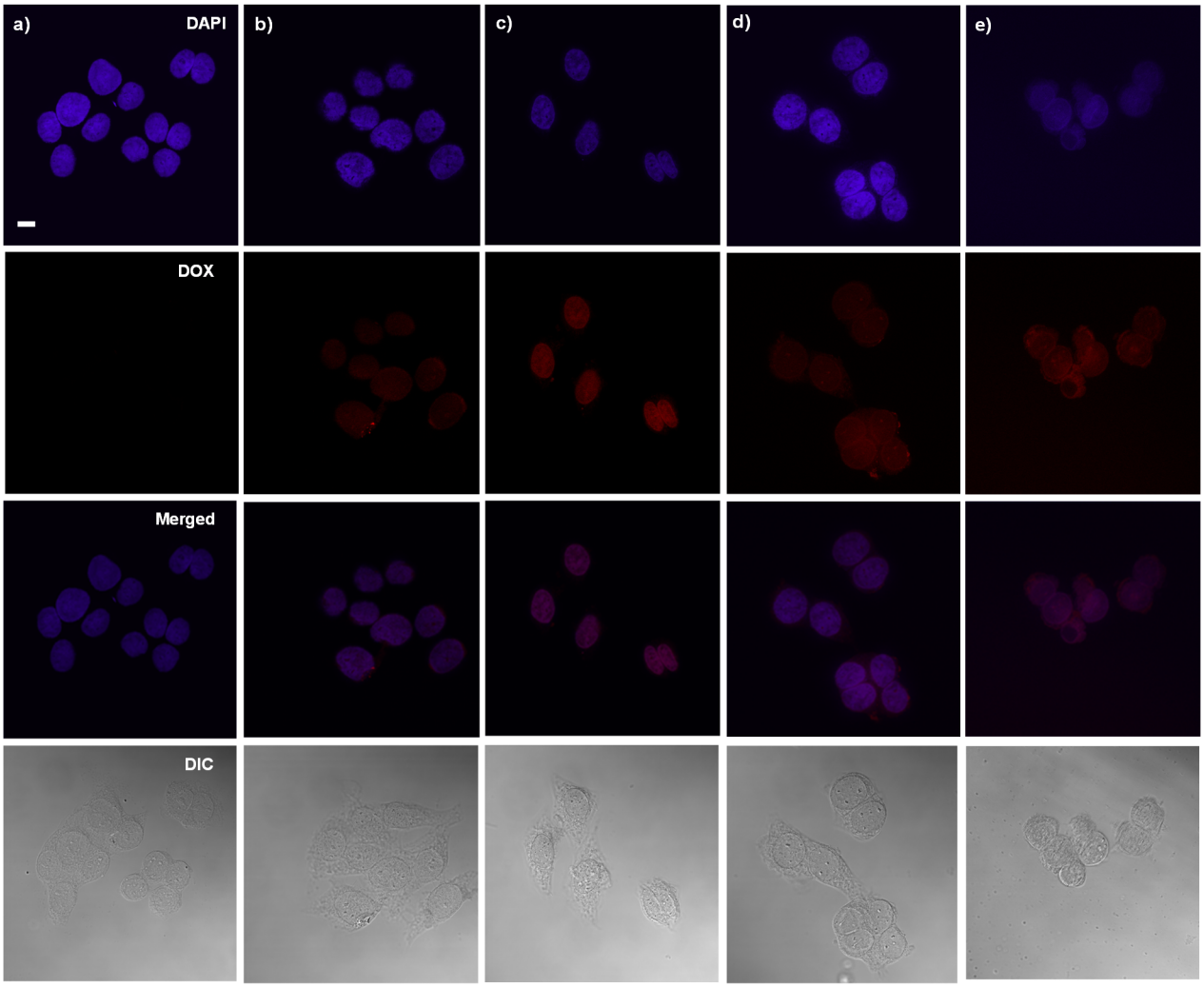

Figure 3.5. CLSM images of HeLa cells incubated with empty ssBNGs for 8 hrs (a), DOX-loaded ssBNGs for 2 (b) and 8 hrs (c), as well as free DOX for 2 (d) and 8 hrs (e). Scale bar = 20 μm.

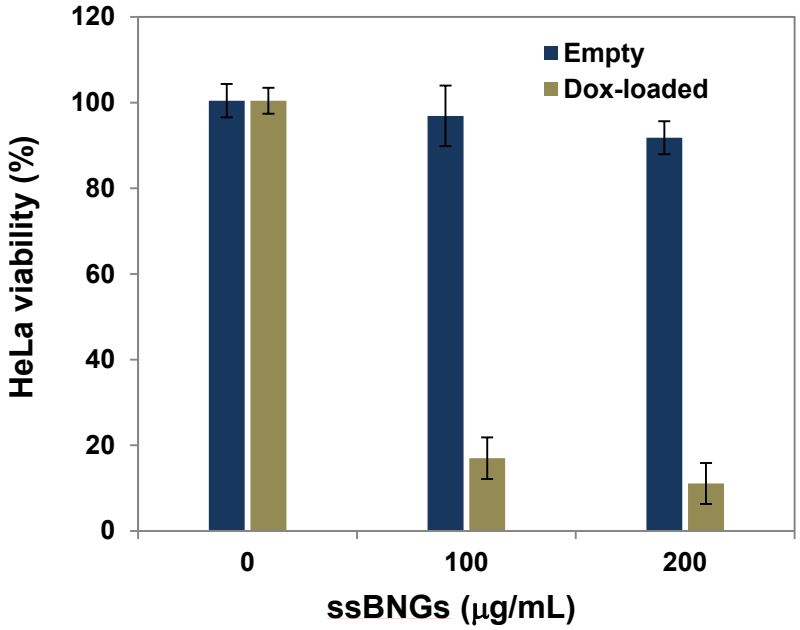

Figure 3.6. Viability of HeLa cells incubated with empty and DOX-loaded ssBNGs for 48 hrs determined by MTT assay. Data are presented as the average ± standard deviation (n = 12)

3.3.5 Bioconjugation for active targeting

Active targeting to specific cells through bioconjugation of delivery vehicles with cell targeting agents is a desired property for PDDS. Specific targeting could reduce the serious side effects of drugs as well as enhance the drug efficiency.[254, 255] Polysaccharides including CMC possess a high content of functional groups including hydroxyl and carboxylic acid groups. These functional groups can be further utilized for bioconjugation with cell targeting agents. To assess an applicability of ssBNGs based on crosslinked POEOMA-g-CMC toward targeted delivery, the conjugation of COOH groups in CMC with a water-soluble APTS dye was examined in aqueous solution through an EDC-coupling reaction.

A known amount of ssBNGs was mixed with free APTS in the presence of EDC at room temperature for 1 day. The mole ratio of [COOH]/[APTS]/[EDC] = 1/0.5/4.5. The mole of COOH was calculated from the carboxylate content = 70% (from supplier's catalog). Unreacted APTS dyes were removed by intensive dialysis against water. Figure 3.7 shows the UV/Vis spectra of APTS-conjugated ssBNGs and free APTS in aqueous solutions at pH = 7. The maximum absorption at λ_{max} = 424 nm for free APTS dyes was shifted to λ_{max} = 372 nm for

APTS-bound ssBNGs. As a control experiment, the pH-dependence of UV absorption of free APTS was examined in aqueous solutions at a broad range of pH from 2 to 10 (Figure A.5). At above pH = 2, its UV/Vis spectra retained similar with its maximum absorption at λ = 424 nm, while it was blue-shift at below pH = 2. Note that the UV/Vis spectrum of APTS-conjugated ssBNGs was recorded at pH = 7. Consequently, the blue-shift after conjugation is attributed to the formation of new amide linkages, suggesting the successful conjugation of ssBNGs with APTS to form APTS-conjugated ssBNGs (see Scheme 3.1).

For quantitative analysis, the extinction coefficient of APTS at λ_{max} = 424 nm was determined to be ε = 21,700 M^{-1} cm^{-1} in water (pH = 6.5) (Figure A.6). UV/Vis spectra of the mixture consisting of ssBNGs, APTS, and EDC before and after the occurrence of EDC coupling reaction are compared in Figure 3.7. Using the extinction coefficient and the difference of the absorbance at λ = 424 nm, the conjugation efficiency of COOH groups in ssBNGs with APTS was estimated to be 15% under these conditions.

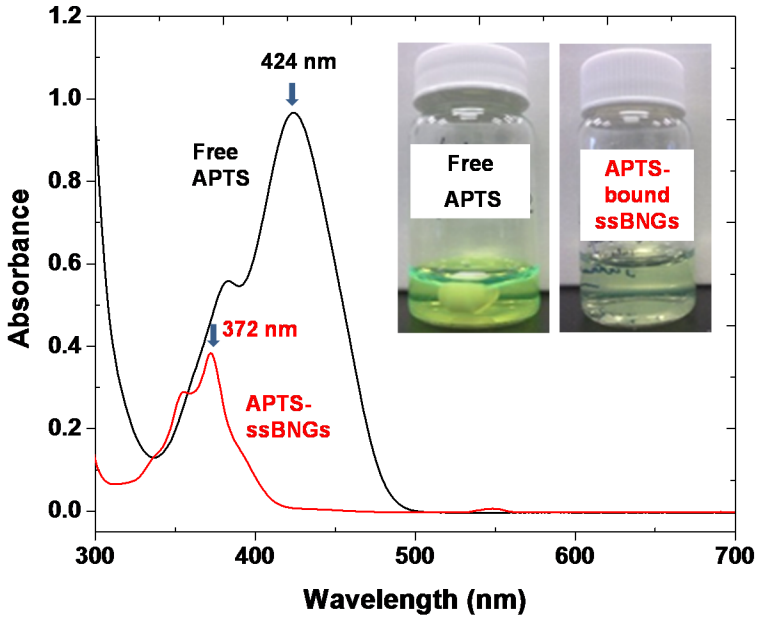

Figure 3.7. UV/Vis spectra and digital photos (insect) of aqueous solution of APTS-conjugated ssBNGs and free APTS at pH = 7.

3.4 Conclusion

Polysaccharide-based ssBNGs crosslinked with disulfide linkages of POEOMA-g-CMC exhibiting dual-stimuli reduction and acidic pH responses were synthesized by a facile aqueous free radical crosslinking polymerization of OEOMA in the presence of CMC and ssDMA at ambient temperature. In the absence of crosslinkers, the initiator concentration, temperature, and OEOMA concentrations were revealed to be important parameters that significantly influence the polymerization kinetics and grafting of POEOMA from CMC chains. Introduction of ssDMA yielded dual stimuli-responsive ssBNGs with diameter ≈ 24 nm, confirmed by DLS and TEM. Toward intracellular anticancer drug delivery, DOX was encapsulated at loading level = 3.4%. The results from UV absorbance measurements suggest the enhanced release of DOX in response to acidic pH as well as in the presence of GSH; interestingly, acidic pH-response is more significant than GSH-response in enhancing DOX release. Furthermore, the intracellular release of anticancer drugs after internalization into HeLa cancer cells is confirmed with the results from CLSM and MTT viability assay. These results, combined with the ability to facile bioconjugation with a cell-targeting model biomolecule in aqueous solution, suggest that the ssBNGs are a promising intracellular nanocarrier platform exhibiting multi-controlled drug release.

Chapter 4

Development of pH/temperature-responsive CMC-based bionanogels

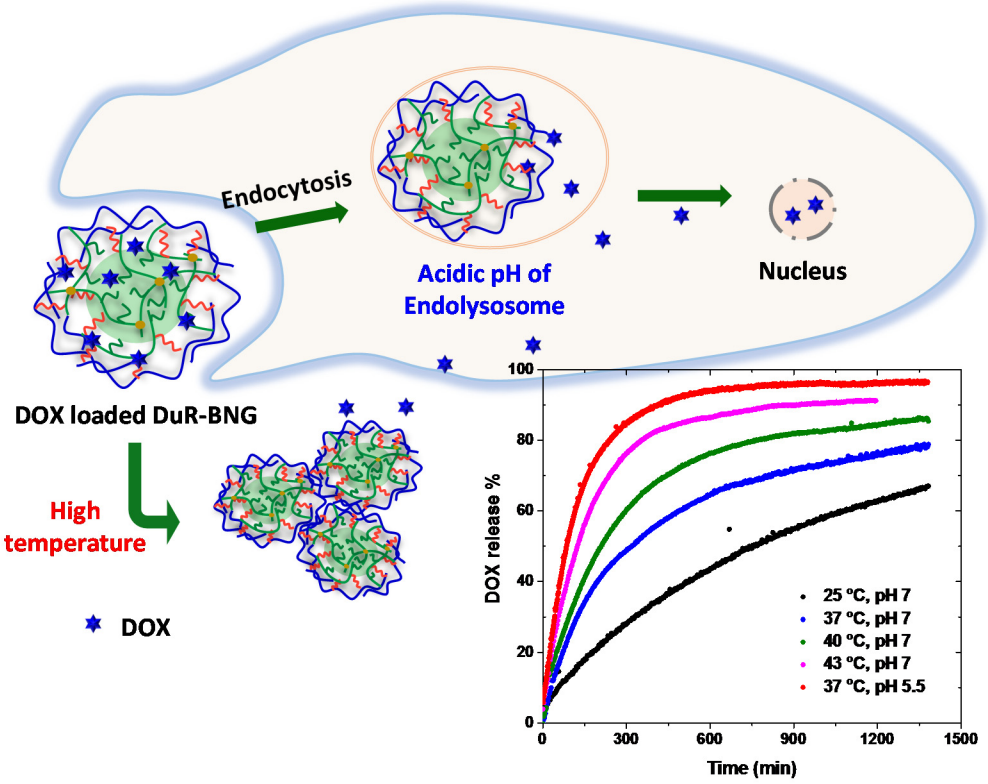

Polysaccharide-based crosslinked nanogels (bionanogels) exhibiting multiple stimuli-responsive release of encapsulated therapeutics hold a great potential as tumor-targeting intracellular drug delivery nanocarriers. Herein, we report the synthesis of monodisperse dual temperature/acidic pH-responsive bionanogels (DuR-BNGs) by aqueous crosslinking polymerization through temperature-induced self-association method. The DuR-BNGs have prolonged colloidal stability and negligible non-specific interactions with proteins. In response to acidic pH and higher temperature (above LSCT), they exhibit synergically rapid release of anticancer drugs as a consequence of both acidic pH-sensitivity of CMC and temperature-induced volume changes of grafted thermoresponsive copolymers. *In vitro* cell culture results suggest that

new DuR-BNG is a promising candidate with enhanced colloidal stability and dual stimuli-responsive drug release for chemotherapy.

This chapter contains information that was submitted in *Colloids and Surfaces B: Biointerfaces* and part of the chapter is reproduced from the article with the permission from the publisher.

4.1 Introduction

In recent decades polymer based drug delivery systems (PDDS) have been a choice of materials that can overcome limitations in conventional chemotherapy: undesired side effects and low drug efficiency common to small drugs.[178-182] Therapeutic molecules are commonly incorporated into PDDS through physical encapsulation or covalent attachment.[256-258] These drug-loaded PDDS are designed to retain prolonged blood circulation. They are then specially extravasated into tumor tissues through enhanced permeability and retention (EPR) effect. This passive targeting enables to improve bioavailability and biodistribution of small drugs in tumor tissues.[3-5] Typical examples of PDDS include self-assembled block copolymer micelles[108, 193, 194, 259, 260] and nanocapsules.[190, 191] However, due to their formation driven by physical association of polymeric chains, they often suffer from the premature release of encapsulated drugs during blood circulation upon the dilution in blood (≈ 4 L).[28] In contrast, well-defined nanogels possess inherent colloidal stability due to being crosslinked.[195-198] Promisingly, polysaccharide-based nanogels (bionanogels, BNGs) offer a number of unique features. Polysaccharides are biocompatible, intrinsically biodegradable, and easily obtained from a variety of natural resources. They possess a plenty of functional groups such as -OH, -COOH and -NH_2 groups, which can facilitate further modification of BNGs, particularly their bioconjugation with cell-targeting molecules.[56, 199-206]

Toward successful tumor-targeting applications of BNGs, however, a critical challenge to be addressed is the slow and uncontrolled release of encapsulated drugs from BNGs.[10] The rapid release of cargoes is highly desired for cancer treatment.[215] One promising approach is to design smart (or stimuli-responsive) BNGs that undergo either volum change or chemical degradation of dynamic covalent linkages in response to external stimuli. This stimuli-responsive platform leads to rapid release of encapsulated drugs. While most smart BNGs have been designed to exhibit single stimulus-response such as temperature,[218, 219] pH,[220-222] salts,[225] enzymatic[226-228] and reductive reactions,[229-232, 261] dual or multiple stimuli-responsive BNGs exhibit more desirable drug release kinetics.[122] However, the exploration to synthesize dual responsive BNGs is in infancy, with few reports describing dual enzyme/light[122] and pH/reduction-responsive[33] systems.

Another challenge involves the facile synthesis and purification of monomodal BNGs. Inverse (mini)emulsion method could yield nanometer-sized BNGs; however, the method requires the removal of oil-soluble surfactants to purify BNGs after polymerization.[213, 240] In contrast, aqueous polymerization is a convenient method that proceeds with no aid of surfactants. The method allows for the synthesis of polysaccharide-grafted polymethacrylates and crosslinked BNGs whose properties can be tuned with varying grafted polymethacrylates.[125, 244] Although this method does not require tedious purification steps for the removal of surfactants, it yields multimodal BNGs with broad size distributions due to undesired inter-chain couplings.[33] Monomodal size distribution of BNGs is highly desired for prolonged blood circulation and cellular uptake to cancer cells through endocytosis.

Herein, we report new dual temperature/acidic pH-responsive BNGs (denoted DuR-BNGs) with narrow size distribution exhibiting enhanced release and excellent colloidal stabiltiy for cancer therapy. As illustated in Scheme 4.1, well-defined monodisperse DuR-BNGs were synthesized by aqueous crosslinking polymerization via temperature-driven self-association method in aquous solution. Biocompabile carboxymethyl cellulose as a promising polysaccharide contains pendant COOH groups that promote the release of encapsulated anticancer drugs in acidic tumor tissues, such as pH = 6.5 in extracellular enviroments and 5.0 - 6.5 in endosomes and lysosomes inside cancer cells. Grafted thermoresponsive oligo(ethylene oxide)-based copolymers are designed to be sensitive to temperatures close to body temperature, leading to thermoresponsive enhanced drug release. Further, both stimuli present at higher temperature in acidic pH promoted synergic release of encapsulated drugs from the DuR-BNGs. Their versatile applicability toward intracellular anticancer drug delivery was further evaluated with the results from *in vitro* cellular uptake and cell viability.

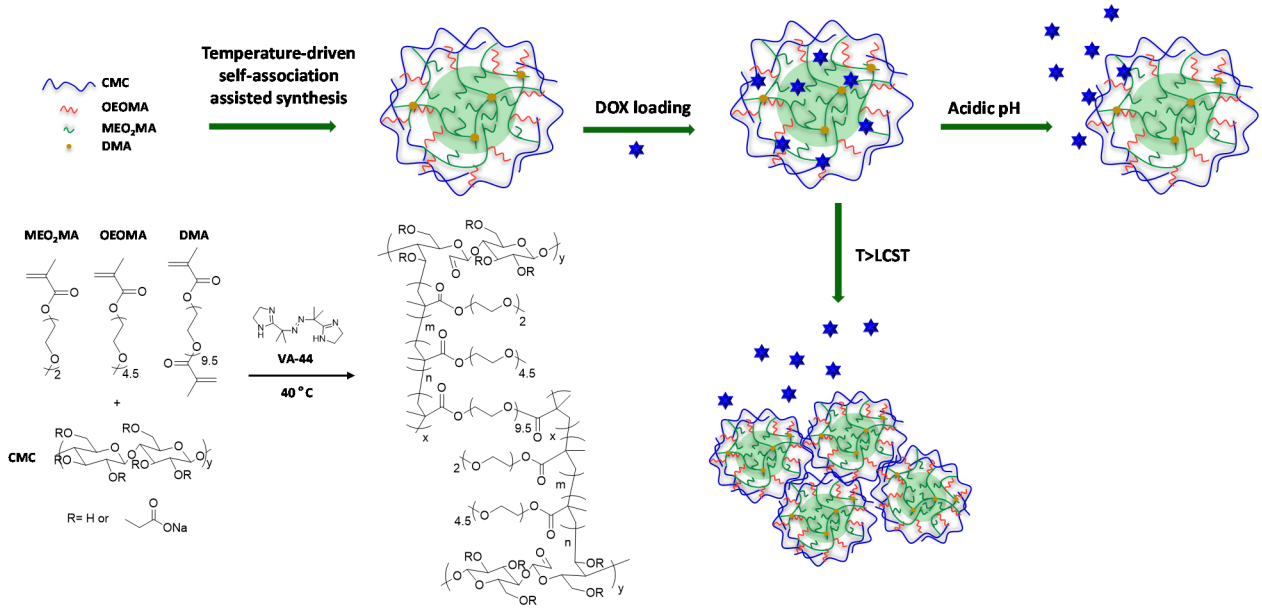

Scheme 4.1. Illustrations of synthesis of dual temperature/acidic pH-responsive DuR-BNGs via temperature-driven self-association method and their stimuli-responsive DOX release.

4.2 Experimental

4.2.1 Materials

Carboxymethylcellulose sodium salts (CMC) (MW ≈ 250 kg/mol and viscosity = 400 - 800 cP at 2 wt% in water, provided by supplier), doxorubicin hydrochloride (DOX, $NH_3^+Cl^-$ salt form, > 98%), potassium hydrogen phthalate (KHP), and KBr (FT-IR grade, ≥ 99%) from Aldrich; bovine serum albumin (BSA, > 95%) from MP biomedicals; as well as 2,2'-azobis[2-(2-imidazolin-2-yl)propane]dihydrochloride (VA-44) from Wako Chemie were purchased and used as received without purification. Dialysis tubing with MWCO = 12,000 g/mol were purchased from Spectrum Laboratories. Oligo(ethylene oxide) monomethyl ether methacrylate (OEOMA) with MW = 300 g/mol and #EO units ≈ 5.5, di(ethylene oxide) methyl ether methacrylate (MEO_2MA), and oligo(ethylene oxide) methyl ether dimethacrylate (OEODMA) was purchased from Aldrich Canada and purified by passing through a column filled with basic alumina to remove inhibitors before used.

4.2.2 Aqueous polymerization to synthesize CMC-g-P(MEO_2MA-co-OEOMA)

A series of aqueous polymerization was carried out in water containing CMC (3.3 mg/mL), a mixture of MEO_2MA and OEOMA (3.3 mg/mL), and VA-44 (0.23 mg/mL) at 40 °C. The amount of MEO_2MA in the monomer mixtures was varied from 0 to 75 mol%. As a typical example for the synthesis of CMC-g-P6 (see Table S1), CMC (50 mg, 0.2 μmol), MEO_2MA (32 mg, 0.17 mmol), and OEOMA (17 mg, 0.057 mmol) were dissolved in water (15 mL) in a 25 mL Schlenk flask. The resulting clear solution was purged with nitrogen for 30 min, and immersed into a pre-heated oil bath at 40 °C. A nitrogen pre-purged aqueous stock solution of VA-44 (0.35 mL, 10 mg/mL, 10.8 μmol) was added to initiate polymerization. Polymerization was stopped after 5 hrs by cooling to room temperature. Monomer conversion was determined by ^{1}H-NMR. The resulting grafted polymers were purified by an intensive dialysis against water for 24 hrs to remove unreacted monomers and initiating species.

4.2.3 Synthesis of DuR-BNGs by temperature-driven self-association assisted method

CMC (50 mg, 0.2 μmol), MEO_2MA (32 mg, 170 μmol), OEOMA (17 mg, 57 μmol), and an aqueous stock solution of OEODMA (0.25 mL, 20 mg/mL, 9.1 μmol) were dissolved in water (15 mL) in 25mL of Schlenk flask. The resulting clear mixture was purged with nitrogen for 30 min under magnetic stirring and then heated to 40 °C in a water bath for 10 min. A nitrogen-prepurged aqueous stock solution of VA-44 (0.35 mL, 10 mg/mL) was added using a syringe to initiate the polymerization. The polymerization was stopped after 14 hrs by cooling down to room temperature. Similarly, the resulting DuR-BNGs were purified by an intensive dialysis against water for 24 hrs.

4.2.4 Instrumentation and analysis

^{1}H-NMR spectra were recorded using a 500 MHz Varian spectrometer. The D_2O doublet at 4.8 ppm was selected as the reference standard. FT-IR spectra were recorded on Nicolet 6700 FT-IR spectrometer using KBr pellets. All spectra were recorded with 32 scans in resolution of 4 cm^{-1} at room temperature in the range of 500 - 4000 cm^{-1}. Background noises were corrected with pure KBr. For FT-IR measurements, the purified, dried BNGs were mixed with KBr

powders to prepare pellets. UV/Vis spectra were recorded on Agilent Cary 60 UV/Vis spectrometer equipped with an external probe.

4.2.5 Size and morphology analysis

The sizes in hydrodynamic diameters by volume of grafted copolymers and DuR-BNGs in aqueous solution were measured by dynamic light scattering (DLS) at a fixed scattering angle of 175° at 25 °C with a Malvern Instruments Nano S ZEN1600 equipped with a 633 nm He-Ne gas laser. Transmission electron microscopy (TEM) images were taken using a Philips Tecnai 12 TEM, operated at 120 kV and equipped with a thermionic LaB6 filament. An AMT V601 DVC camera with point to point resolution of 0.34 nm and line resolution of 0.2 nm was used to capture images at 2048 by 2048 pixels. To prepare specimens, the DuR-BNG dispersions were dropped onto copper TEM grids (400 mesh, carbon boated), blotted and then allowed to air dry at room temperature.

4.2.6 Determination of LCST using DLS

Light scattering (LS) intensity (count rates) of aqueous solution of CMC-g-P(MEO2MA-co-OEOMA) and DuR-BNGs at 4.6 mg/mL was measured in quartz cuvette, which were sealed with a Teflon stopper. The change in light scattering intensity with temperature was then recorded from 20 to 90 °C at increments of 1 °C. The LCST was determined from the onset of increase in LS intensity.

4.2.7 Colloidal stability

An aliquot of DuR-BNG dispersion (1 mL) was mixed with KHP buffer (pH = 5.5) to adjust pH to be 5.5 at 4.3 mg/mL. DLS was used to follow their sizes over time, along with DuR-BNG dispersion at pH = 7.0.

4.2.8 Non-specific BSA absorption of DuR-BNGs

Aliquots of DuR-BNG dispersion (0.3 mL) was mixed with two different volumes (0.8 and 1.1 mL) of aqueous BSA solution (80 mg/mL) in PBS. The final volume of the mixtures was adjusted to be 2 mL with extra PBS. The resulting mixtures were then incubated at 4 ºC for 3

days. DLS was used to follow their sizes. Aliquots of the mixtures (DuR-BNGs + BSA) were then subjected to centrifugation (13,000 rpm x 30 min) to precipitate the formed DuR-BNG/BSA aggregates. Non-specific interaction of DuR-BNGs with BSA was measured using bicinchoninic acid (BCA) assay (Pierce® BCA Assay Kit) according to manufacturer's instruction. Briefly, aliquots of the supernatants (25 μL) were transferred into a 96-well plate and mixed with BCA reagent (200 μL). Blank controls (BSA only) were run simultaneously. The mixtures were then incubated at 37 °C for 30 min. Their absorbance was measured at $\lambda = 562$ nm using a Powerwave HT Microplate Reader (Bio-Tek). The percentage of free BSA was calculated as the wt ratio of BSA in the supernatants of the mixtures containing DuR-BNGs to that in control (with no DuR-BNGs).

A calibration curve was constructed as follows; a series of BSA solutions at various concentrations ranging 0 - 2000 μg/mL was prepared by diluting standard BSA solution (2 mg/mL, provided by the manufacture) with different amounts of PBS. The resulting solutions (25 μL) were transferred into a 96-well plate, and mixed with BCA reagent (200 μL). After the mixtures were then incubated at 37 °C for 30 min, their absorbance was measured at $\lambda = 562$ nm.

4.2.9 DOX Loading

DOX-loaded DuR-BNGs were prepared by mixing an aqueous stock solution of DOX (1.3 mg/mL, 1 mL, 5 wt% of DuR-BNGs solids) with aqueous purified DuR-BNGs (6.1 mg/mL, 4 mL). After being incubated for 24 hrs at 37 °C, the resulting mixture was dialyzed against water (1 L) to remove free DOX for 48 hr. Outer water was changed every 12 hrs, yielding aqueous DOX-loaded DuR-BNG solution at 4.1 mg/mL. UV/Vis spectra were recorded to determine loading level of DOX by the weight ratio of loaded DOX to dried DuR-BNGs.

4.2.10 Dual stimuli-responsive release of DOX using UV/Vis spectroscopy

For acidic pH-responsive release, aliquots of aqueous DOX-loaded DuR-BNG solution (2 mL) were placed in a dialysis tubing and immersed in aqueous KHP buffer solutions at different pH values (50 mL). For thermoresponsive release of DOX, the similar procedure was applied. Experiments were performed at 25, 37, and 42 °C respectively (pH = 7). The absorbance of DOX in outer water was recorded at 3 min intervals of using a UV/Vis spectrometer equipped with an

external probe at λ_{ex} = 497 nm. For quantitative analysis, solution in the tubing was combined with outer water and the UV/Vis spectrum of the resulting mixture was recorded.

4.2.11 Cell culture

HeLa cancer cells were cultured in DMEM (Dulbecco's modified Eagle's medium) containing 10% FBS (fetal bovine serum) and 1% antibiotics (50 units/mL penicillin and 50 units/mL streptomycin) at 37 °C in a humidified atmosphere containing 5% CO_2.

4.2.12 Cell viability using MTT assay

Cells were plated at 5 x 10^5 cells/well into a 96-well plate and incubated for 24 hrs in DMEM (100 μL) containing 10% FBS for the following experiments. They were then incubated with various concentrations of empty and DOX-loaded DuR-BNGs for 48 hrs. Blank controls (cells only) were run simultaneously. Cell viability was measured using CellTiter 96 Non-Radioactive Cell Proliferation Assay kit (MTT, Promega) according to manufacturer's instruction. Briefly, 3-(4,5-dimethylthiazol-2-yl)-2,5-diphenyltetrazolium bromide (MTT) solutions (15 μL) was added into each well. After 4 h incubation, the medium containing unreacted MTT was carefully removed. DMSO (100 μL) was added into each well in order to dissolve the formed formazan blue crystals, and then the absorbance at λ = 570 nm was recorded using Powerwave HT Microplate Reader (Bio-Tek). Each concentration was 12-replicated. Cell viability was calculated as the percent ratio of absorbance of mixtures with nanogels to control (cells only).

4.2.13 Confocal laser scanning microscopy (CLSM)

Cells plated at 2×10^5 cells/well into a 6-well plate were incubated with DOX-loaded DuR-BNGs (80μL, DOX = 1 μg/mL), free DOX (10μL, DOX = 1 μg/mL) and pure DuR-BNGs (60μL, DuR-BNGs = 45μg/mL) as a control at 37 °C for 5h. After culture medium was removed, cells were washed with PBS thee times. After the removal of supernatants, the cells were fixed with cold methanol (-20 °C) for 20 min at 4 °C. The slides were rinsed with tris-buffered saline Tween-20 (TBST) thee times. Cells were stained with 2-(4-amidinophenl)-6-indolecarbamidine

(DAPI) for 5 min. The fluorescence images were obtained using a LSM 510 Meta/Axiovert 200 (Carl Zeiss, Jena, Germany).

4.2.14 Flow cytometry

HeLa cells were plated at 5×10^5 cells/well into a six-well plate and incubated in DMEM (2 mL) at 37 °C. After 24 h, cells were treated with DOX-loaded DuR-BNGs (80μL, DOX = 1 μg/mL), free DOX (10μL, DOX = 1 μg/mL) and pure DuR-BNGs (60μL, DuR-BNGs = 45μg/mL) as a control at 37 °C for 4h. After the culture medium was removed, the cells were washed with PBS solution and treated with trypsin. The cells were suspended in DMEM (500 μL) for flow cytometry measurements. Data analysis was performed by means of a BD FACSCANTO II flow cytometer and BD FACSDiva software.

4.3 Results and Discussion

4.3.1 Synthesis of DuR-BNGs

The synthesis of dual temperature and acidic pH-responsive CMC-grafted bionanogels (DuR-BNGs) was accomplished by aqueous crosslinking polymerization assisted via temperature-driven self-association method (see Scheme 4.1). OEOMA (MW = 300 g/mol, #EO = 5.5) and MEO_2MA (MW = 188 g/mol, #EO = 2) were selected as biocompatible thermoresponsive monomers to demonstrate the feasibility of our system. All polymerizations were initiated with a water soluble azo-initiator (VA-44) at 40 ºC in the presence of CMC.

To study thermal properties of uncrosslinked CMC-grafted thermoresponsive copolymers, aqueous polymerization of a mixture of OEOMA and MEO_2MA in the presence of CMC was examined. Their mole ratios were varied to synthesize a series of CMC-g-P(MEO_2MA-co-OEOMA) copolymers with different amounts of hydrophobic MEO_2MA units (see appendix B for detailed synthesis). DLS technique to follow the change in LS intensity was used to examine their thermal properties (Figure B.3). As seen in Figure 4.1, the phase transition temperature (called LCST) of CMC-g-P(MEO_2MA-co-OEOMA) decreased from 57 to 29 ºC as the amount of hydrophobic MEO_2MA units increased in grafted P(MEO_2MA-co-OEOMA) from 0 to 75 mol%. Such decrease has been reported for P(MEO_2MA-co-OEOMA) copolymers with no CMC.[46]

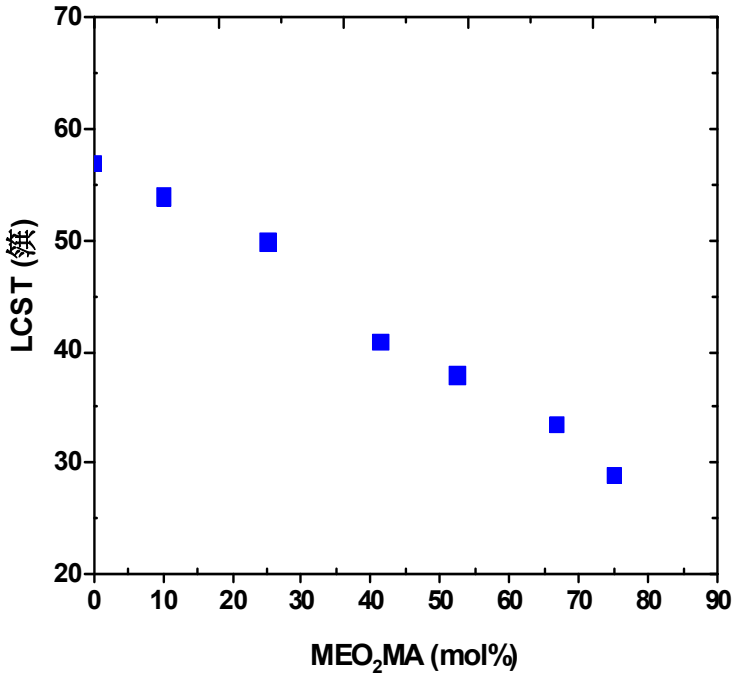

Figure 4.1. LCST of CMC-g-P((MEO$_2$MA-co-OEOMA) as a function of the amount of hydrophobic MEO$_2$MA units.

To synthesize crosslinked DuR-BNGs, the optimized procedure that allows for the synthesis of CMC-g-P(MEO$_2$MA-co-OEOMA) with its LCST = 29 ºC was applied in the presence of OEODMA crosslinker. During the polymerization at 40 ºC, above the LCST, the thermoresponsive P(MEO$_2$MA-co-OEOMA) chains grafted from CMC become hydrophobic thereby collapse with each other. Because CMC backbones retain hydrophilic at 40 ºC, the formed grafted chains tend to self-associate to form micelle-like aggregates; concurrently they are crosslinked in the presence of OEODMA crosslinkers, yielding well-defined DuR-BNGs with narrow size distribution through temperature-driven self-association assisted method.[262]

The resulting DuR-BNGs were characterized for their thermal property as well as size and morphology by DLS and TEM techniques. The resulting DuR-BNGs exhibit LCST = 32 ºC at 4.6 mg/mL (Figure B.4). The LCST is slightly greater than that (29 ºC) of the corresponding uncrosslinked CMC-g-P6 (Table B.1), which is presumably due to the introduction of OEODMA having relatively long hydrophilic OEO chains (#EO = 9.5) increasing the hydrophilicity of the DuR-BNGs. The size of DuR-BNGs was determined to be 10.5 nm in diameter by DLS and 16.7±4.6 nm with spherical morphology by TEM (Figure 4.2).

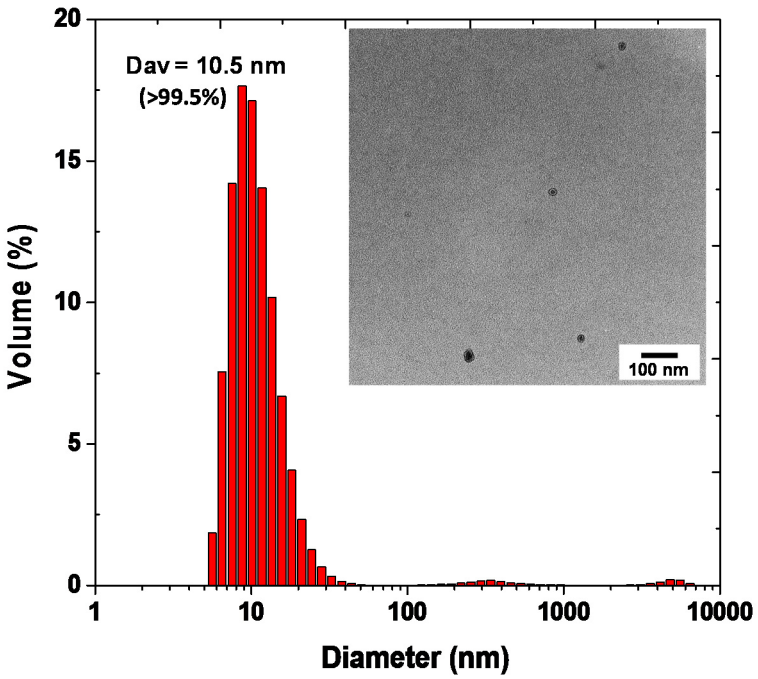

Figure 4.2. DLS diagram and TEM image (inset) of DuR-BNGs measured at 25 ºC.

4.3.2 Prolonged colloidal stability and non-specific protein absorption

Prolonged colloidal stability during blood circulation and after extravasation into tumor tissues (pH < 6.5) is an important property for tumor-targeting nanocarriers. Herein, two experiments were designed to examine colloidal stability of the resulting DuR-BNGs. In an experiment, DuR-BNGs were incubated in buffer solutions at different pH values of 5.5 and 7.0 over time at room temperature. As seen in Figure 4.3, their diameter as measured by DLS did not significantly change over two weeks, suggesting excellent colloidal stability of DuR-BNGs in the range of pHs. In another set of experiment, DuR-BNGs were incubated with a typical serum protein: bovine serum albumin (BSA) at pH = 7.4 (mimic physiological conditions) as a model to test their non-specific interaction with serum proteins *in vitro*. Human serum albumin is one of the most abundant protein in blood serum and is found at concentrations ranging from 35 - 50 g/L. Herein, two different amounts of BSA, as a model protein, at the wt ratio of DuR-BNGs/BSA = 1/30 and 1/45 in PBS were examined. After 72 hrs, the DLS diagrams of the mixtures show monomodal distribution with diameter ≈ 7 nm and no occurrence of significant aggregation (Figure 4.4a). Furthermore, BCA assay was used to evaluate the non-specific

interaction of DuR-BNGs with BSA by quantifying the concentration of free BSA in the supernatants of DuR-BNGs/BSA mixtures after incubation of 48 and 72 hrs. A calibration curve was first constructed with absorbance at λ = 562 nm over BSA concentrations (Figure B.5). The curve was then used to determine the amount of free BSA within the supernatants. As seen in Figure 4.4b, DuR-BNGs exhibit no significant non-specific interactions with BSA. These results suggest that the DuR-BNGs based on biocompatible CMC and P(MEO_2MA-co-OEOMA) are colloidally stable and enable preventing non-specific protein adsorption in physiological conditions.

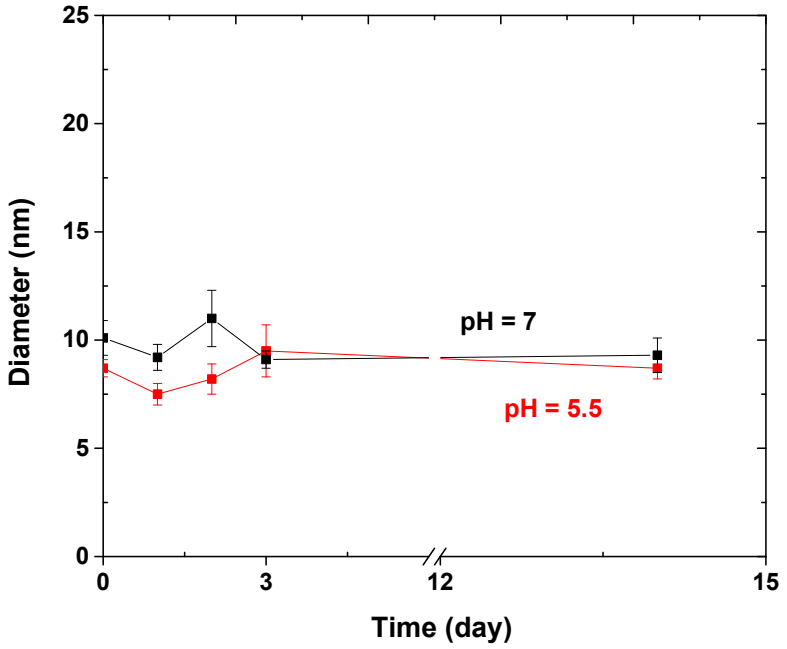

Figure 4.3. Evolution of diameter of DuR-BNGs in buffer solutions at pH = 5.5 and 7.0.

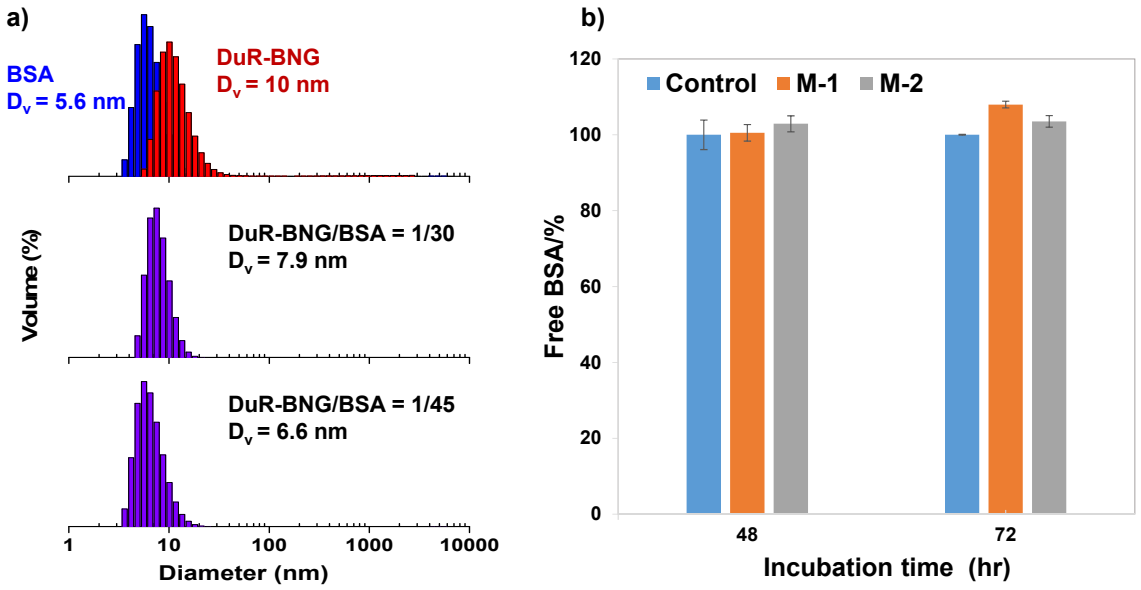

Figure 4.4. DLS diagrams of mixtures consisting of different wt ratios of DuR-BNG/BSA = 1/30 (BSA = 30 mg/mL) (M-1) and 1/45 (BSA = 45 mg/mL) (M-2) in PBS at pH = 7.4 and after 72 hrs (a) and the percentage of free BSA in supernatants at 48 and 72 hrs (b).

4.3.3 Encapsulation of DOX

To preliminarily evaluate the efficacy of DuR-BNGs as tumor-targeting drug delivery nanocarriers, DOX loaded DuR-BNGs were prepared by mixing an aqueous DOX stock solution with aqueous DuR-BNG dispersion. After the aqueous mixtures were incubated at 37 ºC (above LCST) for 24 hrs, they were then subjected to an intensive dialysis for 48 hrs. The removal of free (not encapsulated) DOX was monitored by the change in the UV absorbance of DOX at λ = 497 nm in outer water. Using an extinction coefficient of DOX = 10,000 M^{-1} cm^{-1} in water at λ = 497 nm,[263] the loading level = 2.5 ± 0.3 wt % and loading efficiency = 49.2 ± 5.8 % were determined at the initial wt ratio of DOX/DuR-BNGs = 1/20.

4.3.4 Dual stimuli-responsive release of encapsulated DOX

The enhanced release kinetics of encapsulated DOX from DOX-loaded DuR-BNGs in response to change in temperature and pH was investigated. DOX molecules released from DOX-loaded DuR-BNGs diffuse out of dialysis tubing; the accumulative DOX in outer water was monitored by UV spectrometer with an external probe at λ = 497 nm.

Temperature-responsive release was first examined for DOX-loaded DuR-BNGs in dialysis tubing incubated in KHP buffer (pH = 7) at different temperatures. As seen in Figure 4.5a, the amount of encapsulated DOX released from DOX-loaded DuR-BNGs gradually increased over time. Furthermore, DOX release was faster at temperatures above LCST. Such rapid release is attributed to the hydrophobic transition of thermoresponsive DuR-BNGs, which causes nanogel to shrink and aggregate, thus expelling the encapsulated DOX (Scheme 4.1). Interestingly, a burst release was observed in the initial time of release (mostly within 300 min). To get an insight into the thermoresponsive release of encapsulated DOX, the release kinetics in the early stage (within 300 min) was investigated using Fickian's diffusion model. Figure 4.5a is re-plotted with $\ln(C_o/C_t)$ over time in Figure B.6, where C_o is the initial concentration of DOX and C_t is its concentration at time t within dialysis bag. By fitting the data to linear regression, apparent diffusion constants (D_{app}) were estimated to be 0.30/hr at 43 ºC, 0.20/hr at 40 ºC, 0.16/hr at 37 ºC and 0.06/hr at 25 ºC. The result suggests greater D_{app} value at higher temperature.

Given the enhanced release in response to higher temperature, acidic pH-responsive release of encapsulated DOX was investigated at 37 ºC. DOX release was monitored by immersing DOX-loaded DuR-BNGs in buffer at pH = 5.5 (mimic to cancer cell environment) and pH = 7 (physiological condition). As seen in Figure 4.5b, DOX release was rapid at pH = 5.5, compared with pH = 7. The enhanced release at pH = 5.5 is attributed to less interactions between DOX and CMC. At neutral pH = 7, amine groups of DOX molecules exist in the protonated form ($NH_3^+Cl^-$ forms) because pKa of DOX = 8.3, while carboxylic acid groups on CMC exist in the anionic (COO^-) form (note pKa of COOH = 4.3). Such electrostatic interactions between DOX and DuR-BNGs slow down DOX release. However, at pH = 5.5 (close to the pKa of COOH), more carboxylic acid groups exist as their neutral form (COOH). This could decrease the electrostatic interactions between DOX and DuR-BNGs. Figure B.7 suggests that the change of ionic strength of solution did not significantly affect the DOX release.

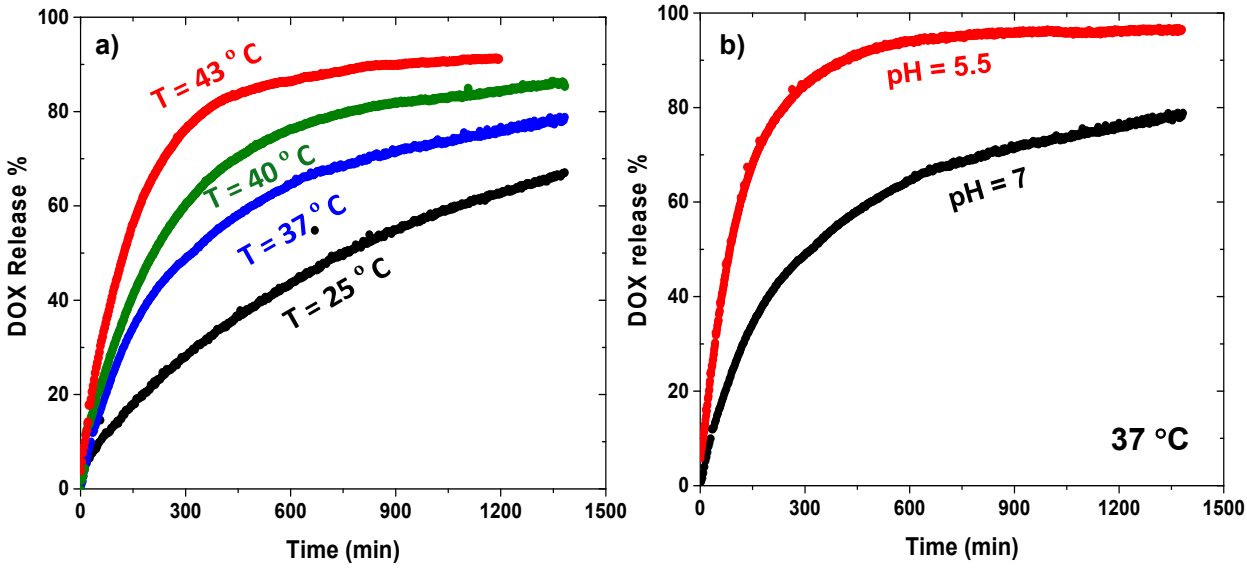

Figure 4.5. Release of DOX from DOX-loaded DuR-BNGs in aqueous buffer solution (pH = 7) at different temperatures of 25, 37, 40, and 43 ºC (a) and at pH = 5.5 and 7 (37 ºC) (b).

4.3.5 Intracellular trafficking and antitumor activity of DOX-loaded DuR-BNGs

Intracellular trafficking of DOX-loaded DuR-BNGs was investigated by flow cytometry and CLSM. Figure 4.6a shows the flow cytometric histograms of HeLa cells incubated with DOX-loaded DuR-BNGs compared with free DOX and empty DuR-BNGs as controls. The amount of DOX in DOX-loaded DuR-BNGs was designed to be the same as free DOX. Histograms present noticeable elevated fluorescence intensity compared to empty DuR-BNGs. Figure 4.6b shows CLSM images of HeLa cells incubated with and without DOX-loaded DuR-BNGs for 5 hrs. For comparison, HeLa cells were also incubated with free DOX. HeLa nuclei were stained with DAPI. The cells nuclei show clear DOX fluorescence signal; this suggest that DOX was released from DOX-loaded DuR-BNGs to reach cell nuclei within 5 hrs. Notice that the fluorescence intensity of DOX from DOX-loaded DuR-BNGs is similar with free DOX. Taking into account both results, DuR-BNGs were able to deliver and rapidly release encapsulated DOX into cells and reach cells nuclei.

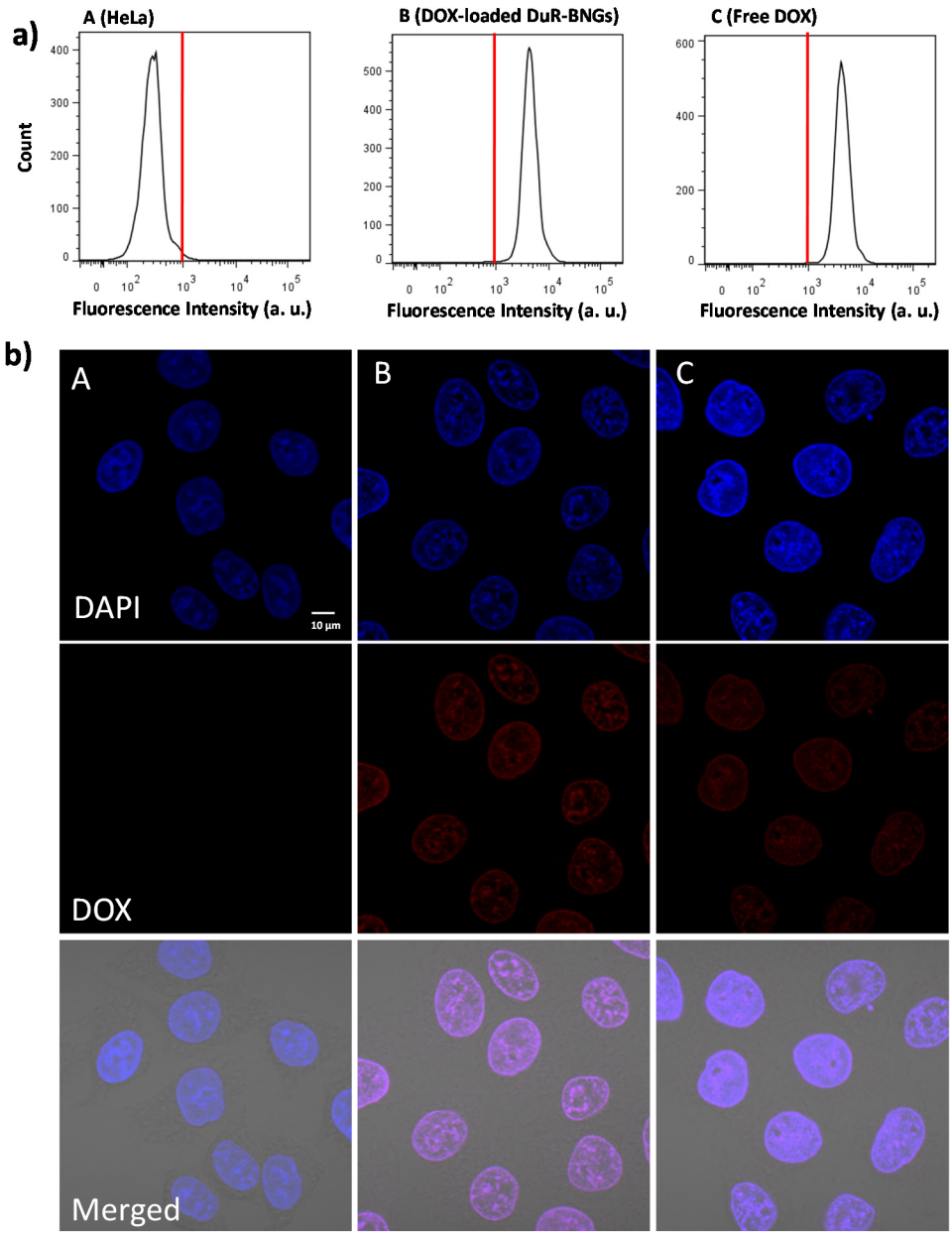

Figure 4.6. Flow cytometric histograms (a) and CLSM images of HeLa cells incubated with DuR-BNGs only (A), DOX-loaded DuR-BNGs (B), and free DOX (C) for 5 hrs (b). Scale bar = 10 μm.

In vitro cytotoxicity of Dox-free and DOX-loaded DuR-BNGs were evaluated by MTT colorimetric assay using HeLa cancer cells. As seen in Figure 4.7a, empty DuR-BNGs exhibit > 90% of HeLa cell viability, suggesting non-toxicity of DuR-BNGs at concentrations up to 1.0 mg/mL. In the presence of DOX-loaded DuR-BNGs, however, the viability of HeLa cells

decreased with an increasing amount of both free and encapsulated DOX (Figure 4.7b). Promisingly, the HeLa cell viability in the presence of DOX-loaded DuR-BNGs is competitive to that with free DOX at all concentrations tested in the experiment. This decrease in HeLa cell viability suggests the inhibition of cellular proliferation due to the effective and rapid release of DOX from DuR-BNGs.

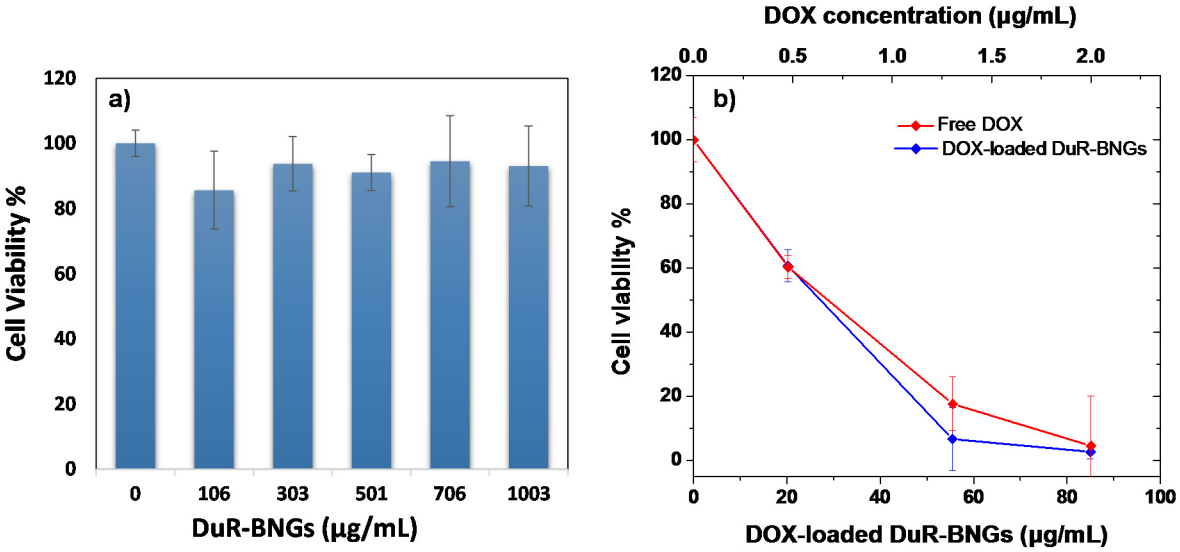

Figure 4.7. Viability of HeLa cells incubated with different amounts of DuR-BNGs only (a), DOX-loaded DuR-BNGs and free DOX for 48 hrs (b) determined by MTT assay

4.4 Conclusion

We have synthesized dual temperature/acidic pH-responsive DuR-BNGs with narrow size distribution by a facile aqueous crosslinking polymerization assisted with temperature-driven self-association method. These well-defined nanogels had excellent colloidal stability at a broad pH range and in the presence of proteins *in vitro*. They exhibited enhanced release upon changes in their morphologies (volumes or ionic interactions) in response to individual stimuli including high temperature and acidic pH; furthermore the DuR-BNGs promoted synergic release of encapsulated anticancer drugs in the presence of both stimuli. Cell culture results from CLSM, flow cytometry, and MTT viability assay suggest intracellular release of anticancer drugs from DOX-loaded DuR-BNGs into HeLa cancer cells. These results suggest that new DuR-BNGs are a promising candidate as tumor-targeting drug delivery vehicles for chemotherapy and hyperthermia.

Chapter 5
Conclusion and Future Work

Polymer-based drug delivery systems have been explored to circumvent challenges facing small drugs: limited drug efficiency and side effects. In particular, naturally-occurring polysaccharides can be considered as promising building blocks in constructing drug delivery nanocarriers. Furthermore, nanocarriers that are able to undergo chemical or physical changes in response to external stimuli offer great opportunities for controlled release of encapsulated drugs. In this thesis, two types of dual stimuli-responsive polysaccharide-based BNGs were developed, and their applications toward tumor-targeting drug delivery were evaluated.

First, well-defined pH/reduction-responsive CMC-based ssBNGs were synthesized by a facile aqueous crosslinking polymerization of OEOMA in the presence of CMC and a disulfide-labeled crosslinker (ssDMA). The resulting ssBNGs had the diameter ≈ 25 nm confirmed by DLS and TEM. DOX was physically encapsulated within ssBNGs through electrostatic interactions. ssBNGs exhibit enhanced drug release in response to acidic pH due to a less interactions between DOX and ssBNGs, and reducing agent due to the reductive cleavage of disulfide bonds. Furthermore, their ability to facile conjugating with cell-targeting ligands was demonstrated using a water soluble UV-active dye as a model cell-targeting biomolecule.

Second, the dual temperature/acidic pH-responsive DuR-BNGs were prepared by aqueous crosslinking polymerization assisted with temperature-driven self-association method, yielding narrow-size distribution of DuR-BNGs with diameter ≈ 11 nm. The DuR-BNGs had good colloidal stability in physiological and acidic pH conditions. For biological perspective, DuR-BNGs show negligible non-specific protein absorption with model protein BSA for up to 72 hrs. In response to high temperature and acidic pH, DuR-BNGs underwent changes in volume or ionic interactions triggering rapid drug release. Potential applications toward drug delivery of two types of BNGs have been evaluated with MTT viability assay and cellular uptake test by CLSM and flow cytometry.

In summary, the thesis presents different dual stimuli-responsive BNGs fabricated via aqueous crosslinking polymerization. Although they display promising features toward drug

delivery applications, further improvements are required toward effective tumor-targeting drug delivery applications. First of all, ssBNGs exhibited insignificant enhancement of DOX release in response to reducing agent possibly due to the low crosslink density of nanogel networks. In the meantime, the use of large amount of crosslinkers can lead to significant inter-particle crosslinking and aggregation. One potential solution is to introduce thiol (SH) groups into polysaccharide backbones. The pendant thiol groups will generate disulfide cross linkages through thiol-disulfide exchange reaction, thereby increasing the crosslink density of polymer networks.[118] Furthermore, the prepared BNGs display some premature drug release within physiological environment. The interaction between drug and polymer matrix plays a key role in determining the drug loading capacity and release profile.[264] Physically encapsulated drugs easily diffuse out of nanogel matrix causing leakage.[50] Chemically attached drug molecules avoid premature release, but they potentially suffer from slow drug release when the cleavage of labile linkage between drug and nanogel are slow or incomplete.[265] Therefore, further understanding is necessary to reduce premature drug release and achieve desirable pharmacokinetics. Finally, DuR-BNGs exhibited enhanced drug release at higher temperature, which makes them to be good candidates for hyperthermia treatment. New thermoresponsive BNGs that sensitive to small change in temperature will be highly desired since the temperature difference a human body can tolerate is very limited. Toward this goal, more work is needed to enhance the sensitivity of the nanocarriers.

References

[1] S. Taurin, H. Nehoff, K. Greish, *Journal of Controlled Release* **2012**, *164*, 265-275.

[2] A. P. Blum, J. K. Kammeyer, A. M. Rush, C. E. Callmann, M. E. Hahn, N. C. Gianneschi, *Journal of the American Chemical Society* **2015**, *137*, 2140-2154.

[3] O. C. Farokhzad, R. Langer, *ACS Nano* **2009**, *3*, 16-20.

[4] A. Prokop, J. M. Davidson, *Journal of Pharmaceutical Sciences* **2008**, *97*, 3518-3590.

[5] Y. H. Bae, K. Park, *Journal of Controlled Release* **2011**, *153*, 198-205.

[6] L. M. Bareford, P. W. Swaan, *Advanced Drug Delivery Reviews* **2007**, *59*, 748-758.

[7] R. T. Chacko, J. Ventura, J. Zhuang, S. Thayumanavan, *Advanced Drug Delivery Reviews* **2012**, *64*, 836-851.

[8] N. Nishiyama, K. Kataoka, *Advances in Polymer Science* **2006**, *193*, 67-101.

[9] D. Peer, J. M. Karp, S. Hong, O. C. Farokhzad, R. Margalit, R. Langer, *Nature Nanotechnology* **2007**, *2*, 751-760.

[10] Y. Wen, J. K. Oh, *Macromolecular Rapid Communications* **2014**, *35*, 1819-1832.

[11] Z. Liu, Y. Jiao, Y. Wang, C. Zhou, Z. Zhang, *Advanced Drug Delivery Reviews* **2008**, *60*, 1650-1662.

[12] T. Coviello, P. Matricardi, C. Marianecci, F. Alhaique, *Journal of Controlled Release* **2007**, *119*, 5-24.

[13] M. Tizzotti, A. Charlot, E. Fleury, M. Stenzel, J. Bernard, *Macromolecular Rapid Communications* **2010**, *31*, 1751-1772.

[14] K. E. Sapsford, W. R. Algar, L. Berti, K. B. Gemmill, B. J. Casey, E. Oh, M. H. Stewart, I. L. Medintz, *Chemical Reviews* **2013**, *113*, 1904-2074.

[15] C. Alvarez-Lorenzo, B. Blanco-Fernandez, A. M. Puga, A. Concheiro, *Advanced Drug Delivery Reviews* **2013**, *65*, 1148-1171.

[16] D. Klemm, B. Heublein, H. P. Fink, A. Bohn, *Angewandte Chemie International Edition in English* **2005**, *44*, 3358-3393.

[17] J. A. Yang, K. Park, H. Jung, H. Kim, S. W. Hong, S. K. Yoon, S. K. Hahn, *Biomaterials* **2011**, *32*, 8722-8729.

[18] B. C. Bae, K. Na, *Biomaterials* **2010**, *31*, 6325-6335.

[19] N. Morimoto, X.-P. Qiu, F. o. Winnik, K. Akiyoshi, *Macromolecules* **2008**, *41*, 5985-5987.

[20] K. Peng, C. Cui, I. Tomatsu, F. Porta, A. H. Meijer, H. P. Spaink, A. Kros, *Soft Matter* **2010**, *6*, 3778-3783.

[21] Y. Gao, Z. Zhang, L. Chen, W. Gu, Y. Li, *Biomacromolecules* **2009**, *10*, 2175-2182.

[22] P. Pereira, D. Morgado, A. Crepet, L. David, F. M. Gama, *Macromolecular Bioscience* **2013**, *13*, 1369-1378.

[23] J. Jing, D. Alaimo, E. De Vlieghere, C. Jérôme, O. De Wever, B. G. De Geest, R. Auzély-Velty, *Journal of Materials Chemistry B* **2013**, *1*, 3883.

[24] A. Zhang, Z. Zhang, F. Shi, J. Ding, C. Xiao, X. Zhuang, C. He, L. Chen, X. Chen, *Soft Matter* **2013**, *9*, 2224-2233.

[25] L. Ma, H. Kang, R. Liu, Y. Huang, *Langmuir* **2010**, *26*, 18519-18525.

[26] F. M. Goycoolea, M. E. Fernández-Valle, I. Aranaz, Á. Heras, *Macromolecular Chemistry and Physics* **2011**, *212*, 887-895.

[27] J. K. Oh, D. I. Lee, J. M. Park, *Progress in Polymer Science* **2009**, *34*, 1261-1282.

[28] J. W. Nichols, Y. H. Bae, *Nano Today* **2012**, *7*, 606-618.

[29] H. S. Choi, W. Liu, P. Misra, E. Tanaka, J. P. Zimmer, B. Itty Ipe, M. G. Bawendi, J. V. Frangioni, *Nature Biotechnology* **2007**, *25*, 1165-1170.

[30] F. Sultana, Manirujjaman, M. Imran-Ul-Haque, *Journal of Applied Pharmaceutical Science* **2013**, *3*, S95-S105.

[31] C. A. Schutz, L. Juillerat-Jeanneret, P. Kauper, C. Wandrey, *Biomacromolecules* **2011**, *12*, 4153-4161.

[32] S. Zhou, X. Min, H. Dou, K. Sun, C. Y. Chen, C. T. Chen, Z. Zhang, Y. Jin, Z. Shen, *Chemical Communications (Cambridge, England)* **2013**, *49*, 9473-9475.

[33] Y. Wen, J. K. Oh, *RSC Advances* **2014**, *4*, 229-237.

[34] X. Zhang, S. Malhotra, M. Molina, R. Haag, *Chemical Society Reviews* **2015**.

[35] C. I. Crucho, *ChemMedChem* **2015**, *10*, 24-38.

[36] A. P. Blum, J. K. Kammeyer, A. M. Rush, C. E. Callmann, M. E. Hahn, N. C. Gianneschi, *Journal of American Chemical Society* **2015**, *137*, 2140-2154.

[37] Q. Zhang, N. Re Ko, J. Kwon Oh, *Chemical Communications* **2012**, *48*, 7542-7552.

[38] W. Lv, S. Liu, W. Feng, J. Qi, G. Zhang, F. Zhang, X. Fan, *Macromolecular Rapid Communications* **2011**, *32*, 1101-1107.

[39] J. B. Weaver, *Nature nanotechnology* **2010**, *5*, 630-631.

[40] J. van der Zee, *Annals of Oncology* **2002**, *13*, 1173-1184.

[41] M. A. Ward, T. K. Georgiou, *Polymers* **2011**, *3*, 1215-1242.

[42] D. Roy, W. L. A. Brooks, B. S. Sumerlin, *Chemical Society Reviews* **2013**, *42*, 7214-7243.

[43] C. Duan, D. Zhang, F. Wang, D. Zheng, L. Jia, F. Feng, Y. Liu, Y. Wang, K. Tian, F. Wang, Q. Zhang, *International Journal of Pharmaceutics* **2011**, *409*, 252-259.

[44] C. R. Becer, S. Hahn, M. W. M. Fijten, H. M. L. Thijs, R. Hoogenboom, U. S. Schubert, *Journal of Polymer Science Part A: Polymer Chemistry* **2008**, *46*, 7138-7147.

[45] W. Yuan, J. Zhang, H. Zou, T. Shen, J. Ren, *Polymer* **2012**, *53*, 956-966.

[46] C. Porsch, S. Hansson, N. Nordgren, E. Malmström, *Polymer Chemistry* **2011**, *2*, 1114.

[47] Z. Deng, Z. Zhen, X. Hu, S. Wu, Z. Xu, P. K. Chu, *Biomaterials* **2011**, *32*, 4976-4986.

[48] G. Tamura, Y. Shinohara, I. Akiba, A. Tamura, M. Oishi, Y. Nagasaki, K. Sakurai, Y. Amemiya, *Journal of Physics: Conference Series* **2011**, *272*, 012018.

[49] M. Zan, J. Li, S. Luo, Z. Ge, *Chemical Communications (Cambridge, England)* **2014**, *50*, 7824-7827.

[50] W. Chen, K. Achazi, B. Schade, R. Haag, *Journal of Controlled Release* **2014**.

[51] G. F. Payne, S. R. Raghavan, *Soft Matter* **2007**, *3*, 521.

[52] R. Stern, M. J. Jedrzejas, *Chemical Reviews* **2008**, *108*, 5061-5085.

[53] J. Credou, T. Berthelot, *Journal of Materials Chemistry B* **2014**, 2, 4767-4788.

[54] J. Berger, M. Reist, J. M. Mayer, O. Felt, N. A. Peppas, R. Gurny, *European Journal of Pharmaceutics and Biopharmaceutics* **2004**, *57*, 19-34.

[55] T. C. Laurent, Editor, "*The Chemistry, Biology and Medical Applications of Hyaluronan and its Derivatives. [In: Wenner-Gren Int. Ser., 1998; 72]"*, 1998, p. 341 pp.

[56] S. A. Agnihotri, N. N. Mallikarjuna, T. M. Aminabhavi, *Journal of Controlled Release* **2004**, *100*, 5-28.

[57] J. K. Oh, R. Drumright, D. J. Siegwart, K. Matyjaszewski, *Progress in Polymer Science* **2008**, *33*, 448-477.

[58] E. Vieira, A. Cestari, C. Airoldi, W. Loh, *Biomacromolecules* **2008**, *9*, 1195-1199.

[59] N. Bhattarai, J. Gunn, M. Zhang, *Advanced Drug Delivery Reviews* **2010**, *62*, 83-99.

[60] A. M. Martins, C. M. Alves, F. Kurtis Kasper, A. G. Mikos, R. L. Reis, *Journal of Materials Chemistry* **2010**, *20*, 1638-1645.

[61] S. N. Pawar, K. J. Edgar, *Biomaterials* **2012**, *33*, 3279-3305.

[62] S. Tan, K. Ladewig, Q. Fu, A. Blencowe, G. G. Qiao, *Macromolecular Rapid Communications* **2014**, *35*, 1166-1184.

[63] M. Zan, J. Li, S. Luo, Z. Ge, *Chemical Communications* **2014**, *50*, 7824-7827.

[64] Y. Lee, H. Lee, Y. B. Kim, J. Kim, T. Hyeon, H. Park, P. B. Messersmith, T. G. Park, *Advanced Materials* **2008**, *20*, 4154-4157.

[65] M. Creixell, A. P. Herrera, M. Latorre-Esteves, V. Ayala, M. Torres-Lugo, C. Rinaldi, *Journal of Materials Chemistry* **2010**, *20*, 8539-8547.

[66] S. Taheri, G. Baier, P. Majewski, M. Barton, R. Foerch, K. Landfester, K. Vasilev, *Journal of Materials Chemistry B* **2014**, *2*, 1838-1845.

[67] N. Gogoi, D. Chowdhury, *Journal of Materials Chemistry B* **2014**, *2*, 4089-4099.

[68] K. Y. Choi, K. H. Min, J. H. Na, K. Choi, K. Kim, J. H. Park, I. C. Kwon, S. Y. Jeong, *Journal of Materials Chemistry* **2009**, *19*, 4102.

[69] T. Nakai, T. Hirakura, Y. Sakurai, T. Shimoboji, M. Ishigai, K. Akiyoshi, *Macromolecular Bioscience* **2012**, *12*, 475-483.

[70] M.-H. Alves, H. Sfeir, J.-F. Tranchant, E. Gombart, G. Sagorin, S. Caillol, L. Billon, M. Save, *Biomacromolecules* **2014**, *15*, 242-251.

[71] S. M. Sagnella, H. Duong, A. MacMillan, C. Boyer, R. Whan, J. A. McCarroll, T. P. Davis, M. Kavallaris, *Biomacromolecules* **2014**, *15*, 262-275.

[72] P. S. Pramod, K. Takamura, S. Chaphekar, N. Balasubramanian, M. Jayakannan, *Biomacromolecules* **2012**, *13*, 3627-3640.

[73] B. Cao, L. Li, H. Wu, Q. Tang, B. Sun, H. Dong, J. Zhe, G. Cheng, *Chemical Communications (Cambridge, England)* **2014**, *50*, 3234-3237.

[74] N. Morimoto, S. Hirano, H. Takahashi, S. Loethen, D. H. Thompson, K. Akiyoshi, *Biomacromolecules* **2013**, *14*, 56-63.

[75] P. Liu, B. Shi, C. Yue, G. Gao, P. Li, H. Yi, M. Li, B. Wang, Y. Ma, L. Cai, *Polymer Chemistry* **2013**, *4*, 5793-5799.

[76] Y. Wang, Y. Liu, Y. Liu, Y. Wang, J. Wu, R. Li, J. Yang, N. Zhang, *Polymer Chemistry* **2014**, *5*, 423-432.

[77] R. Novoa-Carballal, C. Silva, S. Moller, M. Schnabelrauch, R. L. Reis, I. Pashkuleva, *Journal of Materials Chemistry B* **2014**, *2*, 4177-4184.

[78] O. Dechy-Cabaret, B. Martin-Vaca, D. Bourissou, *Chemical Reviews* **2004**, *104*, 6147-6176.

[79] S. Penczek, M. Cypryk, A. Duda, P. Kubisa, S. Slomkowski, *Progress in Polymer Science* **2007**, *32*, 247-282.

[80] K. Matyjaszewski, T. P. Davis, "Handbook of Radical Polymerization", John Wiley & Sons Inc., 2002.

[81] P. Marcasuzaa, S. Reynaud, F. Ehrenfeld, A. Khoukh, J. Desbrieres, *Biomacromolecules* **2010**, *11*, 1684-1691.

[82] P. Dobrzynski, D. Fabbri, C. Torri, J. Kasperczyk, B. Kaczmarczyk, M. Pastusiak, *Journal of Polymer Science Part A: Polymer Chemistry* **2008**, *47*, 247-257.

[83] M. P. Bajgai, S. Aryal, S. R. Bhattarai, K. C. R. Bahadur, K.-W. Kim, H. Y. Kim, *Journal of Applied Polymer Science* **2008**, *108*, 1447-1454.

[84] W. Yuan, J. Yuan, F. Zhang, X. Xie, *Biomacromolecules* **2007**, *8*, 1101-1108.

[85] E. Ostmark, D. Nystrom, E. Malmstrom, *Macromolecules* **2008**, *41*, 4405-4415.

[86] M. Kamigaito, T. Ando, M. Sawamoto, *Chemical Reviews* **2001**, *101*, 3689-3745.

[87] K. Matyjaszewski, J. Xia, *Chemical Reviews* **2001**, *101*, 2921-2990.

[88] C. Boyer, V. Bulmus, T. P. Davis, V. Ladmiral, J. Liu, S. Perrier, *Chemical Reviews* **2009**, *109*, 5402-5436.

[89] J. Chiefari, Y. K. Chong, F. Ercole, J. Krstina, J. Jeffery, T. P. T. Le, R. T. A. Mayadunne, G. F. Meijs, C. L. Moad, G. Moad, E. Rizzardo, S. H. Thang, *Macromolecules* **1998**, *31*, 5559-5562.

[90] J. K. Oh, D. I. Lee, J. M. Park, *Prog. Polym. Sci.* **2009**, *34*, 1261-1282.

[91] A. S. Goldmann, M. Glassner, A. J. Inglis, C. Barner-Kowollik, *Macromolecular Rapid Communications* **2013**, *34*, 810-849.

[92] B. S. Sumerlin, A. P. Vogt, *Macromolecules* **2010**, *43*, 1-13.

[93] M. A. Gauthier, M. I. Gibson, H.-A. Klok, *Angewandte Chemie International Edition* **2009**, *48*, 48-58.

[94] B. Le Droumaguet, K. Velonia, *Macromolecular Rapid Communications* **2008**, *29*, 1073-1089.

[95] W. H. Binder, R. Sachsenhofer, *Macromolecular Rapid Communications* **2008**, *29*, 952-981.

[96] Q. He, W. Wu, K. Xiu, Q. Zhang, F. Xu, J. Li, *International Journal of Pharmaceutics* **2013**, *443*, 110-119.

[97] I. Otsuka, C. Travelet, S. Halila, S. Fort, I. Pignot-Paintrand, A. Narumi, R. Borsali, *Biomacromolecules* **2012**, *13*, 1458-1465.

[98] W. Yuan, Z. Zhao, S. Gu, J. Ren, *Journal of Polymer Science Part A: Polymer Chemistry* **2010**, *48*, 3476-3486.

[99] C. E. Hoyle, C. N. Bowman, *Angewandte Chemie International Edition* **2010**, *49*, 1540-1573.

[100] C. E. Hoyle, A. B. Lowe, C. N. Bowman, *Chemical Society Reviews* **2010**, *39*, 1355-1387.

[101] M. J. Kade, D. J. Burke, C. J. Hawker, *Journal of Polymer Science Part A: Polymer Chemistry* **2010**, *48*, 743-750.

[102] B. D. Mather, K. Viswanathan, K. M. Miller, T. E. Long, *Progress in Polymer Science* **2006**, *31*, 487-531.

[103] H. Lee, C. H. Ahn, T. G. Park, *Macromolecular Bioscience* **2009**, *9*, 336-342.

[104] L. Qiu, L. Zhang, C. Zheng, R. Wang, *Journal of Pharmaceutical Sciences* **2011**, *100*, 2430-2442.

[105] X. Wei, X. Lv, Q. Zhao, L. Qiu, *Acta Biomaterialia* **2013**, *9*, 6953-6963.

[106] M. H. Ramadan, J. E. Prata, O. Karacsony, G. Duner, N. R. Washburn, *Langmuir* **2014**, *30*, 7485-7495.

[107] P. Huang, C. Yang, J. Liu, W. Wang, S. Guo, J. Li, Y. Sun, H. Dong, L. Deng, J. Zhang, J. Liu, A. Dong, *Journal of Materials Chemistry B* **2014**, *2*, 4021-4033.

[108] C. Allen, D. Maysinger, A. Eisenberg, *Colloids and Surfaces B: Biointerfaces* **1999**, *16*, 3-27.

[109] J. Zhao, J. Liu, S. Han, H. Deng, L. Deng, J. Liu, A. Meng, A. Dong, J. Zhang, *Polymer Chemistry* **2014**, *5*, 1852-1856.

[110] E. Östmark, D. Nyström, E. Malmström, *Macromolecules* **2008**, *41*, 4405-4415.

[111] Y. Sasaki, Y. Tsuchido, S.-i. Sawada, K. Akiyoshi, *Polymer Chemistry* **2011**, *2*, 1267.

[112] U. Hasegawa, S. Sawada, T. Shimizu, T. Kishida, E. Otsuji, O. Mazda, K. Akiyoshi, *Journal of Controlled Release* **2009**, *140*, 312-317.

[113] X. Yang, S. Kootala, J. Hilborn, D. A. Ossipov, *Soft Matter* **2011**, *7*, 7517-7525.

[114] Q. Zhang, N. R. Ko, J. K. Oh, *Chemical Communications* **2012**, *48*, 7542-7552.

[115] O. J. Cayre, N. Chagneux, S. Biggs, *Soft Matter* **2011**, *7*, 2211-2234.

[116] C. J. F. Rijcken, O. Soga, W. E. Hennink, C. F. van Nostrum, *Journal of Controlled Release* **2007**, *120*, 131-148.

[117] Y. L. Li, L. Zhu, Z. Liu, R. Cheng, F. Meng, J. H. Cui, S. J. Ji, Z. Zhong, *Angewandte Chemie International Edition in English* **2009**, *48*, 9914-9918.

[118] J. Tan, H. Kang, R. Liu, D. Wang, X. Jin, Q. Li, Y. Huang, *Polymer Chemistry* **2011**, *2*, 672-678.

[119] E. Aschenbrenner, K. Bley, K. Koynov, M. Makowski, M. Kappl, K. Landfester, C. K. Weiss, *Langmuir* **2013**, *29*, 8845-8855.

[120] L. Messager, N. Portecop, E. Hachet, V. Lapeyre, I. Pignot-Paintrand, B. Catargi, R. Auzely-Velty, V. Ravaine, *Journal of Materials Chemistry B* **2013**, *1*, 3369-3379.

[121] D. Klinger, E. M. Aschenbrenner, C. K. Weiss, K. Landfester, *Polymer Chemistry* **2012**, *3*, 204-216.

[122] D. Klinger, K. Landfester, *Journal of Polymer Science Part A: Polymer Chemistry* **2012**, *50*, 1062-1075.

[123] M.-H. Hsiao, M. Larsson, A. Larsson, H. Evenbratt, Y.-Y. Chen, Y.-Y. Chen, D.-M. Liu, *Journal of Controlled Release* **2012**, *161*, 942-948.

[124] C.-Y. Chuang, T.-M. Don, W.-Y. Chiu, *Journal of Polymer Science Part A: Polymer Chemistry* **2010**, *48*, 2377-2387.

[125] D. R. Biswal, R. P. Singh, *Carbohydrate Polymers* **2004**, *57*, 379-387.

[126] C. Duan, J. Gao, D. Zhang, L. Jia, Y. Liu, D. Zheng, G. Liu, X. Tian, F. Wang, Q. Zhang, *Biomacromolecules* **2011**, *12*, 4335-4343.

[127] M. F. Leung, J. Zhu, F. W. Harris, P. Li, *Macromolecular Rapid Communications* **2004**, *25*, 1819-1823.

[128] C. Duan, D. Zhang, F. Wang, D. Zheng, L. Jia, F. Feng, Y. Liu, Y. Wang, K. Tian, F. Wang, Q. Zhang, *International Journal of Pharmaceutics* **2011**, *409*, 252-259.

[129] Z. Zhao, Z. Zhang, L. Chen, Y. Cao, C. He, X. Chen, *Langmuir* **2013**, *29*, 13072-13080.

[130] X. Chen, L. Chen, X. Yao, Z. Zhang, C. He, J. Zhang, X. Chen, *Chemical Communications* **2014**, *50*, 3789-3791.

[131] C. Y. Ang, S. Y. Tan, X. Wang, Q. Zhang, M. Khan, L. Bai, S. Tamil Selvan, X. Ma, L. Zhu, K. T. Nguyen, N. S. Tan, Y. Zhao, *Journal of Materials Chemistry B* **2014**, *2*, 1879-1890.

[132] F. M. Goycoolea, G. Lollo, C. Remunan-Lopez, F. Quaglia, M. J. Alonso, *Biomacromolecules* **2009**, *10*, 1736-1743.

[133] C. A. Schutz, L. Juillerat-Jeanneret, P. Kauper, C. Wandrey, *Biomacromolecules* **2011**, *12*, 4153-4161.

[134] F. Maggi, S. Ciccarelli, M. Diociaiuti, S. Casciardi, G. Masci, *Biomacromolecules* **2011**, *12*, 3499-3507.

[135] P. Liu, C. Yue, B. Shi, G. Gao, M. Li, B. Wang, Y. Ma, L. Cai, *Chemical Communications* **2013**, *49*, 6143-6145.

[136] Y. Song, Y. Zhou, L. Chen, *Journal of Materials Chemistry* **2012**, *22*, 2512-25192.

[137] M. J. Moura, H. Faneca, M. P. Lima, M. H. Gil, M. M. Figueiredo, *Biomacromolecules* **2011**, *12*, 3275-3284.

[138] R. P. Narayanan, G. Melman, N. J. Letourneau, N. L. Mendelson, A. Melman, *Biomacromolecules* **2012**, *13*, 2465-2471.

[139] E. Josef, M. Zilberman, H. Bianco-Peled, *Acta Biomaterialia* **2010**, *6*, 4642-4649.

[140] J. R. Roberts, D. W. Ritter, M. J. McShane, *Journal of Materials Chemistry B* **2013**, *107*, 3195-3201.

[141] A. Tokarev, P. Agulhon, J. Long, F. Quignard, M. Robitzer, R. A. S. Ferreira, L. D. Carlos, J. Larionova, C. Guérin, Y. Guari, *Journal of Materials Chemistry* **2012**, *22*, 20232-20242.

[142] J. Picard, S. Giraudier, V. Larreta-Garde, *Soft Matter* **2009**, *5*, 4198-4205.

[143] L.-J. Lin, M. Larsson, D.-M. Liu, *Soft Matter* **2011**, *7*, 5816-5825.

[144] S. Yamanlar, S. Sant, T. Boudou, C. Picart, A. Khademhosseini, *Biomaterials* **2011**, *32*, 5590-5599.

[145] R. Fernandez, C. Ocando, S. C. M. Fernandes, A. Eceiza, A. Tercjak, *Biomacromolecules* **2014**, *15*, 1399-1407.

[146] B. Chen, K. L. Liu, Z. Zhang, X. Ni, S. H. Goh, J. Li, *Chemical Communications (Cambridge, England)* **2012**, *48*, 5638-5640.

[147] F. van de Manakker, L. M. J. Kroon-Batenburg, T. Vermonden, C. F. van Nostrum, W. E. Hennink, *Soft Matter* **2010**, *6*, 187-194.

[148] N. Lin, A. Dufresne, *Biomacromolecules* **2013**, *14*, 871-880.

[149] J. Yu, H. Fan, J. Huang, J. Chen, *Soft Matter* **2011**, *7*, 7386-7394.

[150] J. H. Jang, Y. M. Choi, Y. Y. Choi, M. K. Joo, M. H. Park, B. G. Choi, E. Y. Kang, B. Jeong, *Journal of Materials Chemistry* **2011**, *21*, 5484-5491.

[151] E. Y. Kang, H. J. Moon, M. K. Joo, B. Jeong, *Biomacromolecules* **2012**, *13*, 1750-1757.

[152] D. Mortisen, M. Peroglio, M. Alini, D. Eglin, *Biomacromolecules* **2010**, *11*, 1261-1272.

[153] Y. Lee, H. J. Chung, S. Yeo, C.-H. Ahn, H. Lee, P. B. Messersmith, T. G. Park, *Soft Matter* **2010**, *6*, 977-983.

[154] A. Khanlari, M. S. Detamore, S. H. Gehrke, *Macromolecules* **2013**, *46*, 9609-9617.

[155] E. Hachet, H. Van Den Berghe, E. Bayma, M. R. Block, R. Auzely-Velty, *Biomacromolecules* **2012**, *13*, 1818-1827.

[156] C. M. Valmikinathan, V. J. Mukhatyar, A. Jain, L. Karumbaiah, M. Dasari, R. V. Bellamkonda, *Soft Matter* **2012**, *8*, 1964-1976.

[157] M. Hamcerencu, J. Desbrieres, M. Popa, G. Riess, *Biomacromolecules* **2009**, *10*, 1911-1922.

[158] J. Voepel, U. Edlund, A.-C. Albertsson, *Journal of Polymer Science Part A: Polymer Chemistry* **2009**, *47*, 3595-3606.

[159] Y. Dong, A. O. Saeed, W. Hassan, C. Keigher, Y. Zheng, H. Tai, A. Pandit, W. Wang, *Macromolecular Rapid Communications* **2011**, 120-126.

[160] R. Kennedy, W. Ul Hassan, A. Tochwin, T. Zhao, Y. Dong, Q. Wang, H. Tai, W. Wang, *Polymer Chemistry* **2014**, *5*, 1838-1842.

[161] T. Hirakura, K. Yasugi, T. Nemoto, M. Sato, T. Shimoboji, Y. Aso, N. Morimoto, K. Akiyoshi, *Journal of Controlled Release* **2010**, *142*, 483-489.

[162] A. Takahashi, Y. Suzuki, T. Suhara, K. Omichi, A. Shimizu, K. Hasegawa, N. Kokudo, S. Ohta, T. Ito, *Biomacromolecules* **2013**, *14*, 3581-3588.

[163] B. Sarker, D. G. Papageorgiou, R. Silva, T. Zehnder, F. Gul-E-Noor, M. Bertmer, J. Kaschta, K. Chrissafis, R. Detsch, A. R. Boccaccini, *Journal of Materials Chemistry B* **2014**, *2*, 1470-1482.

[164] B. Guo, A. Finne-Wistrand, A. C. Albertsson, *Biomacromolecules* **2011**, *12*, 2601-2609.

[165] O. P. Varghese, M. Kisiel, E. Martinez-Sanz, D. A. Ossipov, J. Hilborn, *Macromolecular Rapid Communications* **2010**, *31*, 1175-1180.

[166] H. Tan, J. P. Rubin, K. G. Marra, *Macromolecular Rapid Communications* **2011**, *32*, 905-911.

[167] C. Lee, J. Shin, J. S. Lee, E. Byun, J. H. Ryu, S. H. Um, D. I. Kim, H. Lee, S. W. Cho, *Biomacromolecules* **2013**, *14*, 2004-2013.

[168] N. Q. Tran, Y. K. Joung, E. Lih, K. D. Park, *Biomacromolecules* **2011**, *12*, 2872-2880.

[169] W. Lu, J. Sun, X. Jiang, *Journal of Materials Chemistry B* **2014**, *2*, 2369-2380.

[170] K. A. Rieger, N. P. Birch, J. D. Schiffman, *Journal of Materials Chemistry B* **2013**, *1*, 4531-4541.

[171] C. Huang, S. J. Soenen, E. van Gulck, G. Vanham, J. Rejman, S. Van Calenbergh, C. Vervaet, T. Coenye, H. Verstraelen, M. Temmerman, J. Demeester, S. C. De Smedt, *Biomaterials* **2012**, *33*, 962-969.

[172] A. Y. A. Kaassis, N. Young, N. Sano, H. A. Merchant, D.-G. Yu, N. P. Chatterton, G. R. Williams, *Journal of Materials Chemistry B* **2014**, *2*, 1400-1407.

[173] C. E. Pegg, G. H. Jones, T. J. Athauda, R. R. Ozer, J. M. Chalker, *Chemical Communications (Cambridge, England)* **2014**, *50*, 156-158.

[174] S. Arola, T. Tammelin, H. Setala, A. Tullila, M. B. Linder, *Biomacromolecules* **2012**, *13*, 594-603.

[175] J. Miao, R. C. Pangule, E. E. Paskaleva, E. E. Hwang, R. S. Kane, R. J. Linhardt, J. S. Dordick, *Biomaterials* **2011**, *32*, 9557-9567.

[176] L. Meli, J. Miao, J. S. Dordick, R. J. Linhardt, *Green Chemistry* **2010**, *12*, 1883-1892.

[177] J. L. Shamshina, G. Gurau, L. E. Block, L. K. Hansen, C. Dingee, A. Walters, R. D. Rogers, *Journal of Materials Chemistry B* **2014**, *2*, 3924-3936.

[178] R. Langer, D. A. Tirrell, *Nature* **2004**, *428*, 487-492.

[179] R. Langer, *Accounts of Chemical Research* **2000**, *33*, 94-101.

[180] A. S. Hoffman, P. S. Stayton, O. Press, N. Murthy, C. A. Lackey, C. Cheung, F. Black, J. Campbell, N. Fausto, T. R. Kyriakides, P. Bornstein, *Polymers for Advanced Technologies* **2002**, *13*, 992-999.

[181] A. S. Hoffman, *Advanced Drug Delivery Reviews* **2002**, *54*, 3-12.

[182] N. A. Peppas, *Advanced Drug Delivery Reviews* **2004**, *56*, 1529-1531.

[183] J. Khandare, T. Minko, *Progress in Polymer Science* **2006**, *31*, 359-397.

[184] M. J. Vicent, F. Greco, R. I. Nicholson, A. Paul, P. C. Griffiths, R. Duncan, *Angewandte Chemie International Edition* **2005**, *44*, 4061-4066.

[185] S. Liu, R. Maheshwari, K. L. Kiick, *Macromolecules* **2009**, *42*, 3-13.

[186] O. C. Farokhzad, J. Cheng, B. A. Teply, I. Sherifi, S. Jon, P. W. Kantoff, J. P. Richie, R. Langer, *Proceedings of the National Academy of Sciences of the United States of America* **2006**, *103*, 6315-6320.

[187] S. H. Kim, J. H. Jeong, K. W. Chun, T. G. Park, *Langmuir* **2005**, *21*, 8852-8857.

[188] A. E. van der Ende, E. J. Kravitz, E. Harth, *Journal of the American Chemical Society* **2008**, *130*, 8706-8713.

[189] J. Wu, A. Eisenberg, *Journal of the American Chemical Society* **2006**, *128*, 2880-2884.

[190] W. Li, J. A. Yoon, K. Matyjaszewski, *Journal of the American Chemical Society* **2010**, *132*, 7823-7825.

[191] E. Kim, D. Kim, H. Jung, J. Lee, S. Paul, N. Selvapalam, Y. Yang, N. Lim, C. G. Park, K. Kim, *Angewandte Chemie International Edition* **2010**, *49*, 4405-4408.

[192] A. Blanazs, S. P. Armes, A. J. Ryan, *Macromolecular Rapid Communications* **2009**, *30*, 267-277.

[193] A. S. Mikhail, C. Allen, *Journal of Controlled Release* **2009**, *138*, 214-223.

[194] X.-B. Xiong, A. Falamarzian, S. M. Garg, A. Lavasanifar, *Journal of Controlled Release* **2011**, *155*, 248-261.

[195] R. Langer, J. P. Vacanti, *Science* **1993**, *260*, 920-926.

[196] A. S. Hoffman, *Journal of Controlled Release* **1987**, *6*, 297-305.

[197] N. A. Peppas, J. Z. Hilt, A. Khademhosseini, R. Langer, *Advanced Materials* **2006**, *18*, 1345-1360.

[198] B. V. Slaughter, S. S. Khurshid, O. Z. Fisher, A. Khademhosseini, N. A. Peppas, *Advanced Materials* **2009**, *21*, 3307-3329.

[199] J. K. Oh, R. Drumright, D. J. Siegwart, K. Matyjaszewski, *Progress in Polymer Science.* **2008**, *33*, 448-477.

[200] M. Hamidi, A. Azadi, P. Rafiei, *Advanced Drug Delivery Reviews* **2008**, *60*, 1638-1649.

[201] K. Raemdonck, J. Demeester, S. De Smedt, *Soft Matter* **2009**, *5*, 707-715.

[202] J. K. Oh, *Canadian Journal of Chemistry* **2010**, *88*, 173-184.

[203] A. V. Kabanov, S. V. Vinogradov, *Angewandte Chemie International Edition* **2009**, *48*, 5418-5429.

[204] J. K. Oh, D. I. Lee, J. M. Park, *Progress in Polymer Science* **2009**.

[205] Z. Liu, Y. Jiao, Y. Wang, C. Zhou, Z. Zhang, *Advanced Drug Delivery Reviews* **2008**, *60*, 1650-1662.

[206] B. K. Nanjawade, F. V. Manvi, A. S. Manjappa, *Journal of Controlled Release* **2007**, *122*, 119-134.

[207] N. Bhattarai, J. Gunn, M. Zhang, *Advanced Drug Delivery Review* **2010**, *62*, 83-99.

[208] S. Van Vlierberghe, P. Dubruel, E. Schacht, *Biomacromolecules* **2011**, *12*, 1387-1408.

[209] E. Hachet, H. Van Den Berghe, E. Bayma, M. R. Block, R. Auzely-Velty, *Biomacromolecules* **2012**, *13*, 1818-1827.

[210] M. A. J. Mazumder, N. A. D. Burke, F. Shen, M. A. Potter, H. D. H. Stover, *Biomacromolecules* **2009**, *10*, 1365-1373.

[211] A.-F. Che, Z.-M. Liu, X.-J. Huang, Z.-G. Wang, Z.-K. Xu, *Biomacromolecules* **2008**, *9*, 3397-3403.

[212] Y. Wu, P. Ni, M. Zhang, X. Zhu, *Soft Matter* **2010**, *6*, 3751.

[213] D. Klinger, K. Landfester, *Polymer* **2012**, *53*, 5209-5231.

[214] C. Tsitsilianis, *Soft Matter* **2010**, *6*, 2372-2388.

[215] M. Motornov, Y. Roiter, I. Tokarev, S. Minko, *Progress in Polymer Science* **2010**, *35*, 174-211.

[216] N. Rapoport, *Progress in Polymer Science* **2007**, *32*, 962-990.

[217] A. K. Bajpai, S. K. Shukla, S. Bhanu, S. Kankane, *Progress in Polymer Science* **2008**, *33*, 1088-1118.

[218] H. G. Schild, *Progress in Polymer Science* **1992**, *17*, 163-249.

[219] S. Aoshima, S. Kanaoka, *Advances in Polymer Science* **2008**, *210*, 169-208.

[220] N. Murthy, M. Xu, S. Schuck, J. Kunisawa, N. Shastri, J. M. J. Frechet, *Proceedings of the National Academy of Sciences of the United States of America* **2003**, *100*, 4995-5000.

[221] V. Bulmus, Y. Chan, Q. Nguyen, H. L. Tran, *Macromolecular Bioscience* **2007**, *7*, 446-455.

[222] E. Themistou, C. S. Patrickios, *Macromolecules* **2007**, *40*, 5231-5234.

[223] Y. Zhao, *Macromolecules* **2012**, *45*, 3647-3657.

[224] M. W. Tibbitt, A. M. Kloxin, L. A. Sawicki, K. S. Anseth, *Macromolecules* **2013**, *46*, 2785-2792.

[225] S. Nayak, L. A. Lyon, *Angewandte Chemie International Edition* **2004**, *43*, 6706-6709.

[226] R. V. Ulijn, *Journal of Materials Chemistry* **2006**, *16*, 2217-2225.

[227] B. Soontornworajit, J. Zhou, M. T. Shaw, T.-H. Fan, Y. Wang, *Chemical Communications* **2010**, *46*, 1857-1859.

[228] S. G. Levesque, M. S. Shoichet, *Bioconjugate Chemistry* **2007**, *18*, 874-885.

[229] R. A. Petros, P. A. Ropp, J. M. DeSimone, *Journal of the American Chemical Society* **2008**, *130*, 5008-5009.

[230] H. A. Aliyar, P. D. Hamilton, N. Ravi, *Biomacromolecules* **2005**, *6*, 204-211.

[231] J. K. Oh, D. J. Siegwart, H.-i. Lee, G. Sherwood, L. Peteanu, J. O. Hollinger, K. Kataoka, K. Matyjaszewski, *Journal of the American Chemical Society* **2007**, *129*, 5939-5945.

[232] B. Gyarmati, B. Vajna, A. Nemethy, K. Laszlo, A. Szilagyi, *Macromolecular Bioscience* **2013**, *13*, 633-640.

[233] C. Li, J. Madsen, S. P. Armes, A. L. Lewis, *Angewandte Chemie International Edition* **2006**, *45*, 3510-3513.

[234] N. V. Tsarevsky, K. Matyjaszewski, *Macromolecules* **2005**, *38*, 3087-3092.

[235] A. Russo, W. DeGraff, N. Friedman, J. B. Mitchell, *Cancer Research* **1986**, *46*, 2845-2848.

[236] G. Saito, J. A. Swanson, K.-D. Lee, *Advanced Drug Delivery Reviews* **2003**, *55*, 199-215.

[237] W. Lv, S. Liu, W. Feng, J. Qi, G. Zhang, F. Zhang, X. Fan, *Macromolecular Rapid Communications* **2011**, *32*, 1101-1107.

[238] Y.-L. Li, L. Zhu, Z. Liu, R. Cheng, F. Meng, J.-H. Cui, S.-J. Ji, Z. Zhong, *Angewandte Chemie International Edition* **2009**, *48*, 9914-9918.

[239] W. Chen, M. Zheng, F. Meng, R. Cheng, C. Deng, J. Feijen, Z. Zhong, *Biomacromolecules* **2013**, *14*, 1214-1222.

[240] D. Klinger, E. M. Aschenbrenner, C. K. Weiss, K. Landfester, *Polymer Chemistry* **2012**, *3*, 204-216.

[241] X. Yang, S. Kootala, J. Hilborn, D. A. Ossipov, *Soft Matter* **2011**, *7*, 7517-7525.

[242] N. Morimoto, X.-P. Qiu, F. M. Winnik, K. Akiyoshi, *Macromolecules* **2008**, *41*, 5985-5987.

[243] S. A. Bencherif, N. R. Washburn, K. Matyjaszewski, *Biomacromolecules* **2009**, *10*, 2499-2507.

[244] M.-H. Hsiao, K.-H. Lin, D.-M. Liu, *Soft Matter* **2013**, *9*, 2458-2466.

[245] C.-Y. Chuang, W.-Y. Chiu, T.-M. Don, *Journal of Applied Polymer Science* **2011**, *120*, 1659-1670.

[246] L. Brannon-Peppas, *Journal of Controlled Release* **2000**, *66*, 321.

[247] K. Knop, R. Hoogenboom, D. Fischer, U. S. Schubert, *Angewandte Chemie International Edition* **2010**, *49*, 6288-6308.

[248] J. K. Oh, C. Tang, H. Gao, N. V. Tsarevsky, K. Matyjaszewski, *Journal of the American Chemical Society* **2006**, *128*, 5578-5584.

[249] D. W. Jenkins, S. M. Hudson, *Chemical Reviews* **2001**, *101*, 3245-3273.

[250] A. A. Berlin, V. N. Kislenko, *Progress in Polymer Science* **1992**, *17*, 765-825.

[251] S. M. Derkaoui, T. Avramoglou, C. Barbaud, D. Letourneur, *Biomacromolecules* **2008**, *9*, 3033-3038.

[252] L.-M. Zhang, L.-Q. Chen, *Journal of Applied Polymer Science* **2002**, *83*, 2755-2761.

[253] J. Andrew MacKay, M. Chen, J. R. McDaniel, W. Liu, A. J. Simnick, A. Chilkoti, *Nature Materials* **2009**, *8*, 993-999.

[254] J. D. Byrne, T. Betancourt, L. Brannon-Peppas, *Advanced Drug Delivery Reviews* **2008**, *60*, 1615-1626.

[255] O. Veiseh, J. W. Gunn, M. Zhang, *Advanced Drug Delivery Reviews* **2010**, *62*, 284-304.

[256] M. J. Vicent, *The AAPS Journal* **2007**, *9*, E200-E207.

[257] V. Delplace, P. Couvreur, J. Nicolas, *Polymer Chemistry* **2014**, *5*, 1529-1544.

[258] D. Peer, J. M. Karp, S. Hong, O. C. Farokhzad, R. Margalit, R. Langer, *Nature Nanotechnology* **2007**, *2*, 751-760.

[259] N. Nishiyama, K. Kataoka, *Advances in Polymer Science* **2006**, *193*, 67-101.

[260] A. Harada, K. Kataoka, *Progress in Polymer Science* **2006**, *31*, 949-982.

[261] Y. Wang, J. Nie, B. Chang, Y. Sun, W. Yang, *Biomacromolecules* **2013**, *14*, 3034-3046.

[262] S. Zhou, X. Min, H. Dou, K. Sun, C.-Y. Chen, C.-T. Chen, Z. Zhang, Y. Jin, Z. Shen, *Chemical Communications (Cambridge, U. K.)* **2013**, *49*, 9473-9475.

[263] J. Andrew MacKay, M. Chen, J. R. McDaniel, W. Liu, A. J. Simnick, A. Chilkoti, *Nature Materials* **2009**, *8*, 993-999.

[264] W. B. Liechty, D. R. Kryscio, B. V. Slaughter, N. A. Peppas, *Annual review of chemical and biomolecular engineering* **2010**, *1*, 149-173.

[265] L. Jiang, Z.-m. Gao, L. Ye, A.-y. Zhang, Z.-g. Feng, *Biomaterials Science* **2013**, *1*, 1282.

Appendix A

I. Aqueous FRP of OEOMA without CMC

A series of FRP of OEOMA in water were carried out under different conditions. As a typical example, the procedure to synthesize FRP-2 (Table A.1) under the conditions of OEOMA = 10 mg/mL and VA-44 = 2% of OEOMA at 40 °C is described as follows; OEOMA (0.15 g, 0.32 mmol) was dissolved in water (15 mL) in a 25 mL Schlenk flask. The resulting clear solution was purged with nitrogen for 30 min under magnetic stirring, and then heated to 40 °C in a water bath for 10 min. A nitrogen-prepurged aqueous stock solution of VA-44 (0.3 mL, 10 mg/mL, 9.3 μmol) was added using a syringe to initiate the polymerization. For kinetic studies, samples were withdrawn at different time intervals during the polymerization to determine conversion by ^{1}H-NMR. Polymerization was stopped by cooling down to room temperature.

Kinetic studies of aqueous FRP of OEOMA

A series of FRP of OEOMA in aqueous solution was carried out in the presence of a water-soluble VA-44 azo-type free-radical initiator. VA-44 was selected because of its short half-life at lower temperature ($\tau_{1/2}$ = 10 hrs at 44 °C). Important parameters that influence the rate of aqueous FRP were examined; these parameters include the amount of VA-44 and temperature. For kinetic studies, aliquots withdrawn at given time intervals were analyzed for monomer conversion using ^{1}H-NMR in D_2O. Table A.1 summarizes the results. First, the amount of VA-44 was varied at 40 °C. The rate of polymerization increased with an increasing amount of VA-44 in the mixture. For example, OEOMA conversion was 63% in the presence of 1 wt% VA-44 after 2 hrs (FRP-1). The conversion increased to 78% with 2 wt% VA-44 (FRP-2), and further to 83% with 3 wt% (FRP-3) under similar conditions. However, molecular weight decreased when the amount of VA-44 increased. Such decrease is attributed to the increase in flux of free radicals generated by thermal decomposition of VA-44 initiators. Next, the polymerization temperature decreased to 30 °C in the presence of 2 wt% VA-44 (FRP-4). The conversion decreased from 78% to 67% by approximately 10%, compared to FRP-2 at 40 °C. For all polymerization reactions, molecular weight distribution of the resulting POEOMA homopolymers was broad as $M_w/M_n > 2.6$, due to

polymerization being preceded in uncontrolled manner. These results suggest that the rate of polymerization is enhanced in the presence of larger amounts of initiator at higher temperatures.

Table A.1. Characteristics and results for FRP of OEOMA in aqueous solution after 2 hrs.

Recipe	OEOMA (mg/mL)	VA-44 [a)] (wt%)	Temp (°C)	Conv [b)]	M_n [c)] (g/mol)	M_w/M_n
FRP-1	10	1	40	0.63	159,600	2.6
FRP-2	10	2	40	0.78	115,000	3.3
FRP-3	10	4	40	0.83	97,800	3.3
FRP-4	10	2	30	0.67	120,000	3.2

a) Wt% based on OEOMA; b) Determined by ^{1}H-NMR in D_2O; c) Determined by GPC.

II. Aqueous FRP of OEOMA in the presence of CMC

For the synthesis of POEOMA-g-CMC, similar procedure for aqueous FRP of OEOMA was conducted in the presence of CMC at 40 °C. For an example of FRP-C1, CMC (0.15 g) and OEOMA (0.15 g, 0.32 mmol) were dissolved in water (15 mL) in 25mL Schlenk flask. The resulting clear solution was purged with nitrogen for 30 min under magnetic stirring and then heated to 40 °C in a water bath for 10 min. A nitrogen-prepurged aqueous stock solution of VA-44 (0.3 mL, 10 mg/mL, 9.3 μmol) was added using a syringe to initiate the polymerization. Polymerization was stopped by cooling down to room temperature.

Preparation of POEOMA-g-CMC

The results of a series of FRP of OEOMA initiated with a water-soluble VA-44 azo-type free-radical initiator in aqueous solution are described. The optimized procedure was applied to the synthesis of POEOMA-grafted CMC (POEOMA-g-CMC). An aqueous FRP of OEOMA in the presence of CMC was conducted at 40 °C under the conditions of OEOMA = 10 mg/mL, VA-44 = 2 wt% on OEOMA, and OEOMA/CMC = 1/1 wt ratio (FRP-C1 in Table 3.1). Due to the high molecular weight of CMC, the viscosity of its aqueous solution strongly relies on the

concentration of CMC. It was found that 1 wt% aqueous CMC solution is suitable for FRP. For more than 10 repeated polymerization reactions, conversion reached 80.4 ± 4.3% on average after 2 hrs. This value is similar to that (conv = 78%) without CMC (FRP-2 in Table A.1), suggesting no significant effect of the presence of CMC on the course of aqueous FRP under the conditions. DLS was used to measure the size and size distribution of the resulting POEOMA-g-CMC in water. As seen in Figure 3.1 (10 mg/mL), DLS trace shows multimodal size distribution with three populations; the major population of small sizes with an average diameter ≈ 23 nm and two minor populations of larger aggregates with average diameters ≈ 86 and 487 nm. These three populations resulted in the number average diameter, D_n = 32.5 ± 11.5 nm and relatively broad size distribution, D_w/D_n = 1.5. Such multimodal distribution with relatively high standard deviation could be attributed to inter-chain or inter-particle coupling reactions, resulting in the formation of undesired aggregates.

The amount of OEOMA (as well as CMC) in the polymerization mixtures decreased from 10 mg/mL to 2 mg/mL and further to 0 mg/mL (CMC only) for aqueous FRP at 40 °C, while other parameters remained constant (OEOMA/CMC = 1/1 w/w and VA-44 = 0.2 mg/mL). Table A.2 summarizes the characteristics and conversion data. For all polymerization, conversion reached as high as 80%; however, longer polymerization time was required when smaller amount of OEOMA was added. For example, FRP-C4 with 2 mg/mL OEOMA reached 81% conversion in 8 hrs. DLS results indicate that the sizes of the resulting products prepared in the presence of OEOMA are larger than that (diameter = 1 nm) of CMC only in water, suggesting the occurrence of grafting POEOMA from CMC chains (Figure 3.1). Interestingly, their diameter decreased with a decreasing amount of OEOMA; 33 nm at 10 mg/mL (FRP-C1) to 20 nm at 6.7 mg/mL (FRP-C2), and further to 9 nm at 2 mg/mL (FRP-C4). Polydispersity also decreased. These results suggest that the probability to inter-chain or inter-particle coupling reaction could decrease with lower concentration of OEOMA in aqueous solution.

Table A.2. Characteristics and results for aqueous FRP of OEOMA in the presence of CMC at 40 °C.[a)]

Recipe	OEOMA (mg/mL)	Time (hrs)	Conv[b)]
FRP-C1	10	2	0.83
FRP-C2	6.7	4	0.84
FRP-C3	3.3	5	0.86
FRP-C4	2	8	0.81

a) VA-44 = 0.2 mg/mL, OEOMA/CMC = 1/1 wt/wt; b) Determined by ^{1}H-NMR in D_2O.

Figure A.1. DLS diagrams of POEOMA synthesized by aqueous FRP with various concentrations of OEOMA in water ranging from 0 to 10 mg/mL. VA-44 = 0.2 wt% of OEOMA, T = 40 °C.

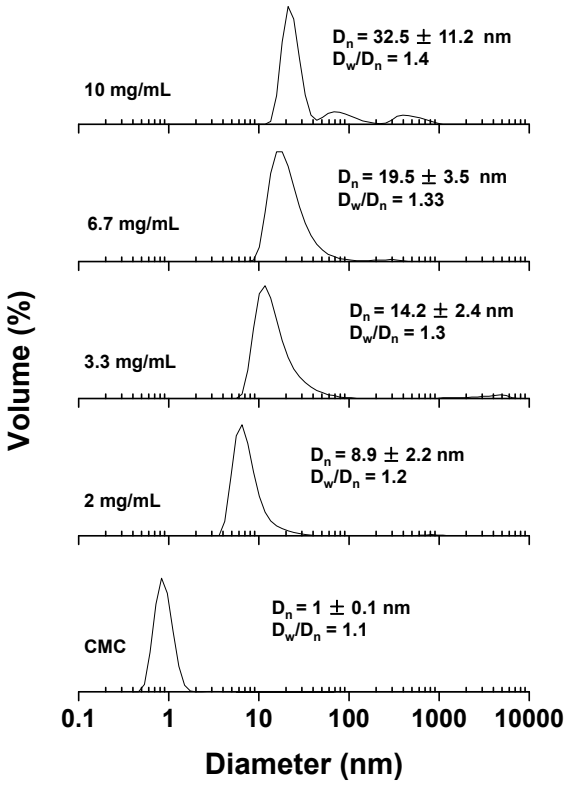

III. Qualitative analysis of POEOMA-g-CMC

Table A.3. Solubility test in various solvents at 5 mg/mL concentration.

Solvent	CMC	POEOMA
Water	Dissolved	Dissolved
Acetone	Undissolved	Dissolved
Ethanol: acetic acid (1:1 v/v)	Undissolved	Dissolved

Figure A.2. FT-IR spectra of POEOMA-g-CMC, CMC and POEOMA homopolymer.

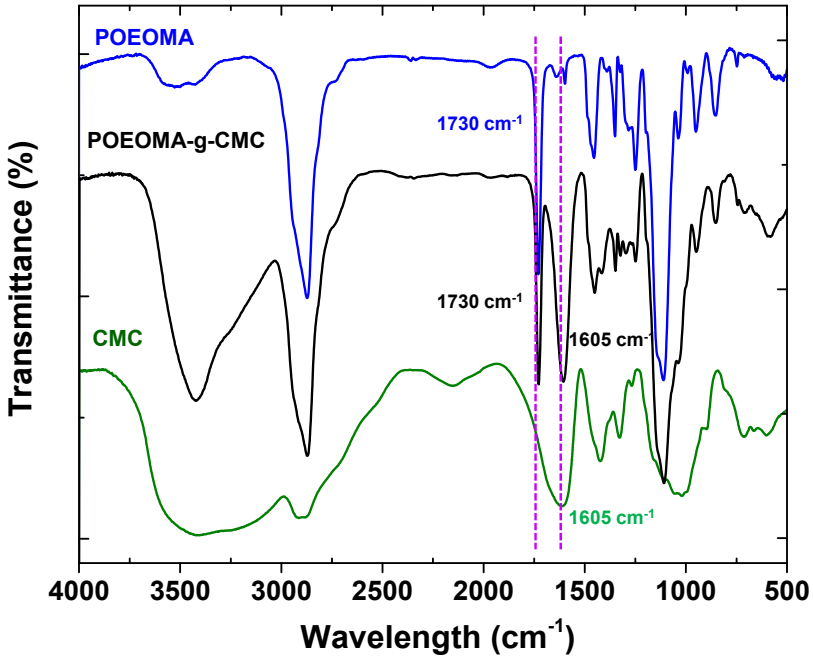

IV. Loading of Dox

Figure A.3. UV absorbance of free DOX in outer water during extensive dialysis at λ = 497 nm.

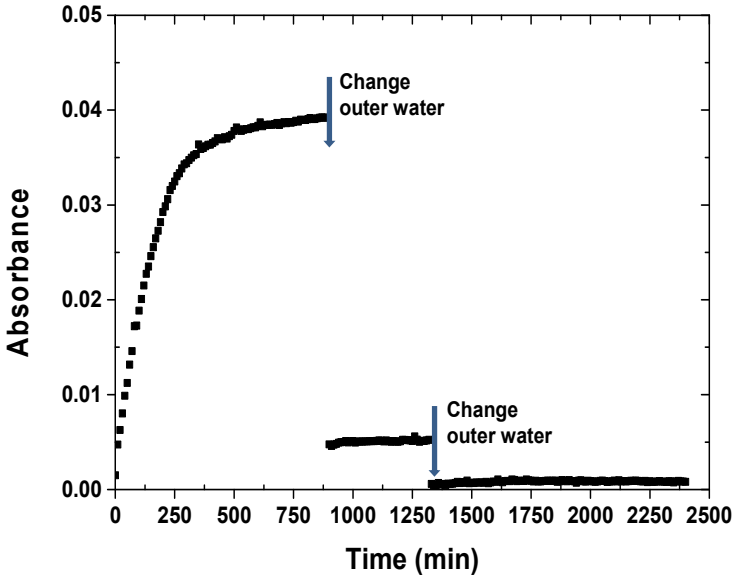

Figure A.4. Comparison of UV/Vis spectra of DOX-loaded ssBNGs (0.2 mg/mL) with free DOX (7.7 μg/mL) in water.

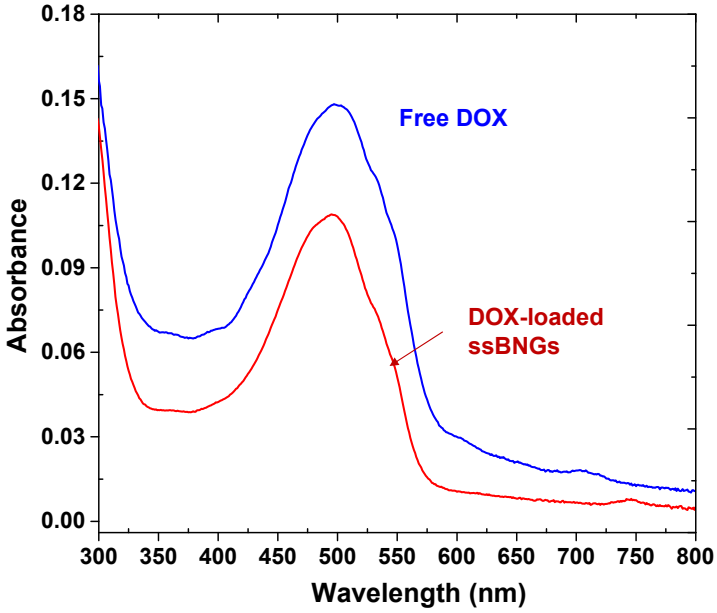

V. Bioconjugation for active targeting

Figure A.5. UV/Vis spectra of free APTS in aqueous solutions at various pH ranging from 2 to 10.

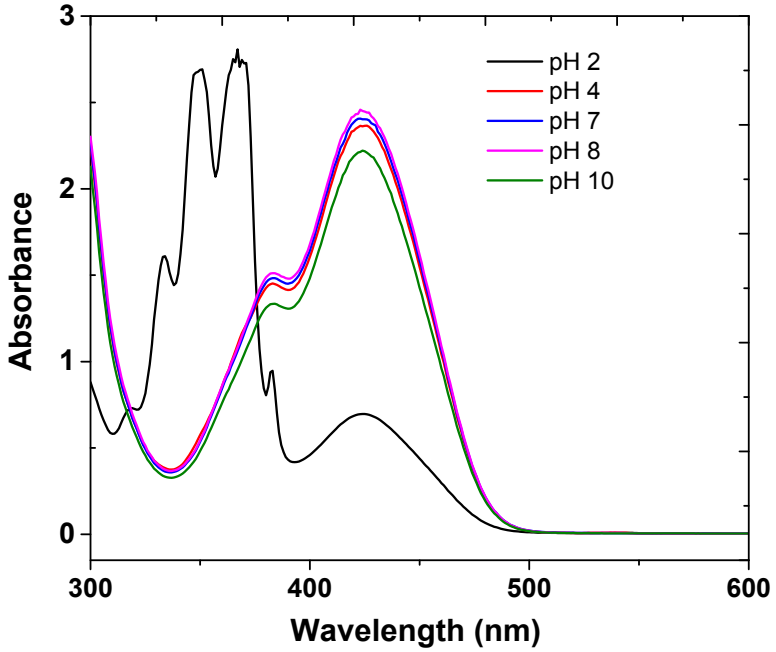

Figure A.6. UV/Vis spectra of (a) absorbance, (b) abs vs different concentrations of APTS in water (pH = 6.5) to determine the extinction coefficient (ε = 21,700 M^{-1} cm^{-1}).

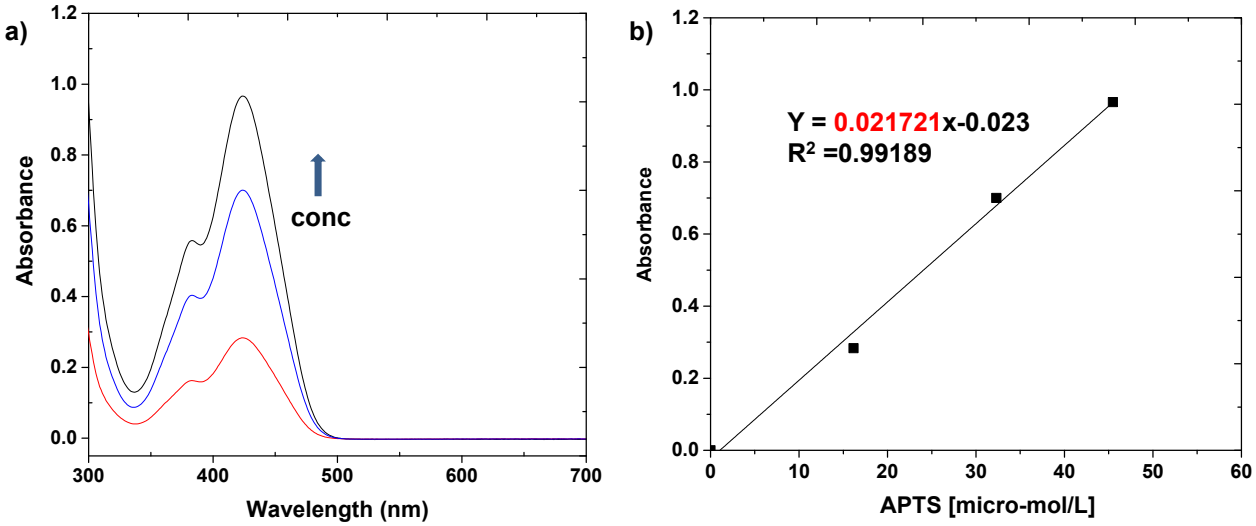

Appendix B

Synthesis and characterization of uncrosslinked CMC-g-P(MEO_2MA-co-OEOMA)

The synthesis of thermoresponsive CMC-grafted polymer (CMC-g-P(MEO_2MA-co-OEOMA)) was conducted by aqueous polymerization of two biocompatible methacrylates having different # of pedant EO units, MEO_2MA and OEOMA, in the presence of CMC. A series of aqueous polymerization was initiated at 40 ºC by a water-soluble azo-type initiator (VA-44) with different feed ratios of MEO_2MA/OEOMA. The results are summarized in Table B.1. Monomer conversion was determined by ^{1}H-NMR spectroscopy using the integrals of the peak at 0.8-1.2 ppm corresponding to 3 protons in methyl groups on polymers to the peak at 6.1 ppm corresponding to one proton in methacrylate groups of monomers (Figure B.1). All polymerization reached > 82% monomer conversion. After the purification by removal of unreacted monomers, the resulting copolymers were characterized by FT-IR technique. As seen in Figure B.2, the FT-IR spectrum of CMC-g-P6 shows two characteristic bands appearing at 1605 cm^{-1} corresponding to carboxylate ($C(=O)O^-$) anion absorption of CMC and at 1730 cm^{-1} corresponding to ester C=O vibrational absorption of grafted P(MEO_2MA-co-OEOMA) copolymers. Furthermore, DLS was used to determine particle size of copolymers in aqueous solutions 25 ºC. Their diameters ranged at 7-13 nm regardless of the amount of MEO_2MA units in copolymers.

Thermal properties of uncrosslinked CMC-g-P(MEO_2MA-co-OEOMA)

The thermoresponsive property of the resulting grafted CMC polymers were characterized using DLS. As seen in Figure S.3, a change in LS intensity of aqueous copolymer solutions was monitored as temperature increased from 20 to 90 ºC. At temperature above their LCST, thermoresponsive CMC-grafted copolymers collapsed to form aggregates, leading to a significant increase in LS intensity. Linear regression of the data points allowed for the determination of their LCST. As summarized in Table B.1, the LCST decreased from 57 to 29 ºC with an increasing amount of MEO_2MA units in the grafted copolymer chains.

Table B.1. Characteristics of physical and thermal properties of CMC-g-P(MEO_2MA-co-OEOMA) prepared by aqueous polymerization in the presence of CMC at 40 ºC.

grafted CMC	MEO_2MA[a] (mol%)	Conv.[b]	Diameter[c] (nm)	LCST[d] (ºC)
CMC-g-P0	0	0.84	13	57
CMC-g-P1	10	0.85	11	54
CMC-g-P2	25	0.87	7	50
CMC-g-P3	41	0.83	11	41
CMC-g-P4	52	0.84	11	38
CMC-g-P5	67	0.83	10	34
CMC-g-P6	75	0.84	8	29

[a] In feed composition of MEO_2MA and OEOMA. [b] By ^{1}H-NMR. [c] By DLS at 4.6 mg/mL at 25 ºC. [d] By DLS with temperature increase from 20 ºC to 90 ºC at an increment of 1 ºC /min.

Figure B.1. ^{1}H-NMR spectrum of CMC-g-P1 in D_2O to determine monomer conversion.

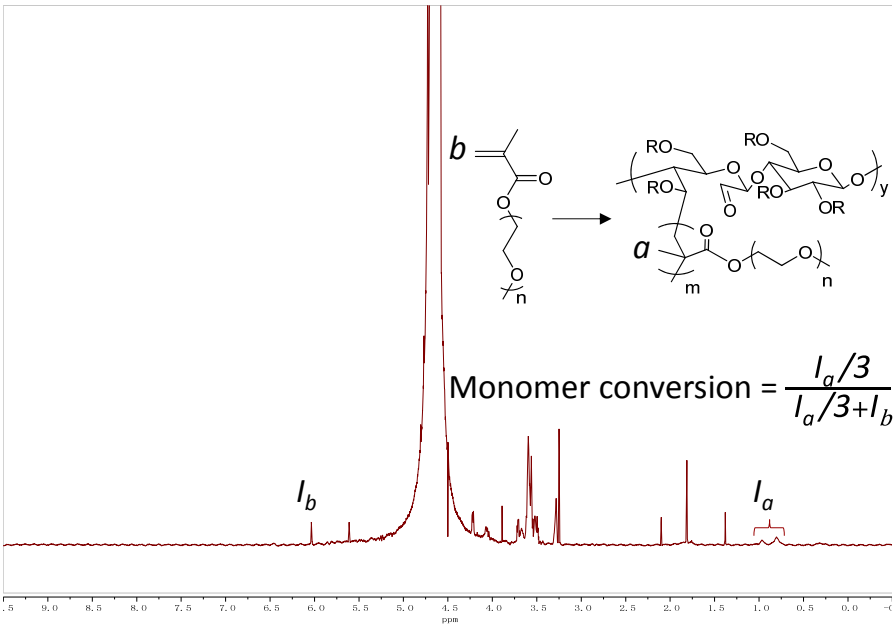

Figure B.2. FT-IR spectrum of CMC-g-P6 (CMC-g-P(MEO_2MA-co-OEOMA)).

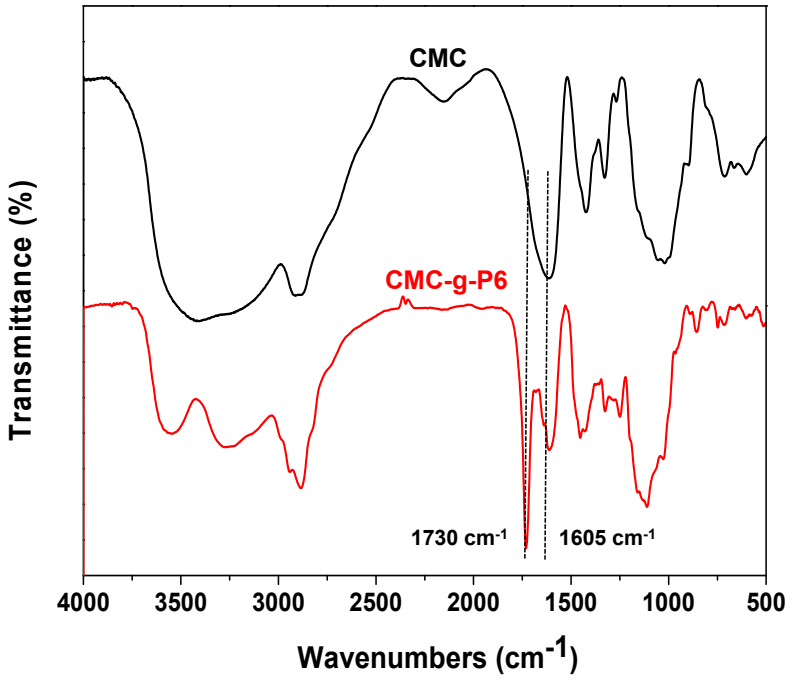

Figure B.3. Temperature dependence of normalized light scattering intensity by DLS for aqueous solutions of LCST vs amount of MEO_2MA units (mol%) in grafted P(MEO_2MA-co-OEOMA) at 4.3 mg/mL.

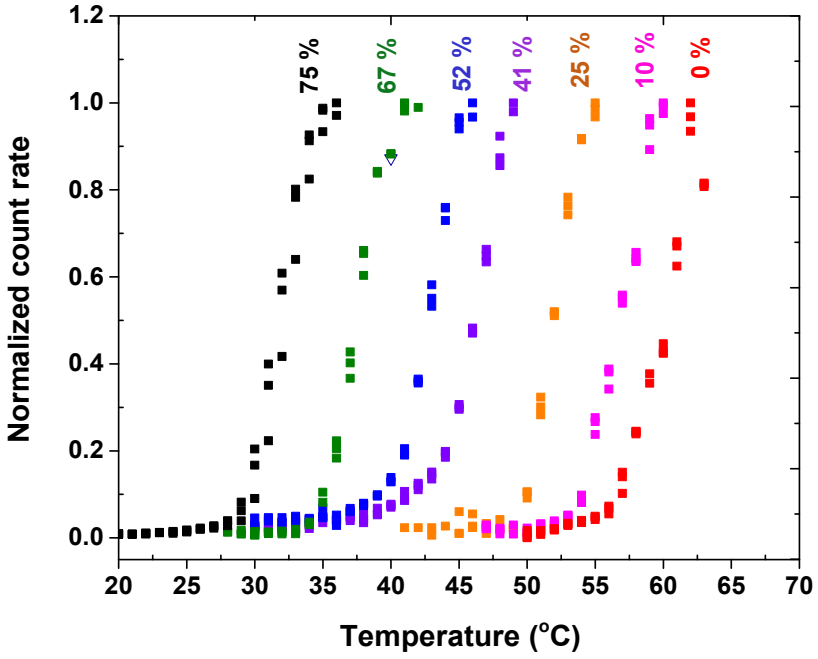

Figure B.4. Temperature dependence of normalized light scattering intensity by DLS for aqueous solutions of DuR-BNGs at 4.6 mg/mL.

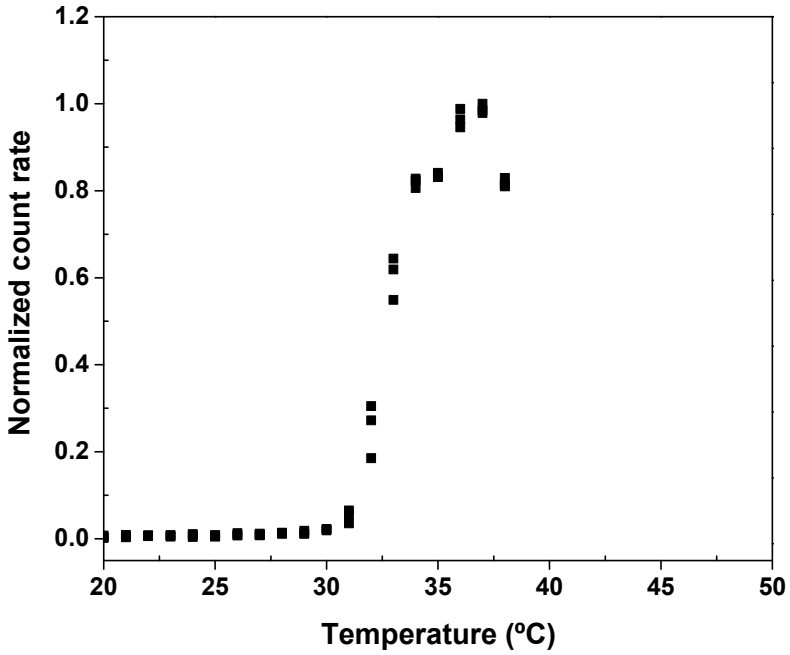

Figure B.5. Calibration curve to determine the concentration of BAS in PBS at pH = 7.4. Fitting function: $y = 0.0384 + 0.0014x - 2.40151E\text{-}7x^2$ ($R^2 = 0.99689$).

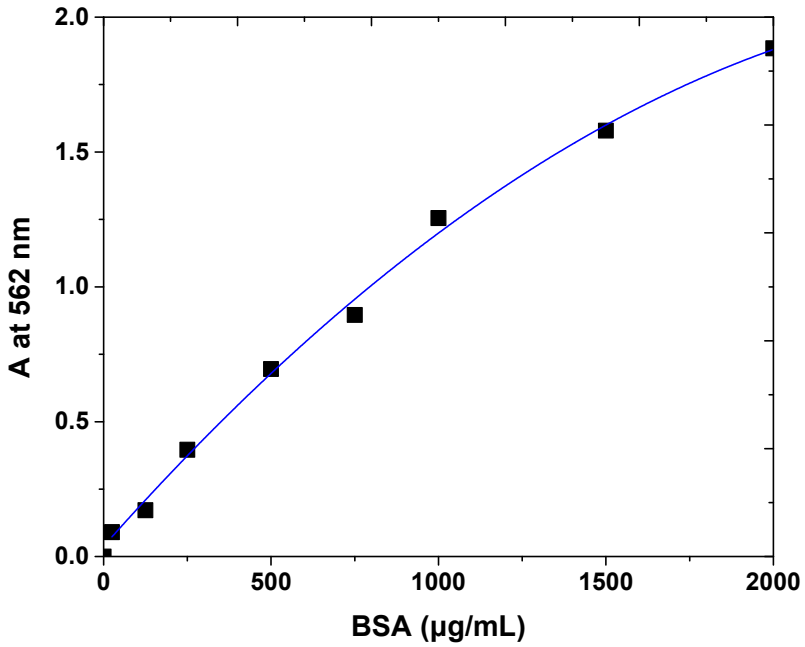

Figure B.6. Release of DOX from DOX-loaded DuR-BNGs in aqueous buffer solution (pH = 7.0) at various temperatures of 25, 37, 40, and 43 ºC. Apparent diffusion constant (D_{app}) is determined from the slopes obtained by fitting the data to a linear regression.

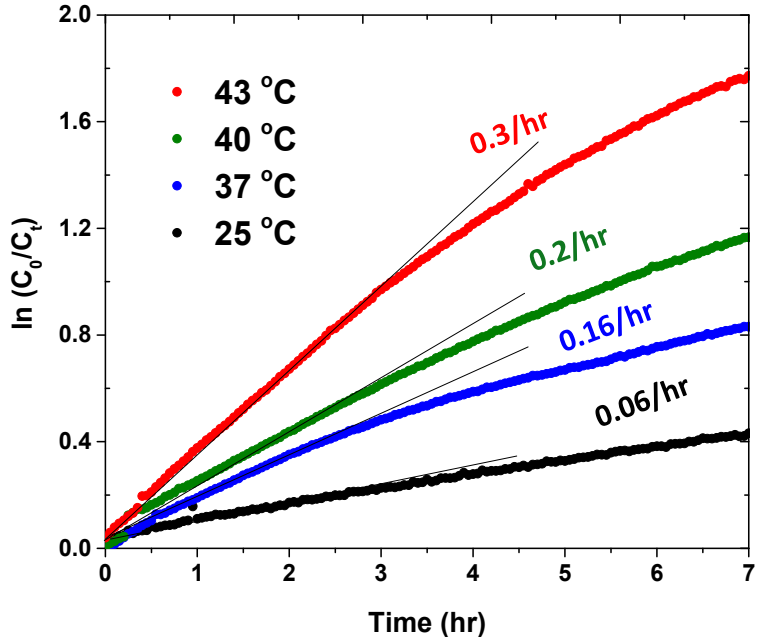

Figure B.7. Release of DOX from DOX-loaded DuR-BNGs in NaCl aqueous solution (pH = 7.0, T = 37 ºC) at different ionic strengths of 154 and 308 mM.

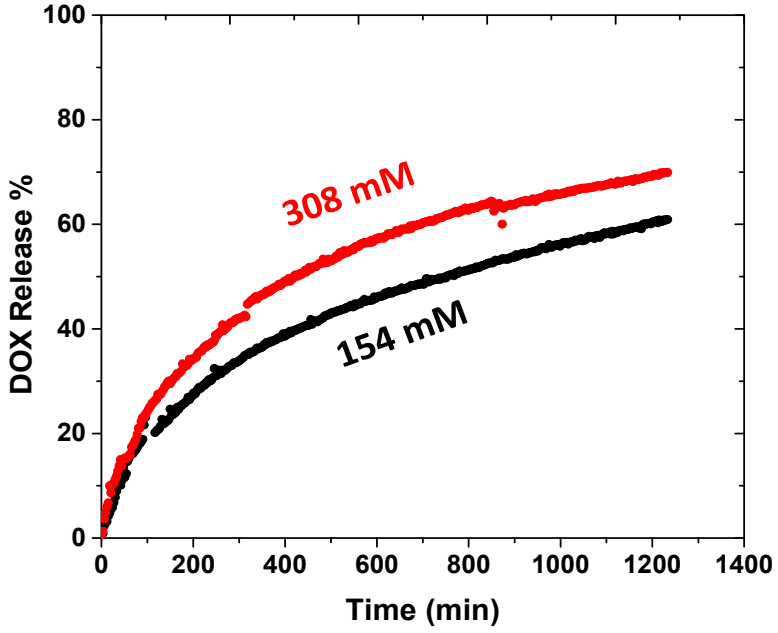

List of publications

K. Rahimian, **Y. Wen**, J. K. Oh.* Redox-responsive cellulose-based thermoresponsive grafted copolymers and in-situ disulfide crosslinked nanogels, *Polymer* **2015**.

Y. Wen, J. K. Oh.* Recent strategies to develop polysaccharide-based nanomaterials for biomedical applications, *Macromolecular Rapid Communications* **2014**, 35, 1819-1832.

Y. Wen, J. K. Oh.* Dual-stimuli reduction and acidic pH-responsive bionanogels: intracellular delivery nanocarriers with enhanced release, *RSC Advances* **2014**, 4, 229-237.

S. Aleksanian; **Y. Wen**; N. Chan; Jung Kwon Oh.* Tuning thermoresponsive kinetics of hydrogels with thiol-responsive degradation. *RSC Advances* **2014**, 4, 3713.